UNIVERSITAT DE BARCELONA

FACULTAT DE QUÍMICA

DEPARTAMENT DE QUÍMICA FÍSICA

Programa de Doctorat de Tecnologia de Materials

Bienni 2004-2006

Electrochemical preparation of Co-Ag nanostructured materials for GMR applications

Memòria que presenta JOSÉ MANUEL GARCÍA TORRES per optar al títol de Doctor per la Universitat de Barcelona

Directores de la tesi:

Dra. Elvira GÓMEZ VALENTÍN
Professora Titular de Química Física
Universitat de Barcelona

Dra. Elisa VALLÉS GIMÉNEZ
Professora Titular de Química Física
Universitat de Barcelona

4.3. Analysis of the first stages during cobalt-silver electrodeposition process

Due to the presence of the $CoAg_3$ metastable phase in thick Co-Ag films, it was of interest to know whether this phase appeared from the very early deposition stages or not. The influence of the growing films and the substrate over the structural and magnetic properties was analyzed. Knowing how those properties vary with film's thickness and kind of substrate will be useful when dealing with the magnetotransport properties results.

The study revealed that after the electrodeposition of a first thin silver layer the incorporation of cobalt took place. However, cobalt was found to be in a different structure depending on the substrate used. Whereas $CoAg_3$ phase was detected from the very beginning of the deposition on Co-Ag films grown over Si/Ti/Ni, the metastable phase was scarcely detected over Si/Cr/Cu and undetected over glass/ITO substrate. This result was attributed to the higher or lesser deposition rate attained over each substrate that clearly affects the structure formation.

On the other hand, the magnetic properties evolved from diamagnetism to superparamagentism and then ferromagnetism by increasing film thickness. The change in the magnetic properties was attributed to the incorporation in the diamagnetic silver layer of nanometric cobalt particles with superparamagnetic behaviour. The coalescence of the cobalt granules led to the ferromagnetic behaviour. However, the ferromagnetic properties of Co-Ag films were also dependent on the substrate and hence on the structure. The coercivity values were higher when the $CoAg_3$ phase was present. These results were in agreement with those found in homogeneous or heterogeneous Co-Cu films for which the H_c values were higher for the homogeneous deposits [106].

Group of articles included in section 4.3.

Page 119: Evolution of magnetic and structural properties from Ag nanolayers to several microns Co-Ag deposits prepared by electrodeposition

Jose Garcia-Torres, Elvira Gómez and Elisa Vallés, Journal of Electroanalytical Chemistry 635 (2009) 63

Evolution of magnetic and structural properties from Ag nanolayers to several microns Co-Ag deposits prepared by electrodeposition

Journal of Electroanalytical Chemistry 635 (2009) 63–68

Contents lists available at ScienceDirect

Journal of Electroanalytical Chemistry

journal homepage: www.elsevier.com/locate/jelechem

Evolution of magnetic and structural properties from Ag nanolayers to several microns Co–Ag deposits prepared by electrodeposition

Jose Garcia-Torres, Elvira Gómez, Elisa Vallés *

Electrodep., Departament de Química Física and Institut de Nanociència i Nanotecnologia (IN²UB) de la Universitat de Barcelona, Martí i Franquès, 1. 08028 Barcelona, Spain

ARTICLE INFO

Article history:
Received 25 May 2009
Received in revised form 29 July 2009
Accepted 6 August 2009
Available online 13 August 2009

Keywords:
Electroplating
Coercivity
Cobalt–silver thin films
Field-emission scanning electron microscopy (FE-SEM)
Selected area electron diffraction-transmission electron microscopy (SAED-TEM)

ABSTRACT

The evolution of composition, morphology, magnetic properties and crystalline structure of Co–Ag electrodeposits from nanometric to micrometric thicknesses has been analyzed. Different substrates (Si/Ti/Ni, Si/Cr/Cu and glass/ITO) have been used to electrodeposit the Co–Ag system. The same trend was observed in all cases: after a first nanometric silver layer, cobalt was gradually incorporated till constant composition was attained. Moreover, a gradual variation of the magnetic response of the films from diamagnetism to superparamagnetism and then ferromagnetism was detected by increasing the deposition charge. fcc-Ag, hcp-Co and a metastable phase hcp-$CoAg_3$ were present in Co–Ag micrometric deposits grown over Si/Ti/Ni from the very early deposition stages, these deposits showing coercivity values around 115 Oe. However, deposits of lower coercivities (around 50 Oe) were obtained over glass/ITO and Si/Cr/Cu substrates, these deposits being constituted by fcc-Ag and hcp-Co.

1. Introduction

Cobalt–silver system has received great attention during the last decades due to its interest in technological applications displaying magnetoresistance, i.e. read-head devices, magnetic sensors, spin-valves [1–3]. This system has attracted much interest not only from a technological point of view but also from a theoretical point of view as a high GMR has been reported in magnetic granular Co–Ag films [4,5].

This material is mainly produced by physical methods [6,7] i.e. sputtering, physical vapour deposition or molecular beam epitaxy. In contrast, electrodeposition has to date not been so extensively investigated to prepare the Co–Ag system [8–10]. However, this technique is a fast and cost-effective way to grow high-quality thin films and multilayers on large-area substrates as compared to vacuum deposition techniques. Films grown by electrodeposition are reproducible and may have properties comparable to samples grown by physical methods [11,12].

The Co–Ag electrodeposition process was previously studied from a bath containing thiourea, sodium gluconate and boric acid over a Si/Ti/Ni substrate [10,13,14]. Those studies mainly dealt with the characterization of several microns thick Co–Ag films. The structural analysis of those deposits revealed the presence of a Co–Ag metastable phase characterized as $CoAg_3$ [14], phase whose percentage varied with different parameters, i.e. applied potential, bath composition and bath temperature. The magnetic properties of the deposits reflected that the higher the $CoAg_3$ content the higher the coercivity. On the other hand, the deposits were characterized by being granular independently of the modified parameters.

Although Co–Ag is a promising system to show GMR due to the total immiscibility of both metals [15], the presence of metastable phases in the deposits exerts a detrimental effect on the magnetoresistance, as it has been previously reported for the Co–Cu system [16]. In this sense, the presence of the $CoAg_3$ metastable phase in electrodeposited Co–Ag films implies that a subsequent annealing of the material would be needed. The thermal treatment will allow the growth of ferromagnetic Co granules within the Ag matrix improving the magnetoresistance values. In this sense, the aim of the present work is to study how the morphology, composition, structure and magnetic properties of Co–Ag electrodeposits vary with the growing film. Special attention is paid on the different crystalline phases present in the Co–Ag electrodeposits from the very early stages of the process and their relation with the magnetic properties. This study is also developed to examine the possibilities of the electrodeposition to obtain films with modulated properties depending on the experimental conditions of deposition rate, thickness of the deposits and specially the nature of the electrode.

* Corresponding author. Tel.: +34 934039238; fax: +34 934021231.
E-mail address: e.valles@ub.edu (E. Vallés).

0022-0728/$ - see front matter © 2009 Elsevier B.V. All rights reserved.
doi:10.1016/j.jelechem.2009.08.003

2. Experimental

The electrodeposition of cobalt–silver coatings was performed from a freshly prepared 0.01 M $AgClO_4$ + 0.1 M $Co(ClO_4)_2$ + 0.1 M thiourea + 0.1 M sodium gluconate + 0.3 M H_3BO_3 + 0.1 M $NaClO_4$ solution, all chemicals being of analytical grade. The solution was freshly prepared with water first doubly distilled and then treated with a Millipore Milli Q system. pH was kept close to 3.7. Before and during experiments, solutions were de-aerated with argon. Temperature was kept constant at 25 °C.

Electrochemical experiments were carried out in a conventional three-electrode cell using an Autolab with PGSTAT30 equipment and GPES software. Working electrodes were vitreous carbon (Metrohm), glass/ITO (indium–tin oxide layer of 25 nm over glass plates), silicon with Ti/Ni seed layer (Si/Ti(100 nm)/Ni(50 nm)) and silicon with Cr/Cu seed layer (Si/Cr(5 nm)/Cu(20 nm)) supplied by IMB-CNM. Vitreous carbon electrode was polished to a mirror finish using alumina of different grades (3.75 and 1.87 μm) and cleaned ultrasonically for 2 min in water. Glass/ITO and Si/seed layer electrodes were firstly cleaned with acetone followed by ethanol and later with water. The counter electrode was a platinum spiral. The reference electrode was an Ag|AgCl|NaCl 1 mol dm^{-3} mounted in a Luggin capillary containing 0.2 mol dm^{-3} $NaClO_4$ solution. All potentials refer to this electrode.

Voltammetric experiments were carried out at 50 mV s^{-1}, scanning at first to negative potentials. Only one cycle was run in each voltammetric experiment. Deposits were obtained potentiostatically on glass/ITO(25 nm), Si/Ti(100 nm)/Ni(50 nm) and Si/Cr(5 nm)/Cu(20 nm) under agitation with magnetic stirring.

The structure of the deposits was studied with X-ray powder diffraction (XRD) using a conventional Bragg–Brentano diffractometer Siemens D-500. The Cu Kα radiation (λ = 1.5418 Å) was selected using a diffracted beam curved graphite monochromator. The X-ray powder diffraction diagrams were created in the 5°–105° 2θ range with a step range of 0.05° and a measuring time of 15 s per step. The structure was also studied by using high resolution transmission electron microscopy (HR-TEM) combined with selected area electron diffraction (SAED) using a JEOL 2100.

Deposit morphology was observed using Hitachi H-4100 FE field-emission scanning electron microscope (FE-SEM). Elemental composition was determined with an X-ray analyser incorporated in Leica Stereoscan S-360 equipment. Thickness of the coatings was measured using a white-light interferometer from Zygo Corporation.

Magnetic measurements were taken in a SQUID magnetometer at room temperature in helium atmosphere.

3. Results and discussion

3.1. Deposits preparation

Deposits were prepared at different deposition times in order to study the initial stages of the Co–Ag electrodeposition process. The gradual variation of the composition, morphology, structure and magnetic properties of the films was analysed. Si/Ti/Ni electrode was used to prepare most of the samples. However, glass/ITO and Si/Cr/Cu substrates were selected to perform the study of the magnetic properties of the thin films because those substrates provide the sufficient conductivity to allow electrodeposition and they do not hide the detection of the magnetic response of the nanometric films prepared.

Similar voltammetric behaviour was observed for all the electrodes (Fig. 1): two reductions peaks corresponding to silver reduction (peak A) and simultaneous cobalt–silver deposition (peak B) prior to hydrogen evolution. A double peak assigned to cobalt

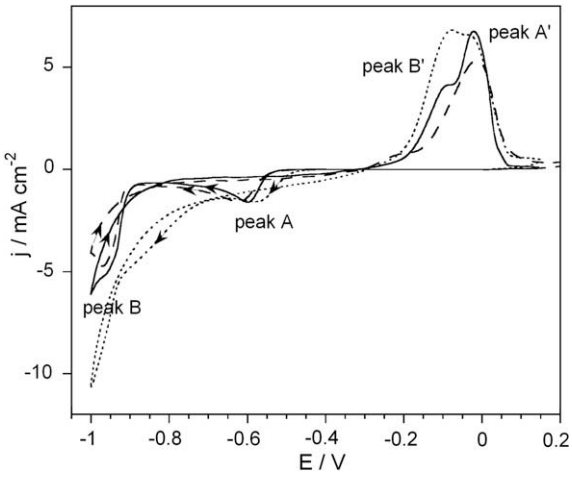

Fig. 1. Cyclic voltammograms recorded from the solution 0.01 M $AgClO_4$ + 0.1 M $Co(ClO_4)_2$ + 0.1 M thiourea + 0.1 M sodium gluconate + 0.3 M H_3BO_3 + 0.1 M $NaClO_4$ over different substrates. (Dotted line) Si/Ti/Ni, (continuous line) vitreous carbon and (dashed line) glass/ITO.

(peak B′) and silver (peak A′) oxidation [13] was recorded during the anodic-going scan. As it was expected, deposition took place at more positive potentials over metallic substrates (Fig. 1, dotted line) than over vitreous carbon or glass/ITO (Fig. 1, continuous line and dashed line) due to the greater ease of nucleation of the initial silver over metallic electrodes. On the other hand, a cobalt-related current density sharp decay is observed over non-metallic substrates, meanwhile a more progressive current increment was recorded over metallic electrodes.

The Co–Ag electrodeposition was carried out potentiostatically and under stirring conditions in order to avoid the depletion of the electroactive species to the electrode. Deposition potentials were selected from the previous voltammetric study according to the shift in the Co–Ag codeposition onset potential over each substrate in order to induce similar deposition rates over each substrate. Different potential ranges were applied depending on the susbtrate: Si/Ti/Ni (−770 mV, −830 mV), Si/Cr/Cu (−810 mV, −870 mV) and glass/ITO (−950 mV, −1100 mV). Deposits were prepared at variable deposition times with the aim to study the evolution of the growing films.

Fig. 2 shows the *j*–*t* transients recorded over the different substrates used to obtain the Co–Ag films. The same initial current density and similar shape of the curves were recorded. However, higher *j*/*t* slopes were observed over metallic substrates (Fig. 2, curves *a* and *b*) than over glass/ITO electrodes (Fig. 2, curve *c*). Hence, different deposition rates were obtained varying them in the way Si/Ti/Ni > Si/Cr/Cu > glass/ITO. These different deposition rates were probably as a consequence of the different electrical conductivity of the seed layers of the substrate, which gradually decreased in the order: Ti(100 nm)/Ni(50 nm) > Cr(5 nm)/Cu(20 nm) > ITO(25 nm). No stabilisation in the *j*–*t* transients was observed, associated with the increment in the film roughness as time goes (this fact will be seen in the next section).

3.2. Evolution of deposit's composition, morphology and structure

Table 1 shows the cobalt percentage of some deposits obtained at fixed potential and different deposition times for the different substrates. Compositional analysis reveals that Ag is initially deposited over the electrode, as can be expected from the voltammetric response of the tested solution. After that, cobalt was progressively incorporated into the deposit as deposition time increased, thus taking cobalt and silver reduction place simulta-

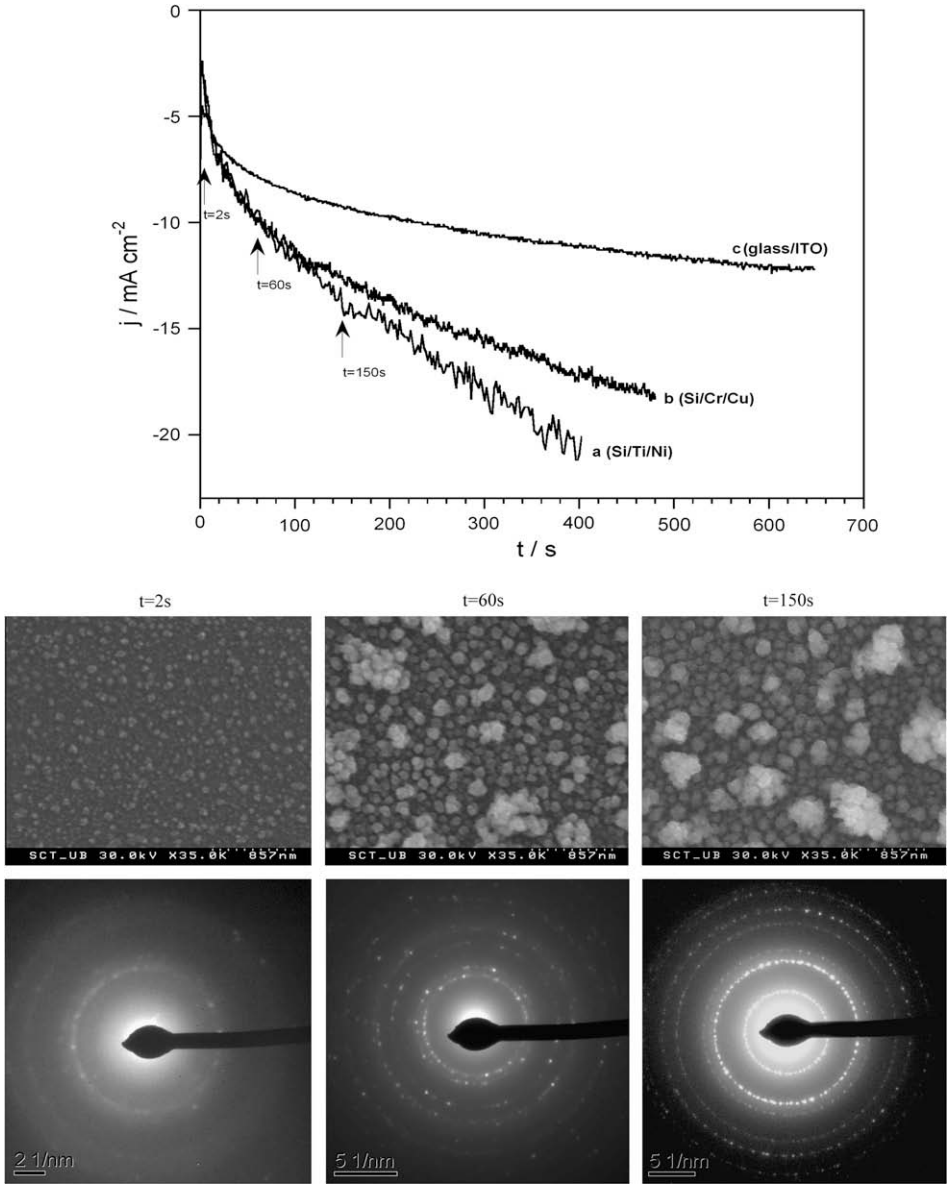

Fig. 2. *j–t* transients recorded from the solution 0.01 M $AgClO_4$ + 0.1 M $Co(ClO_4)_2$ + 0.1 M thiourea + 0.1 M sodium gluconate + 0.3 M H_3BO_3 + 0.1 M $NaClO_4$ over different substrates. (a) Si/Ti/Ni, (b) Si/Cr/Cu and (c) glass/ITO. SEM micrograph and SAED patterns of films prepared over Si/Ti/Ni at different deposition times.

Table 1
Variation of cobalt percentage in Co–Ag films obtained over different substrates.

Si/Ti/Ni		Si/Cr/Cu		Glass/ITO	
Deposition time/s	wt.% Co	Deposition time/s	wt.% Co	Deposition time/s	wt.% Co
2	0	2	0	2	0
60	4	60	32	60	8
100	17	100	42	100	18
150	19	150	42.5	150	29
180	39	200	44	200	40
300	41	480	43	640	41

neously by increasing deposition time. Finally, constant composition was attained over all the electrodes but at different deposition times depending on the substrate used.

The surface morphology evolution of deposits obtained over Si/Ti/Ni at −0.83 V from the very early stages of the process (2 mC cm^{-2}, 1.5 nm thick) to several microns thick deposits (6.7 C cm^{-2}, 4 μm) was examined. Fig. 2 shows the evolution of the deposits from the earliest deposition stages. After 0.5 s of deposition, complete coverage of the electrode surface was attained corresponding to a granular nanometric silver film (1.5 nm), as compositional analysis reveals for this short deposition time. No differences were detected in the silver layer by increasing deposition time (Fig. 2, t = 2 s, 10 nm thick). However, a second growth with higher grain size than that of silver was observed over the initial electrodeposited layer (Fig. 2, t = 60 s, 180 nm thick) which developed to cover entirely the first silver layer (Fig. 2, t = 150 s, 500 nm thick). This second growth started to appear as cobalt was incorporated into the film and its presence was higher and higher as cobalt content increased. Compositional analysis of this second growth revealed the presence of cobalt in it.

The crystalline structure of the growing films obtained at different deposition times was examined by HR-TEM combined with selected area electron diffraction (SAED). In order to perform TEM observations, cross-sections from each sample were prepared, polished mechanically and thinned by means of Ar^+ ion bombardment

Table 2
Comparison between distances measured from the SAED patterns and tabulated data of JCPDS-international centre for diffraction data (*) for the Ag as-deposited samples.

Measured d (Å)	fcc-Ag d*(Å) (h k l)
2.367	2.3587 (1 1 1)
2.048	2.0427 (2 0 0)
	1.4444 (2 2 0)
	1.2318 (3 1 1)
	1.1793 (2 2 2)

Table 3
Comparison between distances measured from the SAED patterns and tabulated data of JCPDS-international centre for diffraction data (*) for the Co–Ag as-deposited samples.

Measured d (Å)	fcc-Ag d*(Å) (h k l)	hep-Co d*(Å) (h k l)	hcp-$CoAg_3$ d*(Å) (h k l)
2.510			2.500 (1 0 0)
2.359	2.3587 (1 1 1)		
2.324			2.337 (0 0 2)
2.206			2.205 (1 0 1)
2.162		2.1697 (1 0 0)	
2.064	2.0427 (2 0 0)	2.0446 (0 0 2)	
1.912		1.9166 (1 0 1)	
1.490		1.4880 (1 0 2)	
	1.4444 (2 2 0)		
		1.2527 (1 1 0)	
	1.2318 (3 1 1)		
	1.1793 (2 2 2)		
		1.1542 (1 0 3)	

to achieve the appropriate thickness to allow electrons to pass through the sample (around 100 nm). After that, the samples were then mounted on a copper holder. Fig. 2 shows the electron diffraction patterns of the samples grown at different times. For all samples, spotty diffraction rings were observed. The measurement of the ring diameter (2R h k l) related to the (h k l) reflection in the pattern allowed us to assess the mean lattice parameters of the present phases.

At very low deposition times, Ag phase was only detected in the films (Fig. 2, t = 2 s), in agreement with the compositional analysis. Table 2 gives the indices of electron diffraction rings in the as-deposited silver films showing that only fcc-Ag (PDF#89-3722) phase is present as all the diffraction spots were assigned to the fcc phase. On the other hand, when the second growth was detected and the compositional analysis revealed the simultaneous cobalt deposition, the SAED patterns (Fig. 2, t = 60 s and 150 s) revealed the presence of the $CoAg_3$ phase (PDF#28-0431) previously detected in thick Co–Ag films [14]. This metastable phase appeared even in short-time deposits in which only a small amount of Co was detected. Moreover, some hcp-Co (PDF#89-4308) was observed being more easily detected when higher amounts of cobalt were present in the films. Table 3 shows the indices of electron diffraction rings of the Co–Ag films showing that they are composed of fcc-Ag, hcp-$CoAg_3$ and hcp-Co.

The same morphological evolution previously described was observed over glass/ITO and Si/Cr/Cu substrates. After a first electrodeposited silver layer a second growth developed over it corre-

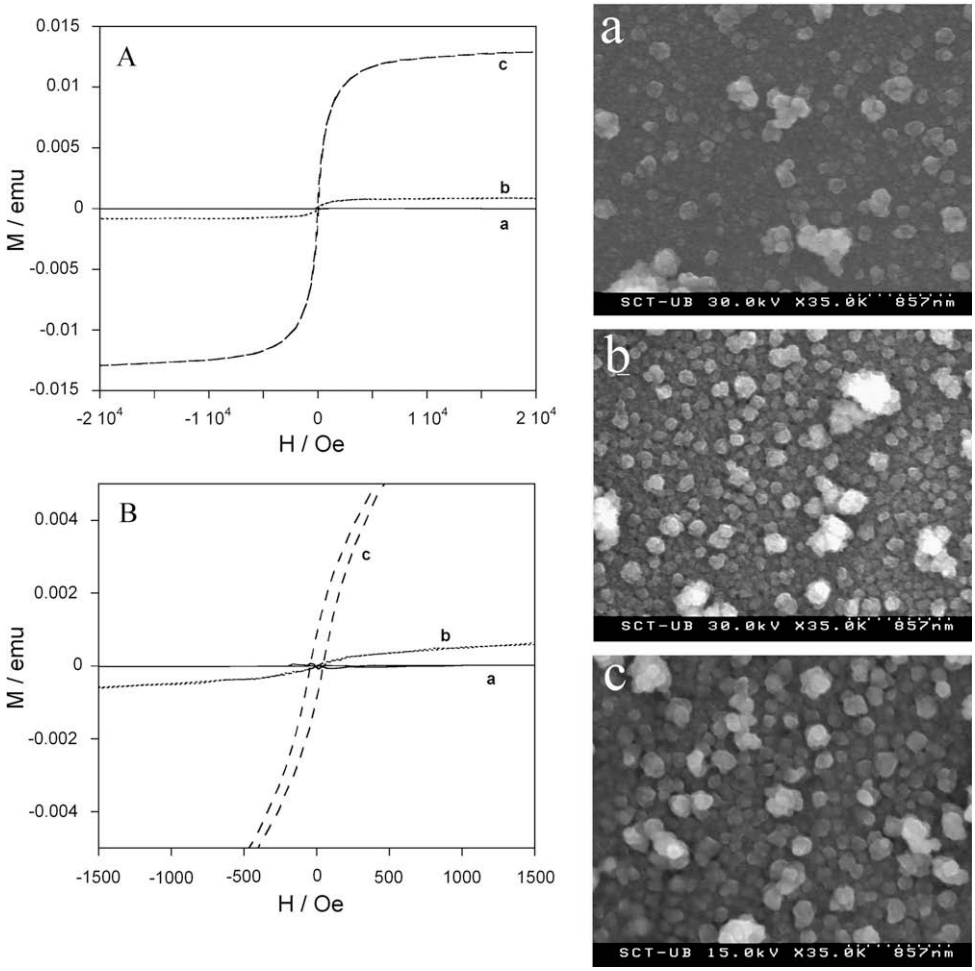

Fig. 3. Magnetization curves of Co–Ag deposits obtained over Si/Cr/Cu at different deposition times, curve *a*) 2 s, 5.3 mC cm^{-2}, 5 nm; curve *b*) 100 s, 0.8 C cm^{-2}, 250 nm and curve *c*) 480 s, 6.6 C cm^{-2}, 4 μm. SEM micrographs of the films at the same times.

sponding to the Co–Ag codeposition. The only difference was the grain size decrease from around 170 nm over Si/Ti/Ni to around 100 nm over glass/ITO on 250 nm thick (t = 100 s) deposits.

Measured thicknesses of the initial layers were smaller than the theoretical ones increasing the difference between both as time goes due to the reduction in the efficiency. However, as film roughness increased with deposition time, more agreement between the experimental thickness and the theoretical one was observed because of the low-packing density of the films. The increment in the roughness throughout all the deposition implies an increment in the electrodeposited surface, fact that justifies the continuous current density increase observed during the electrochemical deposition. The film thickness (h) was estimated by means of Eq. (1) taking into account the deposition charge and the atomic volumes of each metal as well as the composition of the deposits. The efficiency of the process was supposed 100%.

$$h = \frac{QN_A}{100A}(Q_{Co}V_{Co} + Q_{Ag}V_{Ag}). \quad (1)$$

where Q is the total charge, Q_{Co} and Q_{Ag} are the fraction of the total charge related to cobalt and silver, respectively, obtained from the percentage of each metal in the deposit, V_{Ag} and V_{Co} are the atomic volumes in the crystalline lattice, N_A is the Avogadro's number and A is the electrode area.

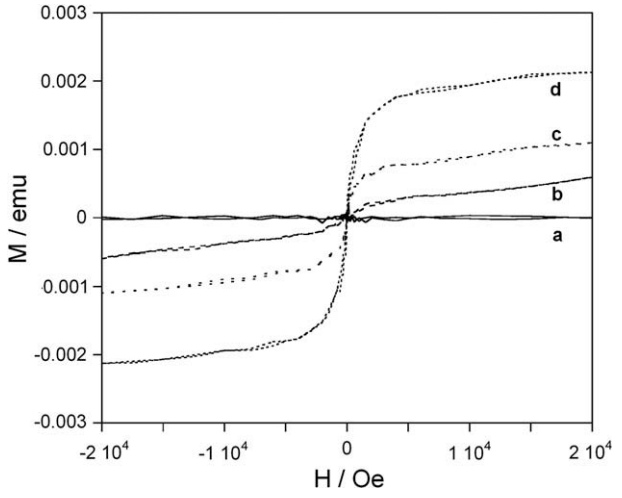

Fig. 4. Magnetization curves, after normalization at the same deposition charge (6.6 C cm^{-2}), of the Co–Ag deposits obtained over glass/ITO substrate at different deposition times, curve *a*) 2 s, 0 wt.% Co, curve *b*) 100 s, 18 wt.% Co, curve *c*) 150 s, 29 wt.% Co and curve *d*) 200 s, 40 wt.% Co.

3.3. Magnetic properties of the growing films

The evolution of the magnetic properties of the electrodeposits prepared over glass/ITO and Si/Cr/Cu as a function of the deposition time was analysed (Figs. 3 and 4). Similar evolution of the magnetic properties with the deposition charge was observed for the deposits prepared over both substrates.

At short deposition times, diamagnetic response of the films grown over Si/Cr/Cu was recorded (Fig. 3, curve *a*) as corresponds to the only silver formation (Fig. 3, SEM micrograph *a*). By increasing deposition time, a certain value of M_s was observed due to cobalt incorporation in the deposits (Fig. 3, curve *b* and SEM micrograph *b*). Under these conditions, superparamagnetic behaviour was detected revealing that the agglomerates observed in the SEM pictures over the initial silver nanolayer would contain nanometric magnetic particles. Poor magnetic signal was recorded due to the small amount of deposit obtained at low deposition charges. On the other hand, ferromagnetic response was clearly detected in thicker deposits (Fig. 3, curve *c* and SEM micrograph *c*). Moreover, the higher the cobalt incorporation in the film the higher the saturation magnetisation, as it was expected.

Similar behaviour was observed for the initial stages of deposits grown over glass/ITO. In order to compare the magnetic response of the samples obtained over this substrate, the magnetic signal was normalized taking into account the deposition charge. In this sense, the increase in the saturation magnetisation of the films was related with a gradual increase of the cobalt percentage in the films (Fig. 4). A stationary value was attained when deposit's composition was constant. At these conditions, constant magnetic hysteresis curves were obtained because deposit composition became constant.

Final deposits (6.7 C cm^{-2}, 4 μm thick) showed hysteresis loops with coercivity values around 50 Oe. However, the magnetic response was different to that obtained for deposits of similar deposition charge but obtained over Si/Ti/Ni substrates [14], for which different M–H hysteresis loops were recorded (Fig. 5A).

In order to explain the different magnetic behaviour of micrometric Co–Ag electrodeposits prepared over the three electrodes studied, XRD analysis were performed. Fig. 5B shows the X-ray patterns of Co–Ag deposits obtained over the different substrates. Besides the diffractions peaks assigned to fcc-Ag, several peaks corresponding only to $CoAg_3$ metastable phase are clearly detected in deposits obtained over Si/Ti/Ni (Fig. 5B, curve *a*). Moreover, peaks place at around 2θ = 38, 65, 77.5 and 81° are due to the reflections of both fcc-Ag and hcp-$CoAg_3$. However, $CoAg_3$ is scarcely detected in deposits prepared over Si/Cr/Cu (Fig. 5B, curve *c*) and undetected over glass/ITO substrates (Fig. 5B, curve *b*). Over these electrodes, the same peaks placed at around 2θ = 38, 65,

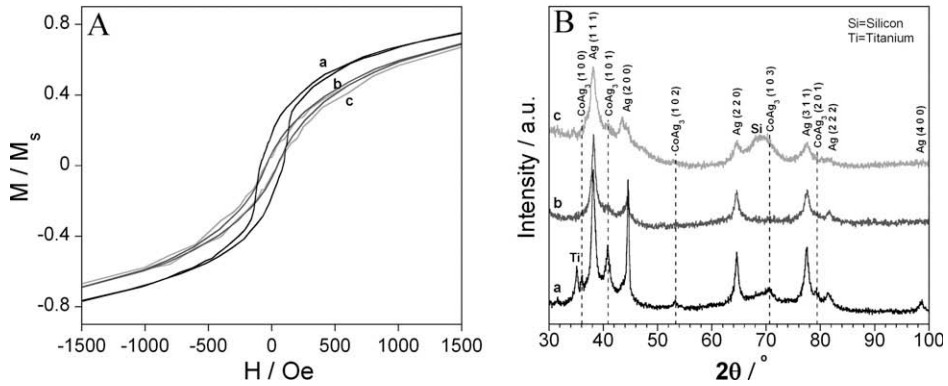

Fig. 5. Magnetization curves of Co–Ag deposits of 6.6 C cm^{-2} obtained over different substrates, curve *a*) Si/Ti/Ni, −830 mV, 40 wt.% Co; curve *b*) glass/ITO, −1000 mV, 40 wt.% Co and curve *c*) Si/Cr/Cu, −850 mV, 40.5 wt.% Co.

77.5 and 81° are only due to silver reflections. In this sense, it seems that Si/Ti/Ni substrate favors the formation of the $CoAg_3$ metastable phase as higher deposition rates are attained. Therefore, the presence of different phases in the Co–Ag samples justifies the different magnetic behaviours observed. The same magnetic response is detected over Si/Cr/Cu and glass/ITO (Fig. 5A, curves *b* and *c*) as the same structure was observed. On the other hand, deposits over Si/Ti/Ni show higher coercivity values (around 115 Oe [14]) due to the $CoAg_3$ phase presence.

The widest peaks in the diffractogram corresponding to the films obtained over Si/Cr/Cu revealed the more nanocrystalline nature of the Co–Ag coatings grown over this substrate. The average grain size was estimated from the full width at half maximum (FWHM) values of the diffraction peaks by using the Debye–Scherrer equation, neglecting the instrumental linewidth (which is acceptable for a nanocrystalline material) and the stress-induced line broadening. A slight decrease in the silver crystal size from around 13 nm observed over Si/Ti/Ni to around 8 nm over Si/Cr/Cu is estimated. The same trend has been observed in the grain size (the values has been previously given in the morphology evolution section), it being higher over Si/Ti/Ni than over Si/Cr/Cu.

4. Conclusions

The electrodeposition technique allowed preparing, from a Co–Ag electrolytic bath, different films with modulated magnetic properties as a function of the film's thickness. Independently of the substrate used, a first electrodeposited diamagnetic layer of silver of several nanometers thick was obtained. Over this layer, Co–Ag codeposition took place leading first to Co agglomerates with superparamagnetic behaviour and then films with ferromagnetic behaviour. The films attained constant composition after a certain time of deposition, time that depended on the substrate used.

The electrical conductance of the layers over the substrate induced different deposition rates that affected the structure of the deposits. Over Si/Ti/Ni, for which the maximum j/t slope was observed in the potentiostatic transients, hcp-$CoAg_3$ metastable phase was present in the films together with hcp-cobalt and fcc-silver. On the contrary, the metastable $CoAg_3$ phase was not detected over substrates leading to lower j/t slopes during the electrodeposition.

No significant difference in the morphology of the deposits obtained over the substrates tested was observed, only a slight difference in the grain size, it being higher over Si/Ti/Ni than over Si/Cr/Cu. This difference was also detected in the crystalline size measured from the XRD pattern.

Acknowledgements

This paper was supported by contract MAT-2006-12913-C02-01 from the *Comisión Interministerial de Ciencia y Tecnología (CICYT)*. J. García-Torres would also like to thank the Departament d'Innovació, Universitats i Empresa of the Generalitat de Catalunya and Fons Social Europeu for their financial support.

References

[1] J. Schotter, P.B. Kanip, A. Becker, A. Pühler, D. Brunkmann, W. Schepper, H. Bruckl, G. Keiss, IEEE Trans. Magn. 38 (2002) 3365.
[2] A. Berkowitz, J.R. Mitchell, M.J. Carey, A.P. Young, D. Rao, A. Starr, S. Zhang, F.E. Spada, F.T. Parker, A. Hutten, G.J. Thomas, J. Appl. Phys. 73 (1993) 5320.
[3] A.J. Fagan, M. Viret, J.M.D. Coey, J. Phys. Condens. Mat. 7 (1995) 8953.
[4] J.Q. Wang, G. Xiao, Phys. Rev. B 49 (1994) 3982.
[5] S.S.P. Parkin, R.F.C. Farrow, T.A. Rabedeau, R.F. Marks, G.R. Harp, Q.H. Lam, M. Toney, R. Savoy, R. Geiss, Euro. Phys. Lett. 22 (1993) 455.
[6] J.Q. Xiao, J.S. Jiang, C.L. Chien, Phys. Rev. B 46 (1992) 9266.
[7] J.Q. Wang, E. Price, G. Xiao, J. Appl. Phys. 75 (1994) 6903.
[8] H. Zaman, A. Yamada, H. Fukuda, J. Ueda, J. Electrochem. Soc. 145 (1998) 565.
[9] S. Kenane, E. Chainet, B. Nguyen, A. Kadri, N. Benbrahim, J. Voiron, Electrochem. Commun. 4 (2002) 167.
[10] E. Gomez, J. Garcia-Torres, E. Valles, J. Electroanal. Chem. 615 (2008) 213.
[11] M. Alper, K. Attenborough, R. Hart, S.J. Lane, D.S. Lashomre, C. Younes, W. Schwarzacher, Appl. Phys. Lett. 63 (1993) 2144.
[12] K.D. Bird, M. Schlesinger, J. Electrochem. Soc. 142 (1995) L65.
[13] E. Gómez, J. Garcia-Torres, E. Vallés, Anal. Chim. Acta 602 (2007) 187.
[14] J. Garcia-Torres, E. Gómez, X. Alcobé, E. Vallés, Cryst. Growth Des. 9 (4) (2009) 1671.
[15] B. Hugh (Ed.), Alloy Phase Diagram ASM Handbook, vol. 3, ASM International, Ohio, 1992.
[16] E. Gómez, A. Labarta, A. Llorente, E. Vallés, J. Electrochem. Soc. 151 (2004) 731.

4.4. Film's optimization process and giant magnetoresistance

Preliminary magnetoresistance measurements performed onto the Co-Ag films obtained from the previously developed bath revealed no changes in the electrical resistance with the applied magnetic field at room temperature. However, by decreasing the measurement temperature down to 40 K magnetoresistance values up to 0.1 % could be measured. At this point, two questions were raised: Does the high roughness detected in the films exert any negative effect on the magnetotransport properties? or Is the presence of sulphur the responsible for such low GMR values measured? Based on the influence of roughness and impurities on the electrical resistance of thin films [107,108], it was decided to investigate the possible influence of both factors on the film properties.

The use of the developed bath at low temperatures led to obtain Co-Ag films with lower roughness. On the other hand, bath reformulation which mainly consisted on decreasing thiourea content allowed obtaining films with lower sulphur incorporation. Whereas roughness seemed to have no effect on the magnetoresistance of Co-Ag films; the diminution of sulphur content led obtaining films with higher giant magnetoresistance values but only at cryogenic temperatures. GMR values up to 0.5 % were measured at 40 K.

Due to the low GMR values measured, it was decided to further investigate sulphur influence over the properties of cobalt-silver films. The objective was to incorporate variable amounts of sulphur into the films to study the influence over the deposit's properties. In this case, the source of sulphur was sodium thiosulphate which is also a known complexing agent for silver. Small concentrations of sodium thiosulphate were enough to obtain variable content of sulphur into the deposit that allowed studying its influence over cobalt-silver film's properties. Important results can be drawn from this study.

Co-Ag nanocrystalline deposits with very low roughness values (of the order of a few hundreds of nanometers) were obtained from the thiosulphate bath. Sulphur content into the deposit amounted from 5 to 11 wt.%. Although the XRD patterns presented similar profiles for the Co-Ag coatings obtained at the different applied potentials, a variation in the magnetic properties was observed. H_c values were dependent on the applied deposition potential. The change in the potential was reflected in different deposition rates, grain sizes and variable cobalt and sulphur incorporation, factors that were responsible for the different magnetic behaviour observed.

The magnetotransport properties of the Co-Ag coatings were also investigated. No significant change in the electrical resistance with the applied magnetic field was recorded either at room temperature or at 40 K. From these results one could state that whereas sulphur was the main responsible for the GMR deterioration in the Co-

Ag granular films, film's roughness seemed no exerting any detrimental effect. It is at this point where the compositional analysis of pure silver, pure cobalt and Co-Ag deposits was very revealing: sulphur was partly dissolved in the cobalt lattice and partly placed in the magnetic/non-magnetic interface. As it has been previously explained, the magnetic/non-magnetic interface plays a central role in the magnetoresistive phenomenon of granular films. In this sense, the sulphur barrier place at this interface always behaves as a scattering centre for the electrons independently of their spin direction (spin-up or spin-down) and independently of the cobalt granules magnetization direction and the applied magnetic field. Therefore, no magnetoresistance is recorded as the electrons with spin-up and spin-down will experience the same resistance/scattering probability in all the applied magnetic fields (Figure 4.5).

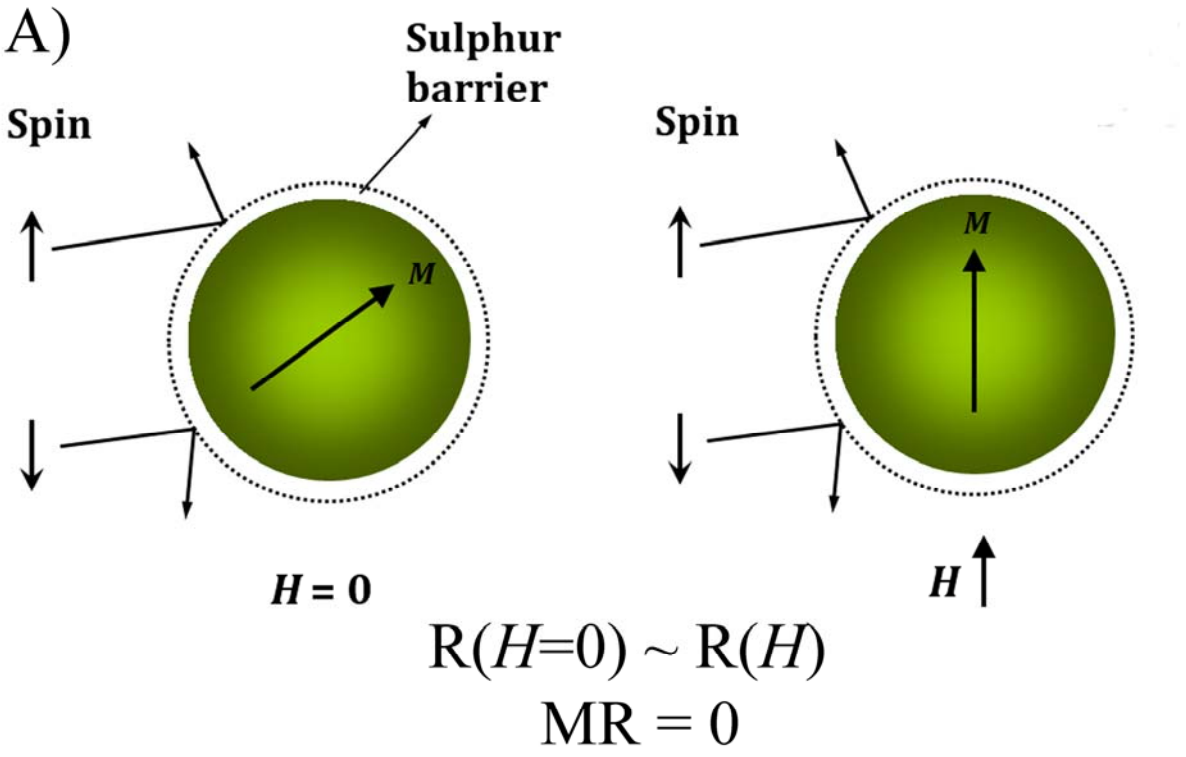

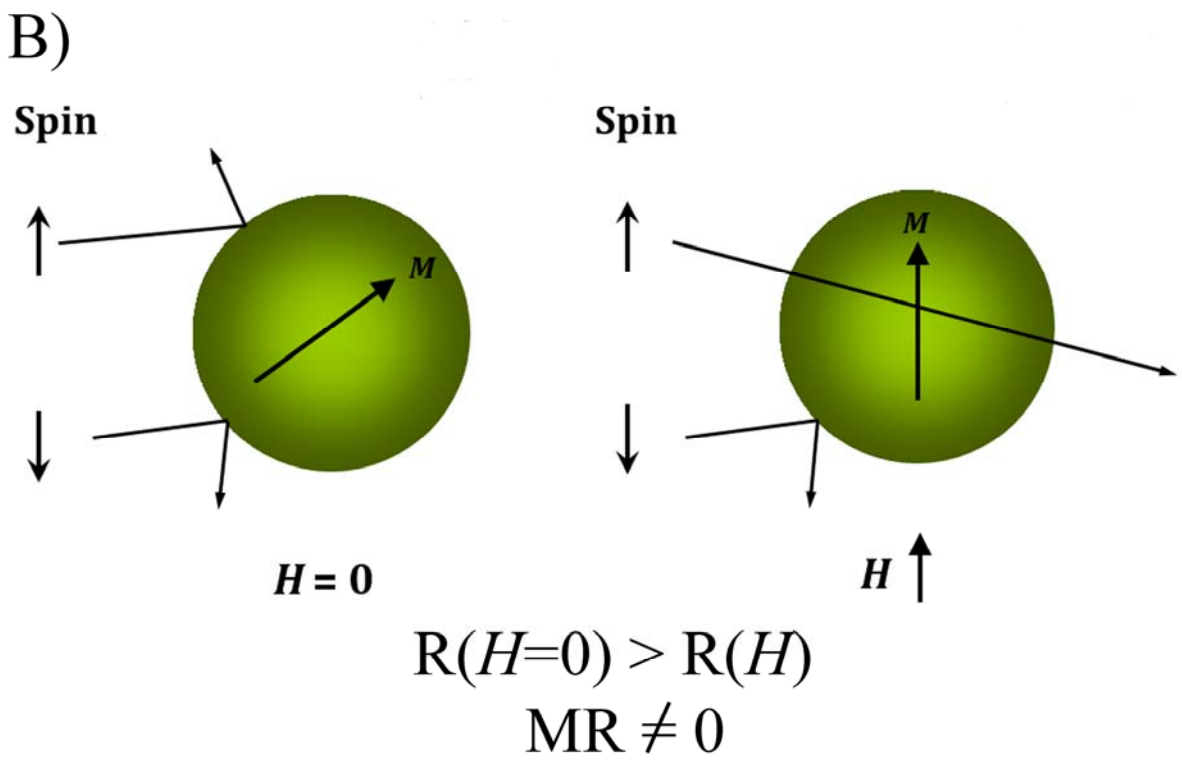

Figure 4.5. The scheme tries to represent the deleterious effect of sulphur on the magnetotransport properties. A) The presence of sulphur at the magnetic/non-magnetic interface always acts as a scattering centre for electrons independently of the electron spin direction, magnetization and applied magnetic field directions, which is detrimental for magnetoresistance. B) Magnetoresistance effect takes place if there is no "sulphur barrier" at the interface.

Group of articles included in section 4.4.

Page 131: Effect of bath temperature and bath composition on Co-Ag electrodeposition

Jose Garcia-Torres, Elisa Vallés and Elvira Gómez, Submitted.

Page 145: Modification of magnetic and structural properties of Co and Co-Ag electrodeposits by sulphur incorporation

Jose Garcia-Torres, Elvira Gómez and Elisa Vallés, Accepted in Materials Chemistry and Physics. DOI 10.1016/jmatchemphys.2010.03.027.

Effect of bath temperature and bath composition on Co-Ag electrodeposition

Submitted

Influence of bath temperature and bath composition on Co-Ag electrodeposition

J. García-Torres, E. Vallés, E. Gómez*
Electrodep, Departament de Química Física i Institut de Nanociència i Nanotecnologia (IN^{2}UB), Universitat de Barcelona, c/ Martí i Franquès, 1. 08028 Barcelona (Spain)

Keywords:
Co-Ag thin films
Electrodeposition
roughness
sulphur impurities

A B S T R A C T

A study of the best conditions to prepare smooth heterogeneous micrometric Co-Ag films with low amounts of S from a thiourea-based electrolytic bath has been performed. Using a 0.01 M $AgClO_4$ + 0.1 M $Co(ClO_4)_2$ + 0.1 M thiourea + 0.1 M sodium gluconate + 0.3 M H_3BO_3 + 0.1 M $NaClO_4$ bath, low temperature (10ºC) allowed obtaining compact and smooth deposits containing 2 wt.% sulphur. Decreasing thiourea content down to 0.06 M and increasing gluconate concentration up to 0.3 M, better deposits (more compact with lower sulphur content (1.2 wt.%)) were obtained. A clear influence of the species present in the bath on the film quality was observed: while gluconate favoured film cohesion, boric acid hindered hydrogen adsorption. For all films, fcc-Ag, hcp-$CoAg_3$ and hcp-Co phases were always detected by XRD, TEM and electron diffraction, their proportions varying with the electrodeposition conditions. Magnetic measurements revealed that the increase in the $CoAg_3$ led to an increase in the film coercivity. GMR values were only measured at cryogenic temperatures, they being higher for the deposits with the lowest sulphur content.

1. Introduction

Thin films of nanometer thickness can nowadays be routinely fabricated by electrodeposition [1,2]. This method has been revealed as a successful one to produce films with real technological applications [3,4]. The possibility to incorporate such materials in certain devices is due to both the high quality of the electrodeposited materials and the advantages of electrodeposition (cost effectiveness, ease of processability, large area deposition or relatively low temperature) opposite to the physical methods usually employed.

Granular films of certain binary or ternary systems (i.e. Co-Cu, Co-Ag, Fe-Ag, Co-Ni-Cu) are interesting from the point of view of their magnetotransport properties [5,6]. Among those systems, Co-Ag is one with the highest GMR values reported [7,8] due to the total immiscibility observed in the phase diagram [9]. It allows obtaining granular films with sharp magnetic/non-magnetic interfaces which is a characteristic required to obtain GMR.

In this sense, the preparation of Co-Ag films by means of electrodeposition was proposed in our laboratory. An electrolytic thiourea (TU)-based bath with [TU]:[Ag+] = 10:1 ratio was previously developed [10] in order to approach the deposition of both metals, delaying silver deposition process to more negative potentials. Sodium gluconate and boric acid were incorporated in the bath in order to improve the deposit's quality. The prepared deposits presented granular morphology and high roughness. Film's composition was somewhat difficult to control as cobalt incorporation greatly varied in a narrow potential range. Moreover, the incorporation of sulphur into the deposit was quantified as 2 wt.%. However, and in spite of the immiscibility deduced from the phase diagram, a metastable Co-Ag phase (CoAg3) was detected in the as-prepared films [11]. Upon annealing the metastable phase at elevated temperatures phase segregation took place.

No sign of giant magnetoresistance at room temperature was detected in the Co-Ag films either in the as-deposited state or after the annealing. However, magnetoresistance was measured at low temperatures. Keeping in mind the deleterious effect of film's roughness or impurities on the electrical resistance [12,13], and hence the detrimental effect that they could exert on the magnetotransport properties, the effect of roughness and impurities on the magnetoresistance was investigated. Bath temperature and bath composition were modified in order to achieve this objective. Structural and magnetic properties of the obtained deposits were also analyzed as a function of the modified variables.

2. Experimental

Chemicals used were $AgClO_4$, $Co(ClO_4)_2$, thiourea (CSN_2H_4), sodium gluconate ($C_6H_{11}NaO_7$), H_3BO_3 and $NaClO_4$, all of

analytical grade. All solutions were freshly prepared with water first doubly distilled and then treated with a Millipore Milli-Q system. pH was adjusted to 3.7 by adding $HClO_4$. Before and during experiments, solutions were de-aerated with argon. Temperature was kept at 25 ºC except when the temperature influence was studied.

Electrochemical experiments were carried out in a conventional three-electrode cell using an Autolab with PGSTAT30 equipment and GPES software. Working electrodes were vitreous carbon (Metrohm) and silicon seed layers supplied by IMB-CNM with either Ti/Ni (Si/Ti(100nm)/Ni(50nm)) or Cr/Cu (Si/Cr(5nm)/Cu(20nm) layers. Vitreous carbon electrode was polished to a mirror finish using alumina of different grades (3.75 and 1.87 μm) and cleaned ultrasonically for 2 min in water. Si/seed layer electrodes were firstly cleaned with acetone followed by ethanol and later with water. The counter electrode was a platinum spiral. The reference electrode was an Ag|AgCl|NaCl 1 M mounted in a Luggin capillary containing 0.2 M $NaClO_4$ solution. All potentials refer to this electrode.

Voltammetric experiments were carried out at 50 mV s^{-1}, scanning at first toward negative potentials. Cyclic voltammetries were recorded at quiescent conditions in order to evaluate mass transfer effect. Only one cycle was run in each voltammetric experiment. Deposits were prepared potentiostatically over Si/seed layer substrates under agitation with magnetic stirring (ω = 800 rpm).

Deposit's morphology was observed using Hitachi S 2300 scanning electron microscope. Elemental composition was determined with an X-ray analyser incorporated in Leica Stereoscan S-360 equipment. Structure of deposits was studied by means of X-ray powder diffraction (XRD) using a conventional Bragg-Brentano diffractometer Siemens D-500. The Cu Kα radiation (λ= 1.5418 Å) was selected by means of a diffracted beam curved graphite monochromator. X-Ray powder diffraction diagrams were obtained in the 20-100 º2θ range with a step range of 0.05º and a measuring time of 30 seconds per step. The structure was also studied by transmission electron microscopy (TEM) and high resolution transmission electron microscopy (HR-TEM) combined with selected area electron diffraction (SAED) and fast fourier transform (FFT) using a JEOL 2100.

Magnetic measurements were taken in a SQUID magnetometer at room temperature in helium atmosphere. The magnetization-magnetic field curves were recorded maintaining the samples parallel to the applied magnetic field. The magnetoresistance (MR) measurements were performed in deposits prepared over Si/Cr(5nm)/Cu(20nm at room temperature and at 40 K with the four-point-in-line method in magnetic fields between –8 kOe and +8 kOe in the field-in-plane/current-in-plane geometry. Only the longitudinal magnetoresistance (LMR) (field parallel to current) component was recorded for each sample. The magnetoresistance was defined as follows:

$$MR(H) = 100*[R(H)-R(0)]/R(0)$$

where R(*H*) is the resistance in the magnetic field *H* and R(0) is the resistance when *H*=0.

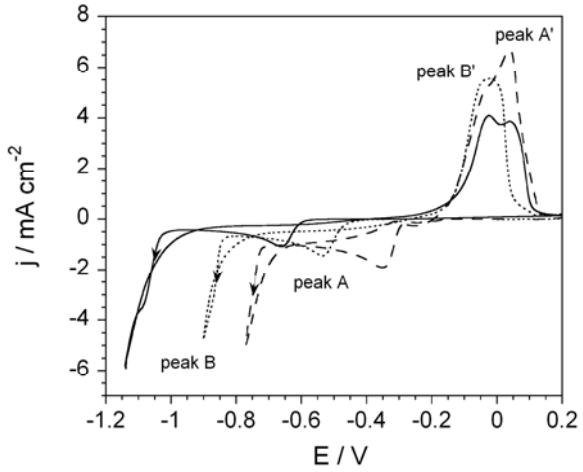

Figure 1. Cyclic voltammograms recorded from *Bath 1* at different temperatures. Dashed line) 60 ºC, dotted line) 30 ºC and continuous line) 5 ºC. Vitreous carbon electrode.

3. Results and discussion

3.1.- Influence of temperature

Temperature influence on the deposition process was studied for the previous developed bath (0.01 M $AgClO_4$ + 0.1 M $Co(ClO_4)_2$ + 0.1 M thiourea + 0.1 M sodium gluconate + 0.3 M H_3BO_3 + 0.1 M $NaClO_4$) (*Bath 1*) [10]. Similar voltammetric behaviour was observed for all temperatures (Fig.1): two reductions peaks prior to hydrogen evolution were recorded during the negative scan being attributed to silver (peak A) and cobalt reduction (peak B). Moreover, a double oxidation peak (peak A' and B') was recorded during the positive-going sweep where the partial contribution of each metal was distinguishable. The couple A/A' is related to silver deposition/oxidation, respectively and peak B' was related with the oxidation of the deposit formed in peak B [10]. The temperature increment led to, as it was expected, an advance in all the reduction processes during the negative-going scan i.e. silver and cobalt deposition as well as hydrogen evolution. On the other hand, the higher the temperature the higher the reduction charge associated with silver, this is because silver

reduction is a mass control process [10] and an important increment in the diffusion coefficient of silver species with temperature took place.

A set of deposits were prepared potentiostatically at different temperatures and at different growth rates for each temperature with the objective to compare composition and morphology. Temperature ranged from 10 to 60 ºC (bath chemical instability was observed at 5 ºC after a short time of deposition). According to the voltammetric results silver incorporation into the films will be higher and higher as temperature rises. Therefore, higher overpotentials were needed to be applied as temperature rose in order to have the same composition at the different temperatures but with the subsequent risk to favour hydrogen evolution. Moreover, it is important to highlight that the dependence of film's cobalt composition on applied potential shows a decrease with decreasing temperature, thus making more easily to control the cobalt percentage into the deposit at low temperatures (Table 1). Sulphur incorporation was similar to that previously obtained at room temperature (around 2 wt.%) [14].

Table 1. Film's composition-applied potential dependence for deposits obtained from *Bath 1* at 10 ºC.

T = 10 ºC							
E / mV	-840	-870	-900	-930	-950	-970	-1000
wt.% Co	20.0	23.0	25.0	26.5	28.0	31.5	35.0

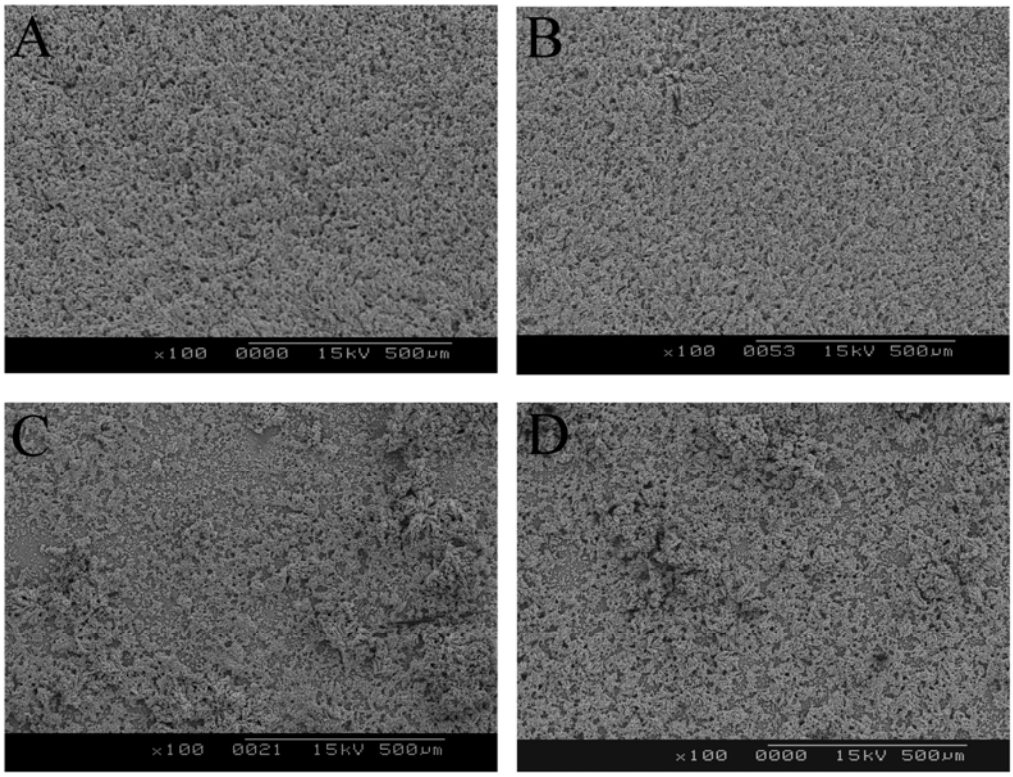

Figure 2. SEM micrographs of Co-Ag deposits obtained from *Bath 1* at different temperatures and applied potentials (A) 10 ºC, E = -950 mV, (B) 10 ºC, E = -1025 mV, (C) 40 ºC, E = -750 mV and (D) 25 ºC, E = -800 mV.

Morphological analysis revealed that the films prepared at low temperatures (10-15ºC) were granular and compact (Fig. 2A). Non-cracked films with a complete and uniform coverage were obtained in all the conditions. Moreover, the deposits kept also the observed compactness even at the more negative applied potentials (Fig. 2B). However, high temperatures exerted a detrimental effect over the deposit quality, leading to films with high roughness and low packing density (Fig. 2C and 2D) being hydrogen evolution responsible for the poor quality of the deposits.

The structural characterization by XRD of Co-Ag deposits prepared in the 10-60 ºC temperature range indicated the presence of fcc-silver and a metastable hcp-$CoAg_3$ phase previously detected [11] (Fig. 3A). The proportion of the $CoAg_3$ phase was higher when the deposits were prepared at low deposition rates (at the lowest temperatures and at the

more positive potentials) (Fig. 3A, curve a). As a consequence, when either the temperature was higher or the potential, for a same temperature, more negative, the proportion of the metastable phase decreased (Fig. 3A, curves b and c). Figure 3B,C shows enlarged regions of the diffractogram for better comparison. No relevant influence of the temperature on the peak width and hence on the grain size was observed.

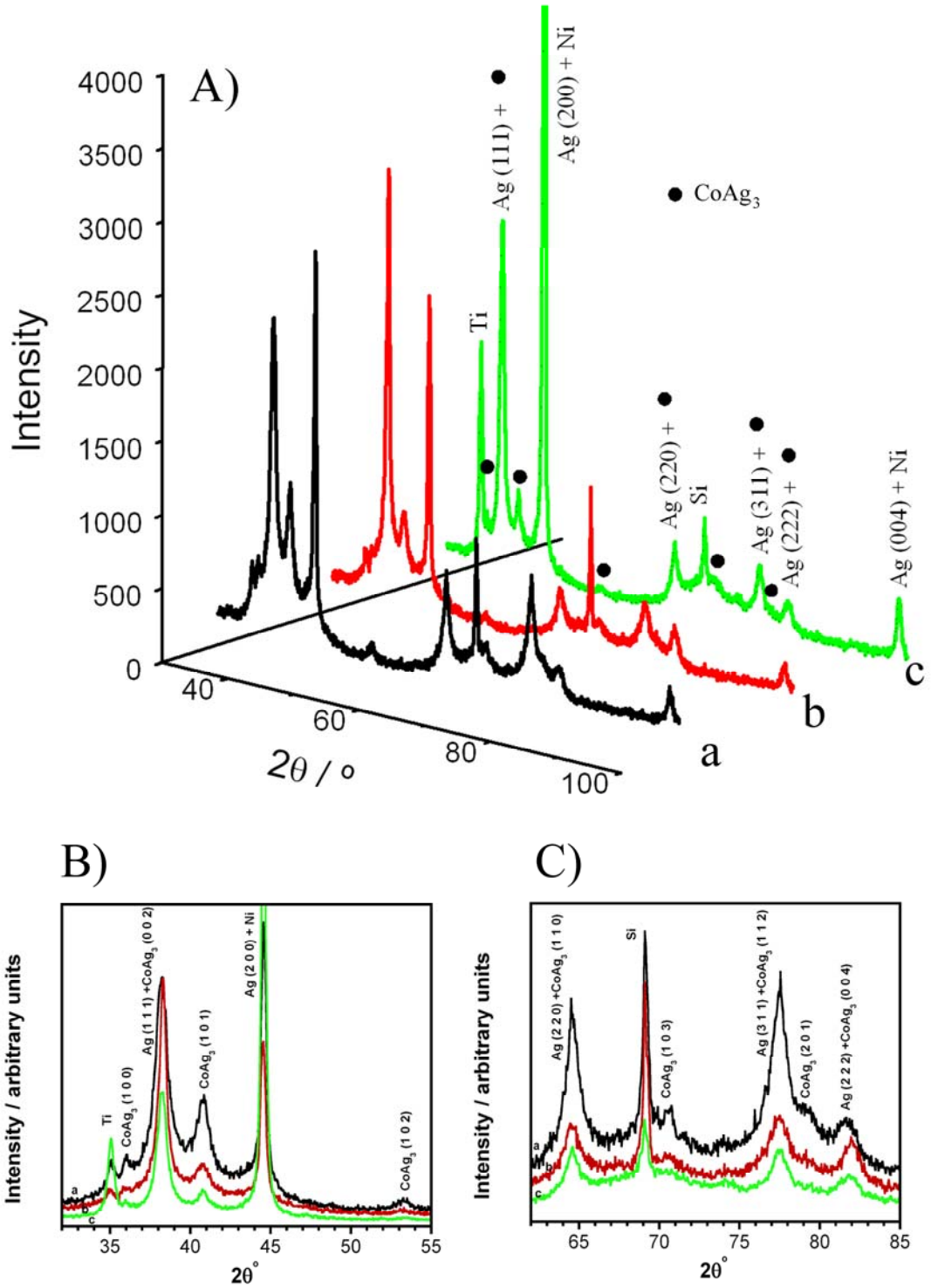

Figure 3. A) XRD pattern of Co-Ag deposits obtained form *Bath 1* at different temperatures and applied potentials. (a) 10 ºC, E = -840 mV, 20 wt.% Co, (b) 10 ºC, E = -970 mV, 31.5 wt.% Co and (c) 40 ºC, E = -800 mV, 33 wt.% Co. B and C) enlargement of two regions of the pattern.

On the other hand, TEM analyses together with selected area electron diffraction (SAED) confirmed the presence of fcc-silver and hcp-$CoAg_3$ but also allowed detecting hcp-Co (Fig. 4A,B): Table 2 gives the indices of the corresponding diffraction rings. The dependence of the $CoAg_3$ content on the electrodeposition conditions was also corroborated when HRTEM and fast fourier transform (FFT) studies were performed (Fig. 4C,D). $CoAg_3$ phase was more easily detected in deposits prepared at low deposition rates (Fig. 4C) than at higher ones (Fig. 4D), as the FFT patterns show.

The differences previously observed on the phase proportion were reflected on the magnetic response of the as-deposited films in which an increase in film coercivity (H_c) with the increase in the $CoAg_3$ phase presence was observed (Fig. 5). It is well-known that the coercivity of magnetic materials depends on different parameters such as grain size, crystalline structure or nonmagnetic inclusions [15] but also on the magnetic anisotropy constants [16]. In the samples reported here, the former parameters were not modified with temperature variation as XRD and compositional analysis revealed (only phase proportion varied). Therefore, magnetic anisotropy seems to be the main responsible for the observed increase in H_c. On one hand, the increase in the hcp-Co lattice constants (a = 2.5054 Å and c = 4.0893 Å [PDF # 89-4308]) when silver replaced some of the cobalt atoms (that is, the hcp-$CoAg_3$ phase, a = 2.887 Å and c = 4.745 Å [11]) suggests that the magnetoelastic anisotropy of the $CoAg_3$ phase is higher. On the other hand, silver presence could enlarge the magnetocrystalline anisotropy of $CoAg_3$ phase. It is also believed that the higher the $CoAg_3$ phase presence is, the smaller the number of cobalt particles is, what makes magnetic interaction among cobalt particles difficult, thus also favouring the H_c increase. Low saturation magnetisations (M_s) were obtained which could be attributed to the moderate film's cobalt percentage and the sulphur presence as it has been previously observed [15]. M_s was dependent on film's cobalt percentage, increasing it with increasing cobalt content (Fig. 5, dashed line and dotted line), as expected.

Magnetotransport properties of Co-Ag films prepared at 10 ºC were measured as they are the most compact deposits obtained. Yet, no change in the electrical resistance with applied magnetic field was detected at room temperature either in the as-deposited state or after an annealing which was made in order to promote $CoAg_3$ metastable phase decomposition. Giant magnetoresistance was only obtained at 40 K, but the measured values (around 0.2 %) were practically the same than those obtained in deposits prepared at 25 ºC. The packing density/roughness of the deposits does not seem to be the main responsible of the lack of MR at room temperature. For this reason, the reformulation of *Bath 1* was proposed in order to decrease the impurity content into the film and to study its influence on the magnetoresistance.

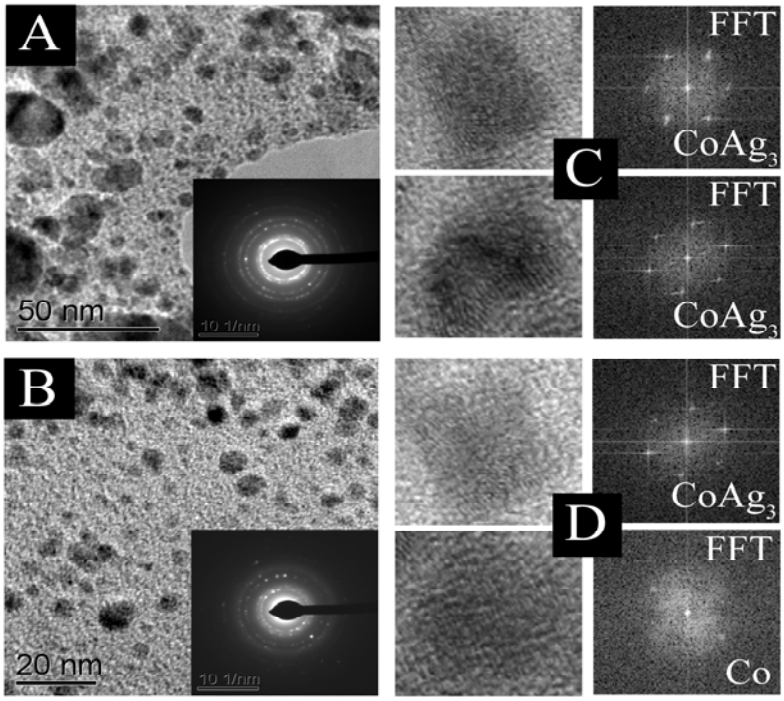

Figure 4. TEM images and SAED patterns of Co-Ag deposits prepared at 10 ºC but different applied potentials A) -840 mV and B) -970 mV. C,D) HRTEM images and corresponding FFT patterns of previous samples.

Table 2. Comparison between Distances measured from the SAED patterns and tabulated data of JCPDS-International Centre for Diffraction Data (*) for the as-deposited samples.

Measured d(Å)	fcc-Ag d*(Å) (hkl)	hcp-$CoAg_3$ d*(Å) (hkl)	hcp-Co d*(Å) (hkl)
2.513		2.500 (100)	
2.353	2.3587 (111)		
		2.337 (002)	
2.196		2.205 (101)	
			2.1697 (100)
			2.0446 (002)
	2.0427 (200)		
1.906			1.9166 (101)
1.531			1.4880 (102)
	1.4444 (220)		
			1.2527 (110)
	1.2318 (311)		
	1.1793 (222)		
			1.1542 (103)

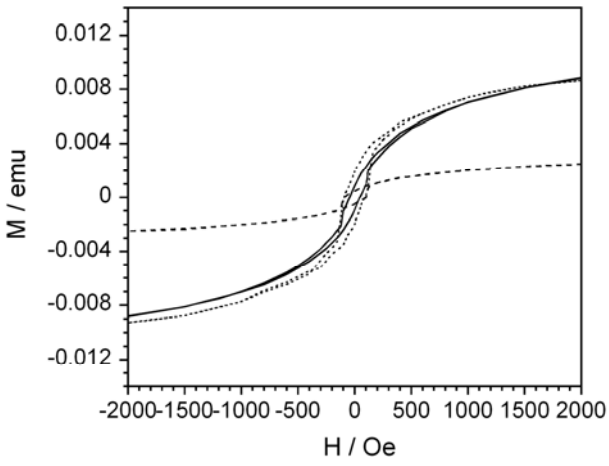

Figure 5. Magnetization curves of the Co-Ag deposits obtained from *Bath 1* at different temperatures and applied potentials. Dashed line) 10 ºC, E = -840 mV, 20 wt.% Co, dotted line) 10 ºC, E = -970 mV, 31.5 wt.% Co and continuous line) 40 ºC, E = -800 mV, 33 wt.% Co.

3.2 Bath reformulation

3.2.1 Decrease in thiourea content

At first, the diminution of thiourea content in the solution was considered with the objective to decrease sulphur incorporation. Solutions containing different thiourea (TU) concentrations in the range 0.04-0.08 M were prepared, keeping the concentration of the rest of Bath 1 components constant. All the solutions presented similar voltammetric behaviour (Fig. 6). However, by decreasing thiourea concentration an advance in both silver reduction and, in less extension, in cobalt deposition was observed. The difference in the deposition potential of both metals was higher and higher and the charge recorded under silver reduction peak increased as thiourea concentration decreased, these differences being attributed to a higher proportion of uncomplexed silver when TU concentration decreased.

Co-Ag deposits show granular morphology in all conditions tested of potential, growth rate and thiourea concentrations (Fig. 7A). A common characteristic of the deposits was the lack of cohesion and the non-homogeneous coverage of the electrode surface. The reduction of TU concentration down to 0.04 M was discarded not only due to the dendritic growth observed (Fig. 7B) but also because of the precipitation process observed during deposition. According to those results, [TU] = 0.06 M was selected as the minimum concentration feasible to prepare Co-Ag films. Regarding sulphur content in the deposits, a decrease of 0.8 wt.% was observed when thiourea was reduced 40 % in the bath composition.

The lesser compactness observed in the deposits prepared from the solution containing 0.06 M thiourea forces to optimize the concentration of both sodium gluconate and boric acid in the electrolyte. The effect of the concentration of these species over the film's properties (electrochemical, morphological, structural and magnetic properties) was also analyzed.

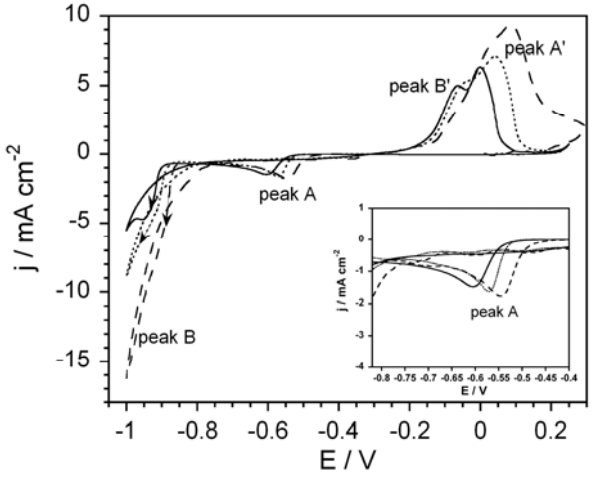

Figure 6. Cyclic voltammograms recorded from *Bath 1* but different TU concentrations. Continuous line) 0.1 M, dotted line) 0.08 M and dashed line) 0.04 M. Inset shows a magnification of peak A. Vitreous carbon electrode.

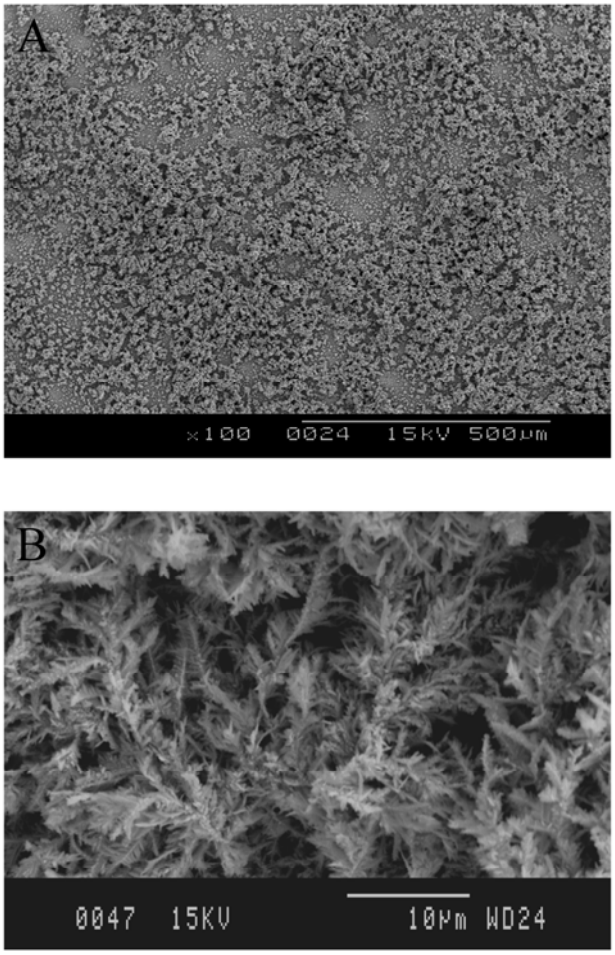

Figure 7. Scanning electron micrographs of Co-Ag deposits prepared from Bath 1 but different TU concentrations. (A) 0.06 M and (B) 0.04 M. Q = -13 C cm-2.

3.2.2 Influence of sodium gluconate

Solutions with sodium gluconate concentration in the range from 0.06 M to 0.7 M and the concentration of the other species constant were prepared. Gluconate concentration increase slightly delays silver deposition process toward more negative potentials and reduces the involved charge under silver reduction peak due to silver-gluconate complex formation (Fig. 8). In the same way, the higher the gluconate concentration the more negative the cobalt deposition potential onset is. The ratio $j_{peak\ A'}/j_{peak\ B'}$ (where j is the current density) diminished as the gluconate concentration increased.

Sets of deposits were prepared at the same growth rate but from solutions containing different gluconate concentrations. The recorded j-t transients always showed a monotonic current increase with deposition time (Fig. 9A). Different growth rates were tested in order to evaluate its influence over deposit's quality. In all conditions deposits showed granular morphology. The increase in gluconate concentration reduces roughness and increases compactness making films more uniform (Fig. 9B-D). However, incipient cracks were detected in the deposits obtained from baths with gluconate concentrations higher than 0.5 M, they being more evident as growth rate increased.

The dependence of the cobalt percentage on the applied potential shows a decrease with increasing sodium gluconate content in the bath (Table 3). The cited dependence shows an increase as the applied potential is made more negative. On the other hand, cobalt percentage is less sensitive to the applied potential than in those deposits obtained from *Bath 1* [10].

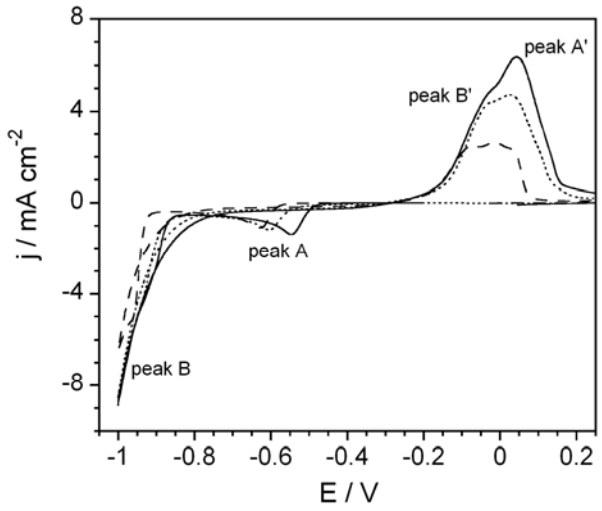

Figure 8. Cyclic voltammograms recorded from the solution 0.01 M $AgClO_4$ + 0.1 M $Co(ClO_4)_2$ + 0.06 M thiourea + x M sodium gluconate + 0.3 M H_3BO_3 + 0.1 M $NaClO_4$. Continuous line) x = 0.06 M, dotted line) x = 0.2 M and dashed line) x = 0.7 M. Vitreous carbon electrode.

Table 3. Film's composition-applied potential dependence for deposits obtained from 0.01 M $AgClO_4$ + 0.1 M $Co(ClO_4)_2$ + 0.06 M thiourea + x M gluconate + 0.3 M H_3BO_3 + 0.1 M $NaClO_4$ solution with different gluconate concentrations (x) and comparison with the results from Ref. [10].

x = 0.3M		x = 0.7M		*Bath 1* [10]	
E / mV	wt.% Co	E / mV	wt.% Co	E / mV	wt.% Co
-710	8.5	-780	13.0	-770	11.0
-740	19.0	-800	16.0	-790	25.0
-770	29.0	-830	22.5	-800	33.0
-790	35.0	-850	31.0	-810	46.0
-810	45.0	-870	39.0	-830	56.0

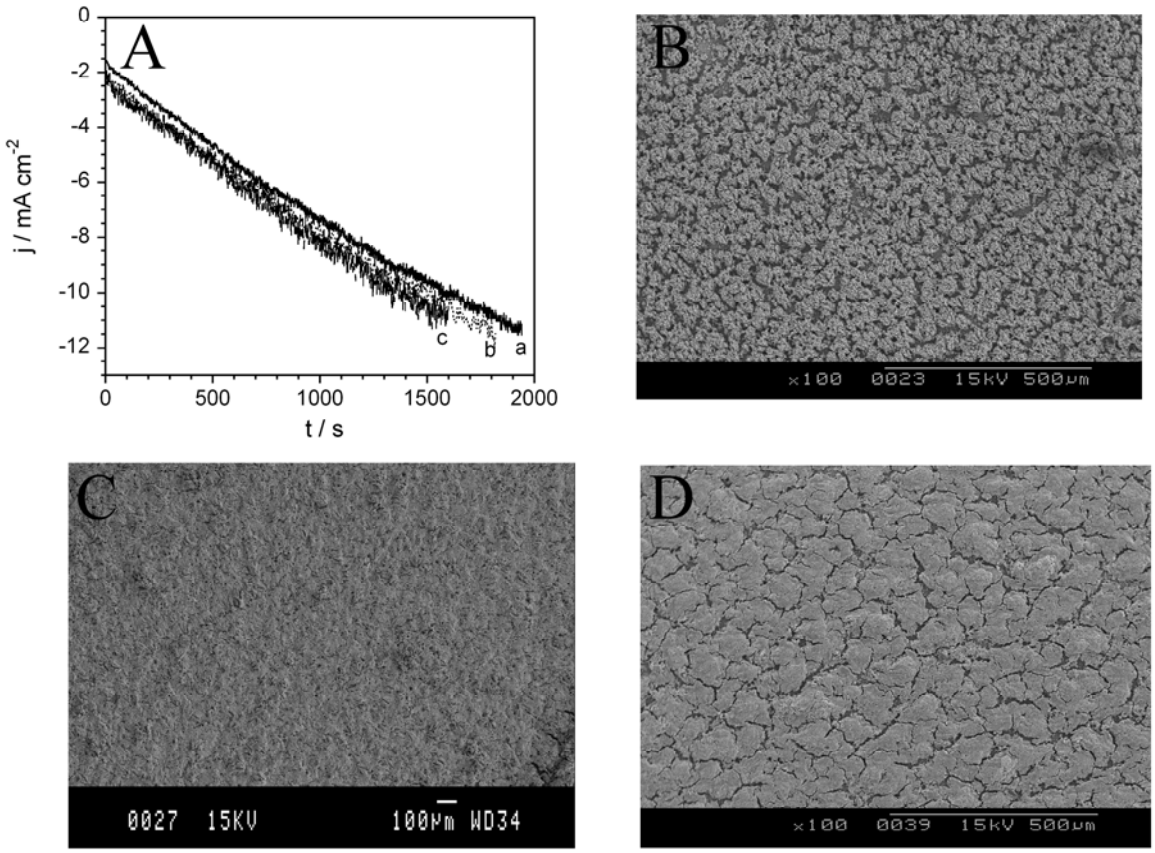

Figure 9. From the solution 0.01 M $AgClO_4$ + 0.1 M $Co(ClO_4)_2$ + 0.06 M thiourea + x M sodium gluconate + 0.3 M H_3BO_3 + 0.1 M $NaClO_4$. (A) j-t transients, (a) x = 0.1 M, (b) x = 0.3 M and (c) x = 0.7 M. SEM micrographs of deposits obtained at the same growth rate, (B) x = 0.1 M, (C) x = 0.3 M and (D) x = 0.7 M. Q = -13 C cm^{-2}.

The structural characterization by XRD of Co-Ag deposits evidenced the same phases previously described (Fig. 10). No significant differences were observed among the X-ray patterns, just a slight decrease in the $CoAg_3$ phase peak intensity as gluconate concentration increased. On the other hand, wide peaks were observed probably attributed to the presence of stress. The similarity in the kind of deposit obtained was also observed in the *M-H* loops as similar H_c values were measured. Deposits of 35 wt.% Co showed a coercivity of around 90 Oe and again low saturation magnetisation.

3.2.3 Influence of boric acid

The influence of boric acid was studied from the bath: 0.01 M $AgClO_4$ + 0.1 M $Co(ClO_4)_2$ + 0.06 M thiourea + 0.7 M gluconate + x M H_3BO_3 + 0.1 M $NaClO_4$. The highest gluconate concentration tested was selected because of the flattest deposits were obtained, as the manner that the

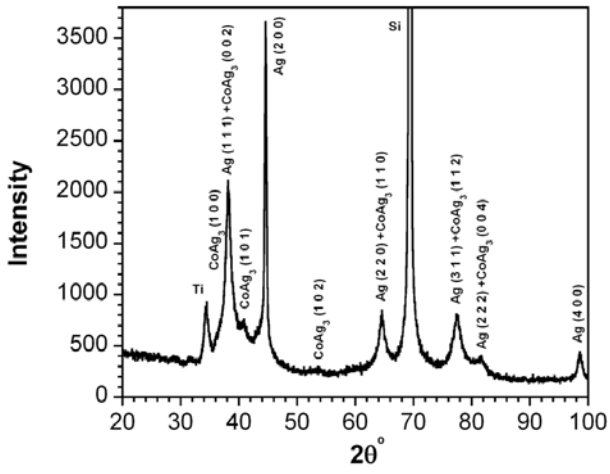

Figure 10. XRD pattern of Co-Ag deposits obtained form 0.01 M $AgClO_4$ + 0.1 M $Co(ClO_4)_2$ + 0.06 M thiourea + 0.7 M sodium gluconate + 0.3 M H_3BO_3 + 0.1 M $NaClO_4$ solution. Q = -13 C cm^{-2}. 35 wt. % Co.

morphological effect of boric acid could be more easily detected. Boric acid concentration in the bath was varied in the range from 0 M to 0.3 M as higher concentrations led to solubility problems.

The effect of boric acid presence in the voltammetric profile was to slightly delay the onset of both silver and cobalt reduction processes toward negative potentials however, successive additions of boric acid did not affect significantly the initio of the deposition (Fig. 11). No effect over silver reduction charge was detected. Nevertheless, important differences were observed during the positive-going scan. Cyclic voltammograms recorded from free-boric acid solution revealed, prior to the oxidation peaks A' and B', a band centred around -375 mV related to the oxidation of hydrogen adsorbed during the negative scan. The current involved in this band decreased until disappearing when boric acid concentration reached 0.3 M (inset Fig. 11) clearly indicating that boric acid presence made hydrogen adsorption difficult.

The influence of boric acid was also detected in the j-t deposition transients recorded on both vitreous carbon and silicon/seed layer substrates. Although the transients recorded at the same potential from solutions with and without boric acid overlap at the beginning of the deposition (Fig. 12A), the curves recorded from solutions containing boric acid reached stationary values at shorter deposition times (Fig. 12A, curves b and c) as a consequence of the decrease in the hydrogen reaction-related current.

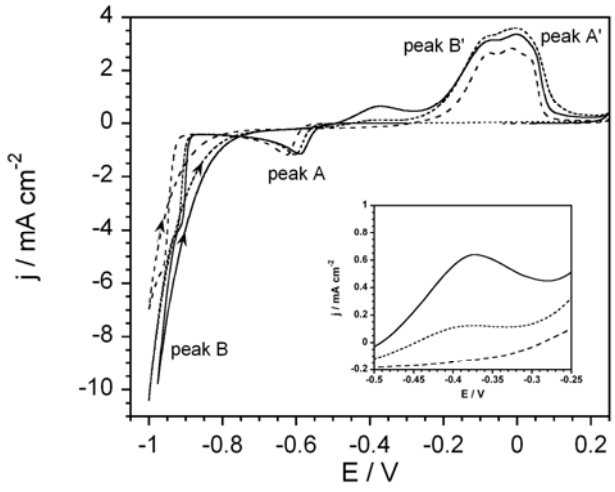

Figure 11. Cyclic voltammograms recorded from the solution 0.01 M $AgClO_4$ + 0.1 M $Co(ClO_4)_2$ + 0.06 M thiourea + 0.3 M sodium gluconate + x M H_3BO_3 + 0.1 M $NaClO_4$. Dashed line) x = 0.3 M, dotted line) x = 0.1 M and continuous line) x = 0 M. Vitreous carbon electrode.

Sets of deposits were prepared at different growth rates from solutions containing different H_3BO_3 concentrations. SEM micrographs of the deposits obtained from free-boric acid solutions corroborated the presence of hydrogen during electrodeposition. Voids due to non-detached bubbles during film growth were observed (Fig. 12B), its number was reduced when 0.1 M concentration in boric acid was present in the bath (Fig. 12C). Co-Ag films with no voids and uniform coverage were obtained from the solution containing 0.3 M in boric acid (Fig. 12D). For this reason, boric acid concentration was maintained at 0.3 M. Note that the cracks observed in the deposit of figure 12D are related to the stress effect (analyzed in section 3.2.2) due to the high gluconate concentration (0.7 M) which was selected in order to clearly evidence the effect of boric acid in this bath.

According to the previous results, the optimized composition for the new bath (*Bath 2*) was: 0.01 M $AgClO_4$ + 0.1 M $Co(ClO_4)_2$ + 0.06 M thiourea + 0.3 M gluconate + 0.3 M H_3BO_3 + 0.1 M $NaClO_4$. This bath allows obtaining Co-Ag films characterized by lower roughness and lower amounts of sulphur than those obtained from *Bath 1*.

Magnetotransport measurements of samples prepared at moderate growth rates showed GMR values up to 0.5 % at 40 K. These values are higher than those obtained when greater amounts of sulphur were present in the deposits. However and despite the reduction of sulphur into the films, no magnetoresistance was observed at room temperature. Two possible explanations are as follows. On one hand, the presence of sulphur reduces the ferromagnetic character of cobalt granules (as low saturation magnetization values have been measured). On the other hand, sulphur acts as scattering centres for the conduction electrons not only at zero magnetic field (*H*) but also with an applied *H*. It is widely known that the reduction in the electrical resistance with *H* (giant magnetoresistance) is due to the reduction in the scatterings number of electrons whose spin is parallel to the magnetization direction of the cobalt granules. However, the presence of sulphur may not allow this reduction in the scatterings number at high magnetic fields as it acts as a scattering centre independently of *H*. Both factors, which could take part simultaneously, are detrimental to the magnetoresistance effect, indicating that the presence of impurities as sulphur or the presence of the other species entrapped into the film, exert a negative effect on the magnetotransport properties.

4. Conclusions

Temperature significantly influences the deposits obtained from the previously developed *Bath 1*. The lower the

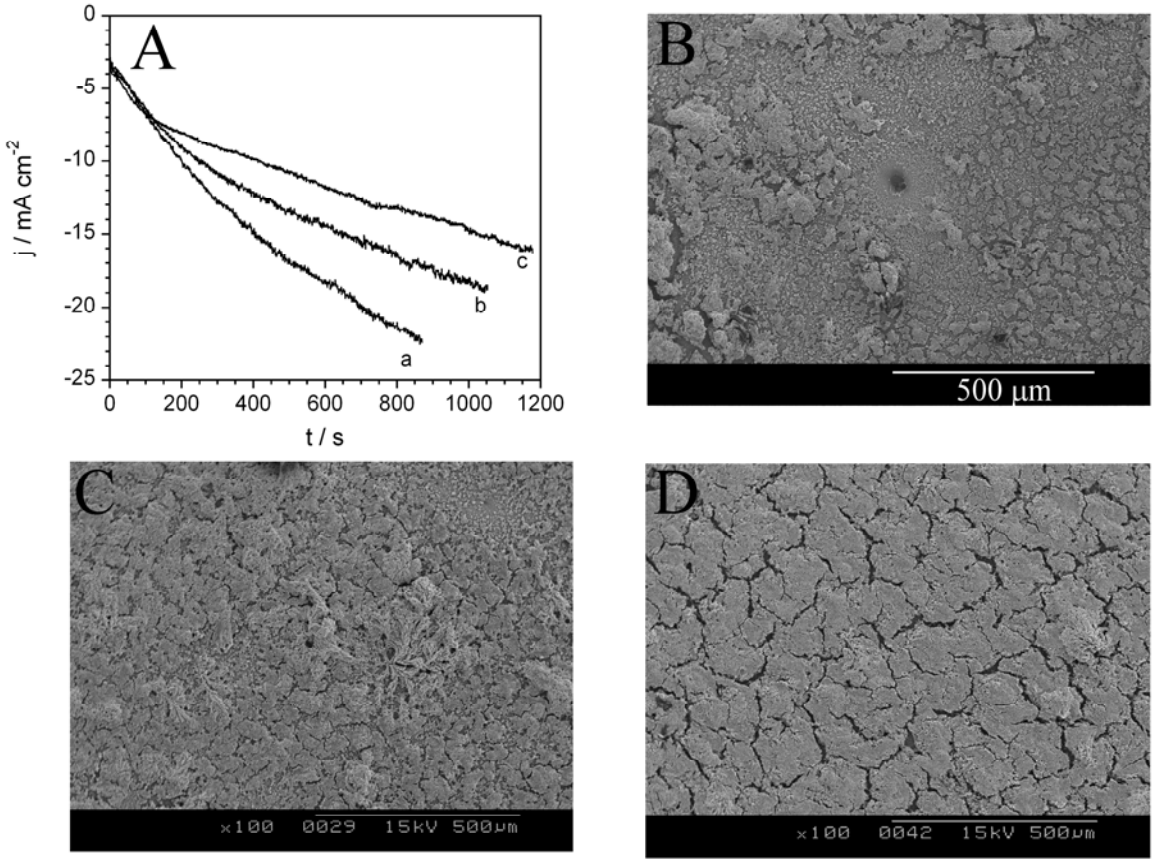

Figure 12. From the solution 0.01 M AgClO4 + 0.1 M Co(ClO4)2 + 0.06 M thiourea + 0.7 M sodium gluconate + x M H3BO3 + 0.1 M NaClO4. (A) j-t transients, (a) x = 0 M, (b) x = 0.1 M and (c) x = 0.3 M. SEM micrographs, (B) x = 0 M, (C) x = 0.1 M and (D) x = 0.3 M. Q = -13 C cm-2.

temperature is, the lower the roughness is and the better the grain-package is. A better control of the film composition was attained at 10 ºC as cobalt incorporation was less sensitive to the applied potential than at higher temperatures. Temperature does not affect the structure of these deposits but do the proportion of the phases which in turn was reflected on their magnetic behaviour. The Co-Ag films prepared at 10 ºC show GMR at low temperatures.

Bath reformulation, which consisted on decreasing TU concentration down to 0.06 M and increasing gluconate one up to 0.3M, also allowed preparing more compact deposits but with lower sulphur content (1.2 wt.%). The detailed study of the gluconate and boric acid effect on the deposition process evidenced the improvement of the packing density and compactness by gluconate presence and the minimization of hydrogen evolution by boric acid. Then, the new bath formulation (*Bath 2*) was 0.01 M $AgClO_4$ + 0.1 M $Co(ClO_4)_2$ + 0.06 M thiourea + 0.3 M gluconate + 0.3 M H_3BO_3 + 0.1 M $NaClO_4$. Film structure was not influenced by the species concentration in the bath. Although no magnetoresistance was observed at room temperature, GMR values measured at low temperature were double than those obtained from *Bath 1*. However, these values are even low to be used in any device.

From the results presented here, one can conclude that sulphur presence is the main detrimental factor for the magnetoresistance effect in our electrodeposited Co-Ag granular films. The mechanism responsible for the suppression of the magnetoresistance could be related to either the reduction of the ferromagnetic behaviour of the cobalt particles or the higher number of scattering centres due to sulphur presence. Thus, the need to employ free-additive electrolytes to prepare Co-Ag with GMR applications is demonstrated.

Acknowledgments

This paper was supported by contract MAT-2006-12913-C02-01 from the Comisión Interministerial de Ciencia y Tecnología

(CICYT). J. García-Torres also thanks the Departament d'Innovació, Universitats i Empresa of the Generalitat de Catalunya and Fons Social Europeu for financial support. The silicon based substrates preparation was supported by the programa de acceso a las ICTS (2009) MICINN NGG-105.

References

[1] Nano plating, Tohru Watanabe, Elsevier Ltd, Oxford, 2004
[2] C. Müller, M. Sarret, T. Andreu., J.Electrochem. Soc. 150(11) (2003) C772.
[3] S. Arana, N. Arana, F. J. Gracia and E. Castaño, Sensors and Actuators A 123-124 (2005) 116.
[4] C. Hierold , J. Micromech. Microeng. 14(2004)S1-S11
[5] A. E. Berkowitz, J. R. Michell, M. J. Carey, A. P. Young, D. Rao, A. Starr, S. Zhang, F. E. Spada, F. T. Parker, A. Hutten and G. Thomas, J. Appl. Phys. 73(10) (1993) 5320.
[6] W. Wang, F. Zhu, W. Lai, J-q.W, G. Yang, J. Zhu and Z. Zhang, J. Phys. D: Appl. Phys. 32 (1999) 1990.
[7] C. L. Chien, J. Q. Xiao and J. S. Jiang, J. Appl. Phys. 73(10) (1993) 5309.
[8] J. Q. Xiao, J. S. Jiang and C. L. Chien, IEEE Trans. Magn. 29(6) (1993) 2688.
[9] Alloy phase diagram in: Hugh Barker (Eds), ASM Handbook, vol 3. ASM International. Ohio 1992.
[10] E. Gómez, J. Garcia-Torres, E. Vallés, Anal. Chim. Acta 602 (2007) 187.
[11] J. Garcia-Torres, E. Gómez, X. Alcobé, E. Vallés, Crystal Growth & Design 9(4) (2009) 1671.
[12] E. Chassaing, J. Electrochem. Soc. 148 (2001) C690
[13] U. Jacob, J. Vancea, H. Hoffman, Phys. Rev. E 41(17) (1990) 11852
[14] E. Gómez, J. Garcia-Torres, E. Vallés, J. Electroanal. Chem. 615 (2008) 213.
[15] J. Garcia-Torres, E- Gómez, E. Vallés, Accepted in Mater. Chem. Phys.
[16] Handbook of Magnetic Materials, K.H.J. Buschow, North Holland, Amsterdam, 1997.

Modification of magnetic and structural properties of Co and Co-Ag electrodeposits by sulphur incorporation

DOI 10.1016/j.matchemphys.2010.03.027

Accepted in Materials Chemistry and Physics

Modification of magnetic and structural properties of Co and Co-Ag electrodeposits by sulphur incorporation

J. García-Torres, E. Gómez, E. Vallés*

Electrodep, Departament de Química Física i Institut de Nanociència i Nanotecnologia (IN^{2}UB), Universitat de Barcelona, c/ Martí i Franquès, 1. 08028 Barcelona (Spain)

Keywords:
Magnetic thin films
Electrodeposition
Crystal structure
Magnetic properties

A B S T R A C T

The influence of sulphur incorporation during electrodeposition on the structural and magnetic properties of both Co and Co-Ag thin films from aqueous thiosulphate solutions has been investigated. Co-Ag deposits containing sulphur showed granular morphology and varying cobalt and sulphur contents as a function of the applied potential. Nanocrystalline soft-magnetic deposits whose coercivity decreased as sulphur incorporation increased were obtained. More influence of the sulphur presence on the cobalt thin film magnetic properties was observed due to the significant structural changes induced by sulphur incorporation into the crystalline lattice. When high amounts of S were present, soft-magnetic amorphous cobalt coatings were obtained. On the other hand, stronger hard-magnetic behaviour was detected on those crystalline thin films where S content was lesser.

1. Introduction

During the last few years, and still today, there is a long-standing interest in the magnetic properties of cobalt alloys [1,2]. Their magnetic properties are determined to large extent by their microstructure which in turn is influenced by the deposition technique and process variables. This is particularly true for electrodeposited cobalt [3] or cobalt-based alloys [4]. Both the modification of the electrodeposition conditions (applied potential, current density, temperature, pH) and the presence of additives in the plating-bath can induce different microstructures and hence different physical properties. However, the use of additives in the plating solutions results in the incorporation of different amounts of nonmagnetic interstitials and inclusions in the magnetic films [5-7], which can modify their physical properties. Sulphur is one of the most common elements present in the films due to the levelling and brightening effect of sulphur-containing additives. It is known that the presence of sulphur can change coercivity, anisotropy and structure of the Fe, Ni, Fe-Ni or Co-Fe films [8,9].

The Co-Ag system is an interesting one since it has been proposed as a potential giant magnetoresistive material [10]. There have been some attempts to fabricate Co-Ag granular films by means of electrodeposition [11-14]. Zaman *et al.* [11] used a sulphate based bath with sodium citrate addition to prepare Co-Ag films by current control. On the other hand, Kenane *et al.* [12,13] reported on the pulse electrodeposition from a bath containing $CoCl_2$, $AgNO_3$ and NaCl. The structural characterization in both cases revealed the fcc structure of cobalt. Moreover, the same magnetic behaviour was present: an evolution from superparamagnetism to ferromagnetism at higher cobalt percentages and associated to the different cobalt cluster size. However, different coercivity values were reported (around 200Oe [11] and 400Oe [12,13]). Lately, a perchlorate-based electrolyte has been developed and characterized in our laboratory [14]. Apart from the perchlorate components, a complexing agent (thiourea) and other additives (sodium gluconate and boric acid) were present in the bath. With this, different structures and different magnetic properties were obtained depending on the electrodeposition conditions. At certain combinations of deposition rate, temperature or bath composition, a $CoAg_3$ metastable phase was detected giving rise to coercivity values of the order of 115Oe. On the other hand, when this metastable phase was missing, H_C values of the order of 50Oe were observed. A low sulphur content (less than 2wt.%) was detected in the deposit due to the presence of thiourea in the bath.

Since not one of the previously mentioned papers studied the influence of inclusions on the physical properties of the deposits and keeping in mind the influence of sulphur over the magnetic properties of thin films, the aim of the present study is to analyze the influence of sulphur in the morphology, crystalline structure, magnetic and magnetotransport properties of Co-Ag thin films. Moreover, the properties of Co and Ag coatings will also be studied for comparison purposes. The electrochemical behaviour was also studied.

2. Experimental

Solutions used for the electrodeposition of cobalt-silver coatings contained $AgClO_4$, $Co(ClO_4)_2$, $Na_2S_2O_3$ and $NaClO_4$, all of analytical grade. The solutions were freshly prepared with water first doubly distilled and then treated with a Millipore Milli-Q system. In the same way, silver and cobalt coatings were also prepared from solutions containing either $AgClO_4$ or $Co(ClO_4)_2$, $Na_2S_2O_3$ and $NaClO_4$. Before and during experiments solutions were de-aerated with argon. Temperature was kept constant at 25ºC.

Electrochemical experiments were carried out in a conventional three-electrode cell using an Autolab with PGSTAT30 equipment and GPES software. Working electrodes were vitreous carbon (Metrohm) and silicon with Ti/Ni seed layer (Si/Ti(100nm)/Ni(50nm)) supplied by IMB-CNM. Vitreous carbon electrode was polished to a mirror finish using alumina of different grades (3.75 and 1.87 μm) and cleaned ultrasonically for 2 min in water. Si/seed layer electrode was firstly cleaned with acetone followed by ethanol and later with water. The counter electrode was a platinum spiral. The reference electrode was an Ag|AgCl|NaCl 1M mounted in a Luggin capillary containing 0.2 M $NaClO_4$ solution. All potentials were referred to this electrode.

Voltammetric experiments were carried out at 50mV s^{-1}, scanning at first to negative potentials. Only one cycle was run in each voltammetric experiment. Deposits were obtained potentiostatically on Si/Ti(100nm)/Ni(50nm) under agitation with magnetic stirring.

The structure of the deposits was studied with X-ray powder diffraction (XRD) using a conventional Bragg-Brentano diffractometer Siemens D-500. The Cu Kα radiation (λ= 1.5418Å) was selected using a diffracted beam curved graphite monochromator. The X-ray powder diffraction diagrams were created in the 20-105º 2θ range with a step range of 0.05º and a measuring time of 15 seconds per step.

Deposit morphology was observed using Hitachi H-4100 FE field emission scanning electron microscope (FE-SEM). Elemental composition was determined with an X-ray analyser incorporated in Leica Stereoscan S-360 equipment. Thickness and roughness of the coatings were measured using a white-light interferometer from Zygo Corporation.

Magnetic measurements were taken in a SQUID magnetometer at room temperature in helium atmosphere. The magnetization-magnetic field curves were recorded maintaining the samples parallel to the applied magnetic field. The magnetoresistance (MR) was measured at 20K and at room temperature with the four-point-in-line method in magnetic fields between -8kOe and +8kOe in the field-in-plane/current-in-plane geometry. The following formula was used for calculating the magnetoresistance ratio: $[R(H)-R(0)]/R(0)$ where $R(H)$ is the resistance in the magnetic field H and $R(0)$ is the resistance at H=0.

3. Results and discussion

3.1. Bath reformulation

The electrolyte used to prepare Co-Ag electrodeposits was composed of $AgClO_4$ and $Co(ClO_4)_2$ as the metals salts, $Na_2S_2O_3$ as the silver complexing agent and $NaClO_4$ as the supporting electrolyte. It was prepared by first dissolving the complexing agent with ultrapure water. After that, a solution containing cobalt and silver salts was added drop by drop to the thiosulphate solution which was continuously stirred in order to obtain the solution of the precipitate formed when the two solutions were brought together. pH was fully controlled during the addition as values lower than 3 lead to chemical instability, probably as a consequence of thiosulphate disproportion [15]. It was therefore imperative to maintain a pH close to 3.5 during solution preparation. The $[Na_2S_2O_3]/[AgClO_4]$ ratio must be higher than 1 as lower ratios led to the appearance of a precipitate as a consequence of the incomplete formation of the argento-thiosulphate complexes [16]. $AgClO_4$ and $NaClO_4$ concentrations were fixed at 0.01M and 0.1M, respectively. The concentration of the other species was varied in order to approach the deposition potentials of both metals as much as possible and to obtain Co-Ag coatings with variable cobalt percentages. Linear sweep and cyclic voltammetries were used to investigate the influence of $Co(ClO_4)_2$ and $Na_2S_2O_3$ concentration on the cited parameters.

Linear sweep voltammetries from the solutions 0.01M $AgClO_4$ + xM $Co(ClO_4)_2$ + 0.05M $Na_2S_2O_3$ + 0.1M $NaClO_4$ with variable amounts of $Co(ClO_4)_2$ are shown in Fig. 1A. Similar voltammograms were obtained independently of the cobalt concentration, two reductions peaks related to silver (peak A) and cobalt reduction (peak B) prior to hydrogen evolution being observed. The higher the cobalt concentration the higher the current density of peak B (j_{Co}) as was to be expected. The j_{Co}/j_{Ag} ratio selected was 3, similar to that obtained in a previously developed bath (containing thiourea as complexing agent) [17] in which cobalt percentages in the range 10-40% were obtained. The j_{Co}/j_{Ag}=3 corresponds to a 0.01M $Co(ClO_4)_2$ concentration.

Fig. 1B shows the influence of thiosulphate content over the voltammetric response. The higher the $Na_2S_2O_3$ concentration the more negative the silver deposition potential, due to the higher proportion of the silver-thiosulphate complex [16]. A $Na_2S_2O_3$ concentration of 0.015M was selected to improve the adhesion to the substrate (because it was observed that the higher the $Na_2S_2O_3$ content, the higher the stress and the lesser the adherence).

From the last results, the 0.01M $AgClO_4$ + 0.01M $Co(ClO_4)_2$ + 0.015M $Na_2S_2O_3$ + 0.1M $NaClO_4$ bath (*cobalt-silver solution*) was selected. The complex stability diagrams of (A) *cobalt-silver solution*, (B) *silver solution* (0.01M $AgClO_4$ + 0.015M $Na_2S_2O_3$ + 0.1M $NaClO_4$) and (C) *cobalt solution* (0.01M $Co(ClO_4)_2$ + 0.015M $Na_2S_2O_3$ + 0.1M $NaClO_4$) were analyzed [16]. Two of Ag (I) complexes with different stability constants ($AgS_2O_3^-$, log K = 8.8 and $Ag(S_2O_3)_2^{3-}$, log K = 13.5) in equimolar concentrations were present in both *silver solution* and *cobalt-silver solution* at the concentrations used and at the working pH. No cobalt-thiosulphate complexes were present in these conditions.

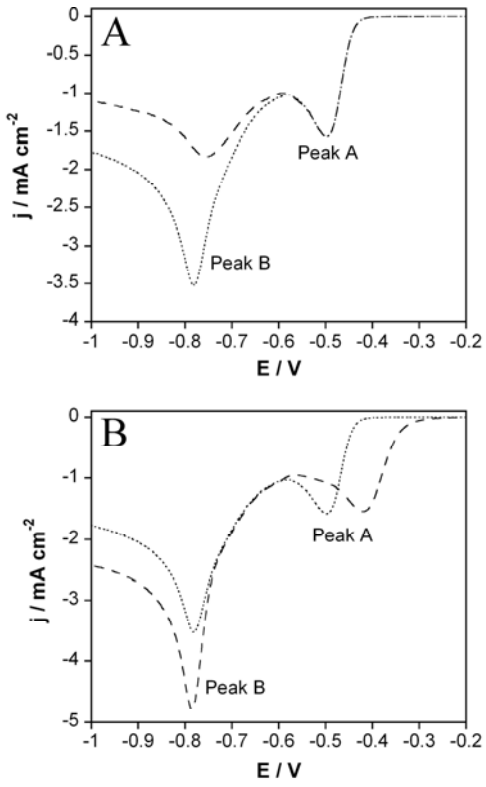

Figure 1. Linear sweep voltammetries recorded from the solution 0.01M $AgClO_4$ + xM $Co(ClO_4)_2$ + yM $Na_2S_2O_3$ + 0.1M $NaClO_4$. (A) Dashed line: x=0.005M, y=0.05M and dotted line: x=0.01M, y=0.05M. (B) Dashed line: x=0.01M, y=0.015M and dotted line: x=0.01M, y=0.05M.

3.2. Electrochemical behaviour

Cyclic voltammetry data for the selected electrolyte (cobalt-silver solution) is presented in Fig. 2A. The cathodic scan shows the two peaks related to silver and cobalt deposition. On the other hand, multiple peaks appear during the anodic scan. In order to identify these peaks, cyclic voltammetries were carried out with each of the following solutions: (1) 0.015M $Na_2S_2O_3$ + 0.1M $NaClO_4$ (*blank solution*), (2) *silver solution* and (3) *cobalt solution* (Fig. 2).

At first, no electrochemical processes were recorded from the *blank solution* when scanning between hydrogen and oxygen evolution and vitreous carbon was used as working electrode (Fig. 2B). The cyclic voltammetry of the *silver solution* (Fig. 2C) confirms that Ag (I) reduction takes place under peak A, being related to a mass control process as, when the solution was stirred, the reduction current maintained a constant value. As it can be observed, electrodeposited silver oxidized in a double peak (peaks A1 and A2) (Fig. 2C, dotted line and dashed line). The formation of the two silver-thiosulphate complexes could explain the double oxidation peak recorded during the positive-going scan. This proposal was confirmed as only a single oxidation peak was recorded from the *silver solution* but with higher thiosulphate concentrations (0.05M). According to the complex stability diagram for these higher concentrations, only the $Ag(S_2O_3)_2^{3-}$ argento-thiosulphate complex formation is expected.

Fig. 2D shows the voltammetric response of the cobalt *solution*. Only one reduction peak (peak B) at around –860 mV, corresponding to a mass control process, and one oxidation peak (peak B1) were recorded (Fig. 2D, dotted line and dashed line, respectively). Moreover, a band located at positive potentials (peak B2) was also observed, which could be related to some cobalt oxides formation as has been previously observed [18].

Once the electrochemical behaviour of the two isolated metals had been investigated, and the stability complex diagram of the *cobalt-silver solution* showed that cobalt and silver behaved as in the *cobalt solution* and *silver solution*, respectively, the interpretation of the voltammograms recorded from the *cobalt-silver solution* (Fig. 2A) became easier. The negative-going scan showed the peaks related with silver (peak A) and cobalt (peak B) reduction processes. Cobalt deposition potential in *cobalt-silver solution* shifted toward more positive values than in *cobalt solution* as the nucleation process is easier over the first electrodeposited silver layer than over vitreous carbon. Regarding the anodic scan, peak B1 was assigned to cobalt oxidation while peak B3 could be related to the oxidation of a cobalt-silver alloy formed during the previous cathodic scan. Peaks A1 and A2 were related to silver oxidation. Moreover, peak B2 was associated to the presence of some cobalt oxides.

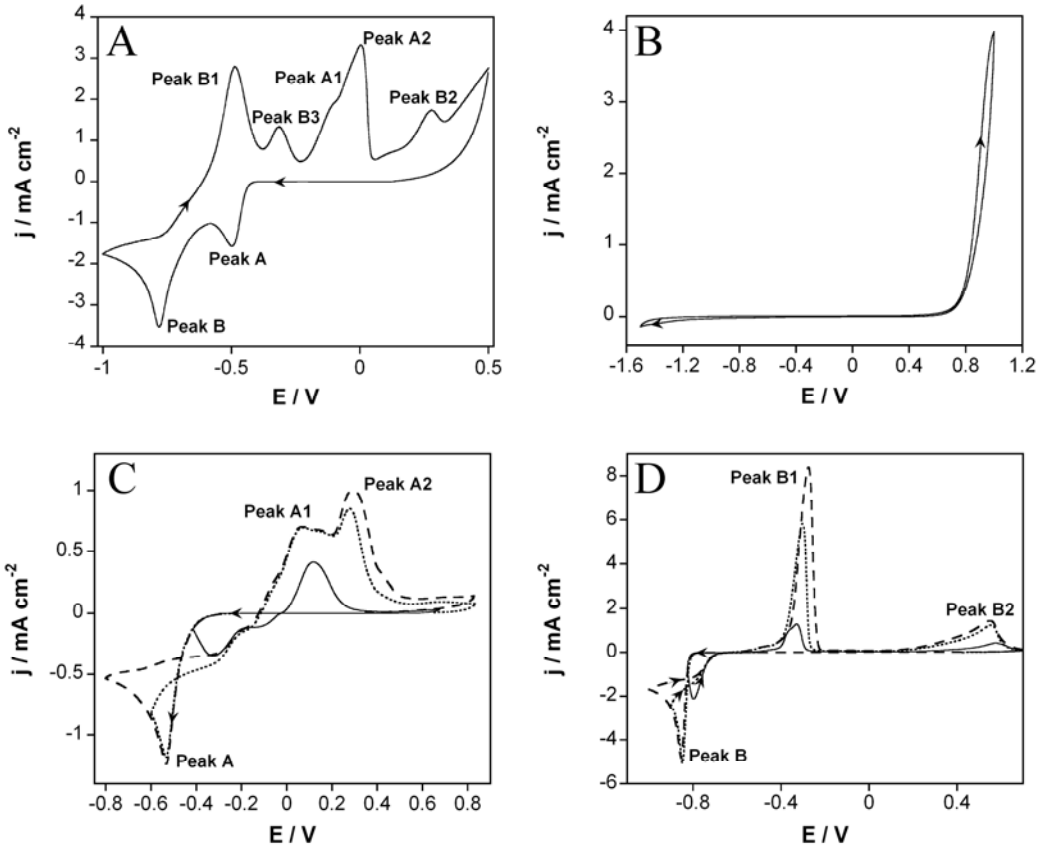

Figure 2. Cyclic voltammograms recorded from the solution xM $AgClO_4$ + yM $Co(ClO_4)_2$ + 0.015M $Na_2S_2O_3$ + 0.1M $NaClO_4$. (A) x=0.01M, y=0.01M (*cobalt-silver solution*). (B) x=0 M, y=0M (*blank solution*). (C) x=0.01M, y=0M (*silver solution*). (D) x=0M, y=0.01M (*cobalt solution*).

3.3. Deposit preparation

Cobalt, silver and cobalt-silver coatings were prepared potentiostatically and under stirring conditions in order to avoid the depletion of the electroactive species over the electrode. Deposition potentials were selected from the previous voltammetric study. Deposits were prepared at different potentials and at variable deposition times with the aim of studying not only the influence of the deposition rate on the morphology but also thickness and roughness evolution.

Fig. 3 shows some representative j-t transients recorded during the Co-Ag electrodeposition process. For all the solutions, these showed a slight current increase with deposition time, j increasing as the applied potential was made more negative. This was associated with an increase in the roughness of the deposits. The same behaviour was observed during silver and cobalt electrodeposition.

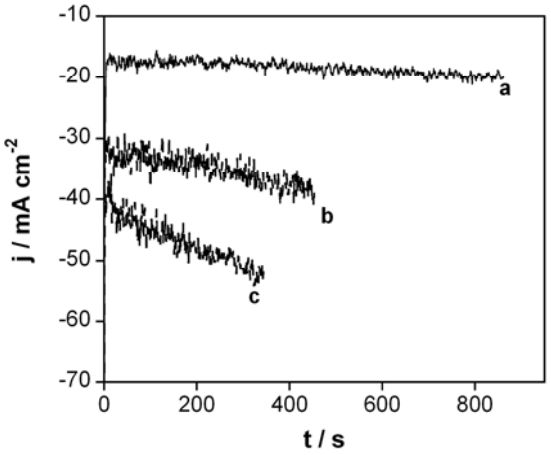

Figure 3. j-t transients recorded from the *cobalt-silver solution* at different applied potentials. Curve (a) -640mV, curve (b) -680mV, curve (c) -770mV.

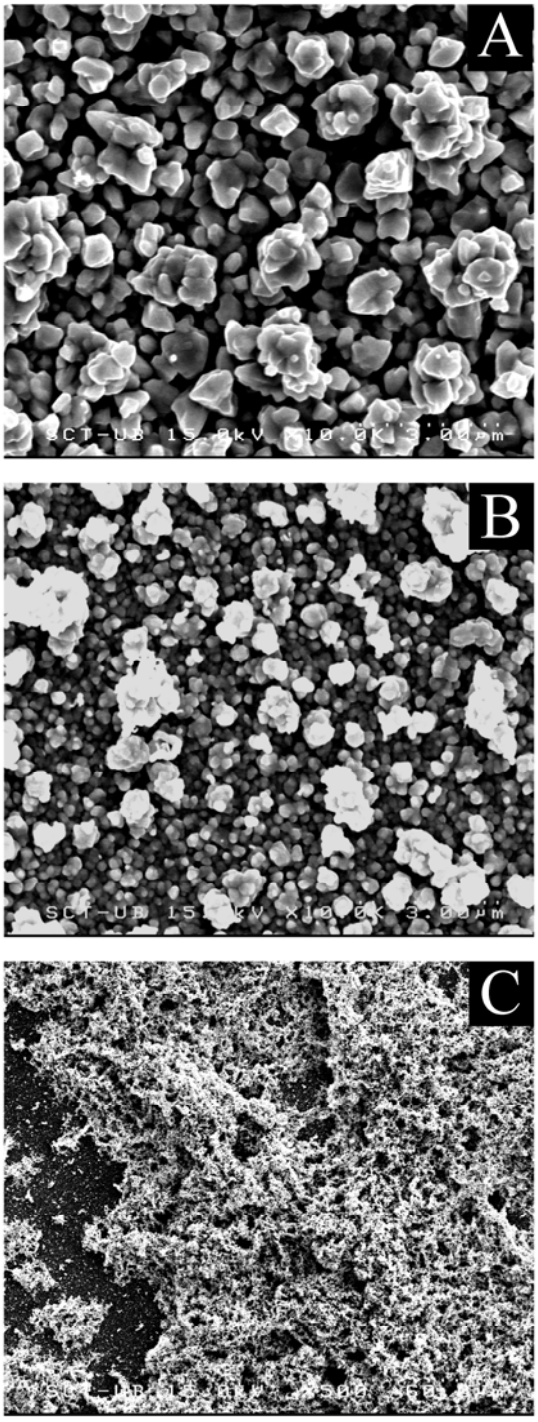

Figure 4. SEM micrographs of silver coatings obtained at different applied potentials.(A) -400mV, (B) -500mV, (C) -700mV.

3.4. Characterization of Ag coatings

Silver deposits showed varying morphologies as a function of the deposition rate (or applied potential) (Fig. 4). A mixture of both granular and faceted grains (Fig. 4A) was observed when deposits were prepared at potentials corresponding to the beginning of the reduction peak. Smaller grain size was detected by applying more negative potentials (Fig. 4B). On the other hand, deposits prepared at highly negative potentials showed a fibrous growth, which tended to become dendritic growth at even more negative potentials, over a first granular layer (Fig. 4C). The compositional analysis of the different coatings prepared revealed no sulphur incorporation into the deposits.

From the XRD patterns of silver deposits no sulphur was deteected. Similar X-ray diffractograms were obtained independently of the deposition rate. Apart from some peaks corresponding to the substrate, several peaks assigned to the silver coating were detected (Fig. 5). These were placed at positions which fitted well enough with fcc-Ag structure, corroborating again that no sulphur was incorporated into the silver lattice. The deposit obtained at the smallest deposition rate (which corresponded to the granular and faceted morphology) showed narrow peaks (Fig. 5, curve a), some of them ((111), (200), (222) and (400)) asymmetric due to the partial overlapping with the substrate peaks. By comparing their relative intensities with those tabulated, these deposits showed the direction (111) as the preferred orientation. On the other hand, the deposit obtained at the highest deposition rate (which corresponded to the fibrous/dendritic morphology) showed broader peaks indicating a smaller crystalline size (Fig. 5, curve b). Moreover, substrate peaks were more clearly seen as a consequence of the lesser compactness of these deposits.

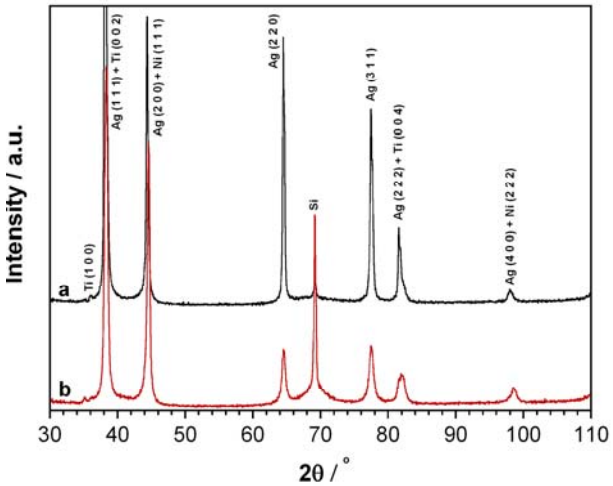

Figure 5. XRD patterns of silver coatings corresponding to (a) Fig. 4A, (b) Fig. 4C.

3.5. Characterization of Co coatings

Cobalt deposits showed important morphology differences depending on growth rate (Fig. 6). At the more positive

potentials deposits were unresolved by FE-SEM indicating a very small grain size (Fig. 6A) whereas, at more negative potentials a granular morphology could be detected (Fig. 6B). The compositional analysis revealed a high sulphur incorporation in all the coatings (6-11wt.%), the content being higher at the slower deposition rates. Although the phase diagram of the Co-S system completely excludes the solubility of sulphur in cobalt, it can possibly be soluble in Co thin films. In fact, it is known that S atoms are to some extent segregated in the grain boundaries and the rest dissolves by substitution in the crystal lattice [19]. Independently of the sulphur location, the higher or lower sulphur quantity could be responsible for the differences observed in the morphology.

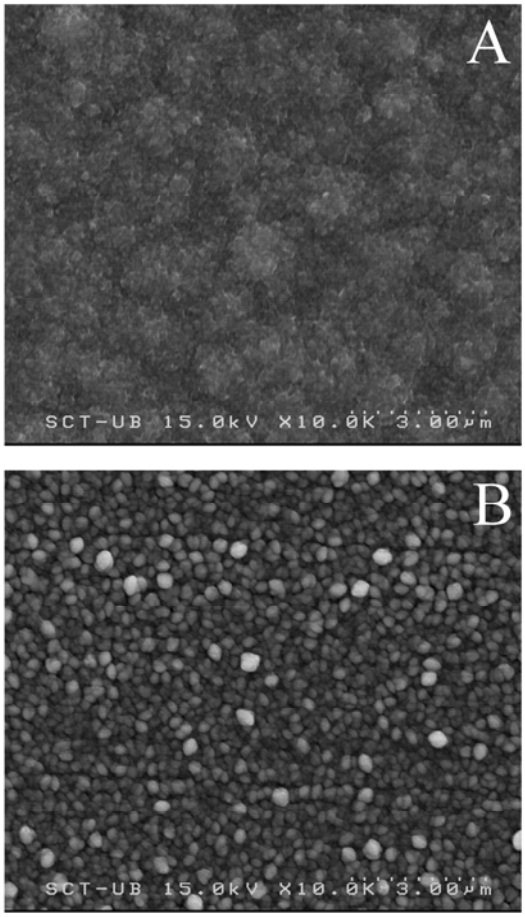

Figure 6. SEM micrographs of cobalt coatings obtained at different applied potentials. (A) -800mV, 11wt.% S, (B) -900mV, 6wt.% S.

Remarkable changes in film structure were also detected as a function of the sulphur content (Fig. 7A). At low sulphur contents (around 6 wt.%) the diffractogram revealed the Co film's polycrystallinity (Fig. 7A, curve a). Next to some peaks attributable to the substrate, several peaks assigned to (1 0 0), (1 0 1), (1 1 0), (2 0 0) and (2 0 1) planes of the hcp structure of cobalt were observed. The reflections were shifted towards smaller angles due to sulphur incorporation into the lattice. The lattice constants of the hcp phase that best fit the position of the observed peaks are a = 2.5225Å, c = 4.1117Å and c/a= 1.6300. The resulting cell volume (22.657Å^3) is higher than that tabulated (22.033Å^3) [20] as the hcp-Co lattice expands due to sulphur incorporation. Moreover, the peak placed at 2θ=23º (see inset Fig. 7A) may correspond to the (1 0 0) reflection of either S_8 or S_6, corroborating once again sulphur presence. No peaks attributable to Co-S compounds were present.

Significant change in the diffractograms was observed by increasing S content in the Co deposits. No peaks assigned to the coating were recorded when sulphur content increased up to 11wt.% (Fig. 7A, curve b), broad band assigned to cobalt being detected centred at 2θ=44º, revealing the film amorphous nature. The high sulphur content could be the responsible for the observed amorphicity.

Due to the significant incorporation of sulphur into the cobalt deposits, modifying both their morphology and crystalline structure, its influence on the magnetic properties of cobalt deposits was also analysed. The substrate magnetic response (silicon/seed-layer) was not significant when compared to that of the Co coatings. Noticeable differences were detected for cobalt deposits with different S percentages (Fig. 7B). Cobalt films with moderate sulphur incorporation (around 6wt.%) showed a coercive field of 240Oe (Fig. 7B, curve a) and a squareness (M_r/M_s) of 0.5 (saturation magnetization is reached at high fields (around 14kOe)). When Co deposits contained higher S percentages (11wt.% S), soft-magnetic behaviour was detected: low coercivity (1-5Oe) and high squareness (around 0.94) was obtained (Fig. 7B, curve b). The sharp decrease in the coercivity value is related to the structural change from crystalline to amorphous previously observed by XRD when sulphur content increased from 6wt.% to 11wt.%. Therefore, the absence of microstructural discontinuities (grain boundaries) on amorphous cobalt, on which magnetic domains can be pinned, makes magnetization by wall motion easy and hence, coercive fields of a few oersteds are achieved. On the other hand, a saturation magnetization of around 120-130emu g^{-1} was obtained for all samples, slightly smaller than that reported for bulk cobalt [21]. This fact could be attributed to the diminution of the magnetic moment per grain because it is known that it depends on both size and packing fraction that is, on the average grain separation [19]. Therefore, the increase in sulphur content, placed mainly in the grain boundaries, increases the average separation between grains thus decreasing M_s (Figure 7B).

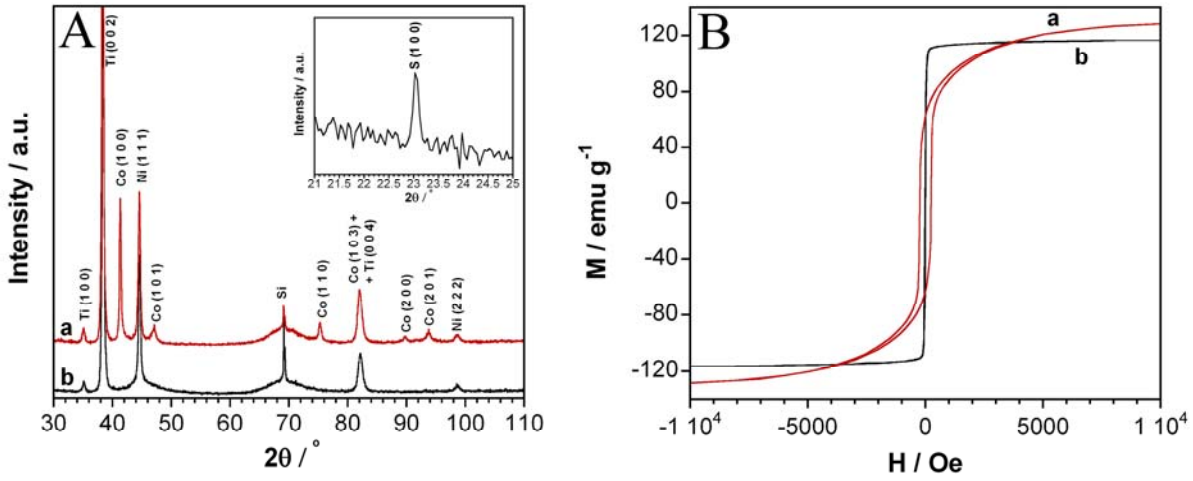

Figure 7. (A) XRD patterns of cobalt coatings with different sulphur content (a) 6wt.%, (b) 11wt.% (B) Magnetization curves of Co deposits with different sulphur content (a) 6wt.%, (b) 11wt.%.

It is widely known that the magnetic properties of cobalt thin films are crystalline structure-dependent. As it is reported elsewhere, cobalt electrodeposits prepared from sulphur-free baths display different coercive field values depending on the structure. Hcp-Co films with coercive field values in the range 200-100Oe were obtained depending on the current density or applied potential [22-25]. A softer magnetic behaviour was observed for the fcc cobalt electrodeposits, for which the coercive field was approximately 40Oe [21], and amorphous cobalt with an H_c value of 15Oe [3]. On the other hand, cobalt deposits with a primitive cubic structure (ε-Co) [14] showed coercivity values close to those of cobalt electrodeposits with an hcp structure. Typical saturation magnetization values of bulk cobalt were reported for all of them.

However, not only the crystalline structure but also the incorporation of a third element can alter the magnetism of cobalt films. In view of the above paragraph important consequences can be derived from sulphur incorporation. H_c values higher than 200Oe (typical of hcp cobalt) and smaller M_s values than the common values have been found in hcp-Co films with small amounts of sulphur (around 6wt.% S). When sulphur segregates at grain boundaries, the S-rich layer decreases the magnetic exchange coupling between grains thus increasing the coercivity. As it has been previously said, the M_s decrease can be due to diminution of magnetic moment per grain. On the other hand, high sulphur incorporations induce an amorphous state in cobalt, leading to H_c values of a few oersteds.

3.6. Characterization of Co-Ag coatings

The influence of both deposition rate and film's thickness in Co-Ag deposits morphology was analyzed. All the deposits were characterized by granular morphology and uniformity (Fig. 8). Deposits were also compact and crack-free, covering the entire cathode surface. Grain size decreased with decreasing the applied potential from -640mV (Fig. 8A) to -900mV (Fig. 8C). The grains were more faceted at the more positive potentials and more rounded at the more negative ones (see insets Fig. 8). In any conditions, dendritic growth was observed.

Deposits roughness analysis by white-light interferometry highlighted the film thickness influence, which led to rougher deposits. Those prepared at the more positive potentials showed roughness values (R_a) of a few tenths of nanometer (around 40nm for 0.8μm thick deposits). However, increasing the thickness up to 1.25μm the roughness increased until reaching R_a values of around 180nm. On the other hand, a variation of around 60nm was observed when the thickness increased from 0.8μm to 1.25μm in deposits prepared at more negative potentials. Despite the increase in the roughness, the R_a values measured were noticeable smaller those for Co-Ag deposits prepared from a previously developed bath containing thiourea (R_a values around 5μm) [18].

Co-Ag deposits varied in composition as a function of the applied potentials (Table 1). As it was to be expected, cobalt percentage moderately increased in the deposit as the

applied potential increased. This weak cobalt percentage-applied potential dependence makes it easier to control deposit composition. Although the sulphur content in the film was kept in the range 5-12wt.%, it initially increased with the potential but then it decreased as the potential was made more negative. No variation of composition was observed throughout the film's thickness.

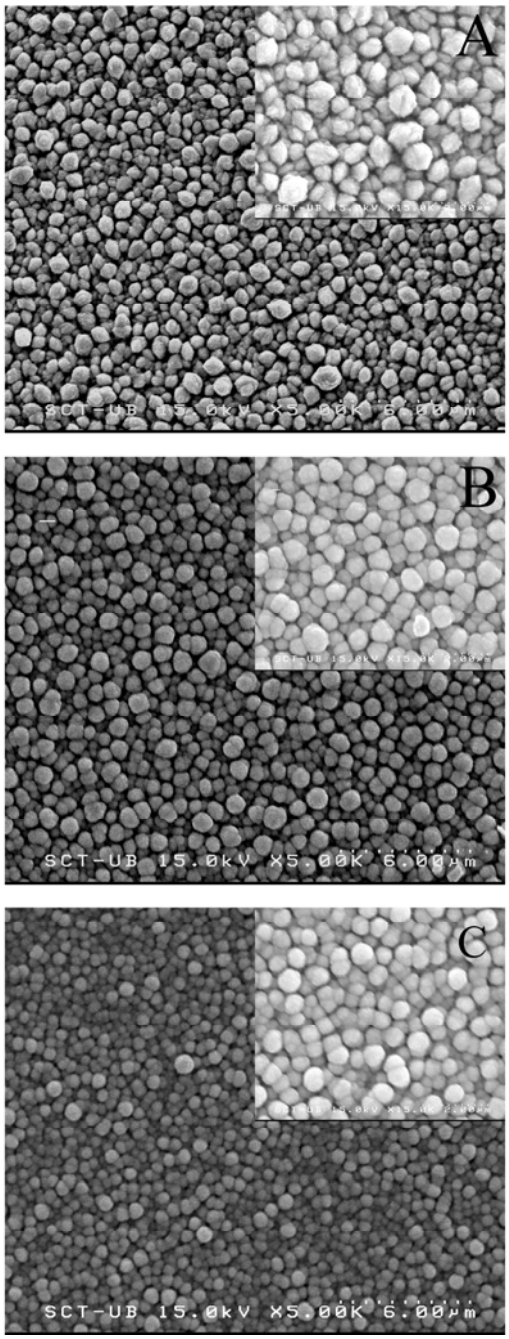

Figure 8. SEM micrographs of Co-Ag coatings obtained at different applied potentials. (A) - 640mV, (B) -770mV, (C) – 900mV. Insets show higher magnification.

Table 1. Variation of cobalt and sulphur content in Co-Ag films.

E / mV	wt.% Co	wt.% S
-640	12	5
-680	18	8
-720	24	10.5
-770	27	12
-820	28.5	10
-900	32	7

X-ray diffractograms of the Co-Ag samples prepared at different deposition rates presented similar profiles. The diffractograms (Fig. 9A, curve b) reveal the only presence of narrow peaks corresponding to the substrate (peaks corresponding to Si, Ti and Ni). However, if one compares these patterns with that of the substrate (Fig. 9A, curve a) some broad bands centred at 2θ=39º, 45º, 64º and 78º can be distinguished (see arrows in Fig. 9A, curve b), these bands being assigned to fcc-Ag. Band broadness is indicative of the nanocrystalline nature of the deposits. On the other hand, neither peaks nor bands associated to cobalt were observed. This result is in agreement with some previous studies in which cobalt was not detected by XRD [26].

The magnetic curves of the Co-Ag deposits showed ferromagnetic behaviour (Fig. 9B) with a soft-magnetic character. Saturation magnetization values increased, as was to be expected, as films cobalt content increased; M_s values were low in comparison to those of pure-cobalt films. The decrease in the saturation magnetization was related again to the magnetic moment per grain diminution but also to the smaller film's cobalt content. On the other hand, coercivity values were dependent on the deposition potential, a more soft-magnetic behaviour being observed as the applied potential was made more negative: coercivity decreased from 30Oe for deposits prepared at -640mV to 1Oe for those obtained at -900mV. This could be attributed to the smaller grain size at the more negative potentials. Moreover, the higher sulphur content could also contribute to grain size reduction, thus promoting the coercivity reduction. This statement is confirmed when comparing these results with those for sulphur-free Co-Ag films. While Co-Ag thin films obtained from free-sulphur baths show H_c values higher than 200Oe [11-13], those prepared from sulphur-containing baths show smaller H_c values (around 115Oe when sulphur amounts up to 2wt.%) [14], diminishing on increasing S content (results reported here). The main difference observed among all the studies is the smaller grain size detected in the films prepared from sulphur-containing baths.

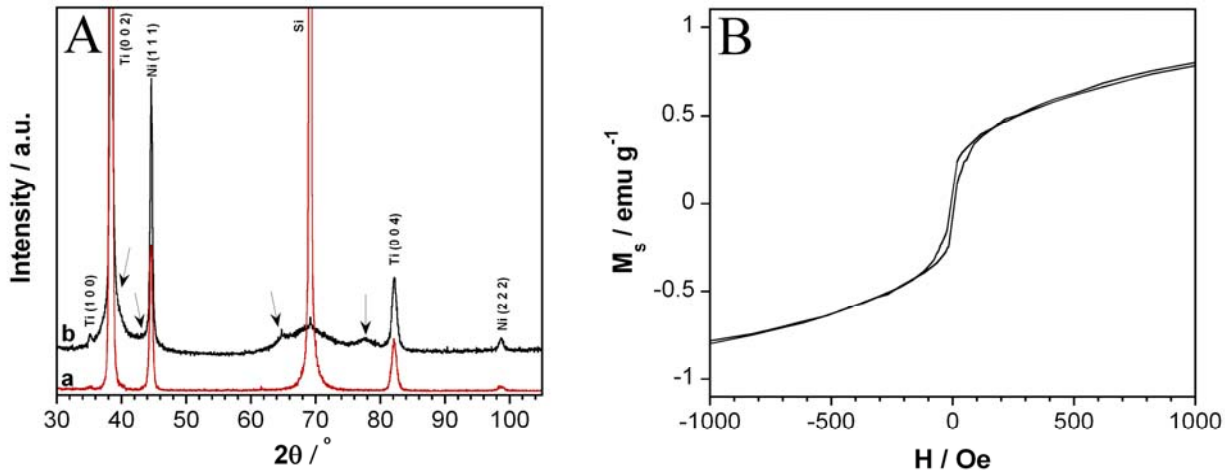

Figure 9. (A) XRD patterns of the (a) substrate (Si/Ti/Ni), (b) Co-Ag coating of Fig. 8A. (B) Magnetization curve of the Co-Ag deposit of Fig. 8A.

The influence of sulphur content on the magnetoresistance of the Co-Ag system was also investigated. As it is known, the magnetic/non-magnetic interface plays a central role in the magnetoresistance of granular films [27]. No change in the electrical resistance with the applied magnetic field was measured at room temperature. The reason may be that the sulphur barrier place at the magnetic/non-magnetic interface always behaves as a scattering centre for the electrons independently of the cobalt granules magnetization direction and the applied magnetic field. Therefore, no magnetoresistance is recorded as the probability for the electrons with spin-up and spin-down to be scattered is the same in all the applied magnetic fields. Another possible explanation of the lack of magnetoresistance is the sulphur's deleterious effect on the magnetic properties of the Co-Ag films as a clear reduction in the M_s has been reported here. Both phenomena can take part simultaneously because of sulphur is located in both the grain boundary and the inner cobalt particle. On the other hand, magnetoresistance values around -0.01% were measured at 20 K. These results highlight the deleterious effect of sulphur on the magnetotransport properties.

4. Conclusions

Thiosulphate electrolytic bath leads to prepare uniform and compact Co-Ag granular films with variable amounts of cobalt. This bath formulation allowed obtaining films with better quality than those previously prepared from other electrolytes containing sulphur species and a clear reduction on the surface roughness has been observed. Simultaneous sulphur incorporation took place during Co-Ag electrodeposition whose composition into the film was in the range 5-12wt.%. It has been proved by studying the separate metals components that sulphur was incorporated in the cobalt particles. Sulphur presence in both Co and Co-Ag deposits modifies their properties. Nanocrystalline Co-Ag deposits with soft-magnetic behaviour (1-30Oe) were obtained. On the other hand, a transition from crystalline cobalt coatings with H_c=240Oe to amorphous soft-magnetic (H_c=1-5Oe) cobalt films was observed when S content was increased.

Acknowledgements

This paper was supported by contract MAT-2006-12913-C02-01 from the Comisión Interministerial de Ciencia y Tecnología (CICYT). J. Garcia-Torres would also like to thank the Departament d'Innovació, Universitats i Empresa of the Generalitat de Catalunya and Fons Social Europeu for their financial support.

References

[1] T. Osaka, Electrochim. Acta 45 (2000) 3311.
[2] W. Brückner, J. Thomas, R. Hertel, R. Schäfer, C. M. Schneider, J. Magn. Magn. Mater. 283 (2004) 82.
[3] J. Garcia-Torres, E. Gómez, E. Vallés, J. Appl. Electrochem. 39 (2) (2009) 233.
[4] D. Kim, D.-Y. Park, B. Y. Yoo, P. T. A. Sumodjo, N. V. Myung, Electrochim. Acta 48 (2003) 819.
[5] T. Osaka, T. Sawagnchi, F. Mizutani, T. Yokoshima, M. Takai, Y. Okinaka, J. Electrochem. Soc. 146 (1999) 3295.
[6] S. R. Brankovic, K. Vasiljevic, T. J. Klemmer, E. C. Johns, J. Electrochem. Soc. 152 (2005) C196.
[7] J. Edwards, Trans. Inst. Met. Finish. 39 (1962) 52.

[8] J. George, J. Rantshler, S. Bae, D. Litvinov, S. R. Brankovic, J. Electrochem. Soc. 155 (2008) D589.
[9] S. Kuriki, M. Sato, M. Maeda, Jpn. J. Appl. Phys. 10 (1971) 604.
[10] A. Berkowitz, J. R. Mitchell, M. J. Carey, A. P. Young, D. Rao, A. Starr, S. Zhang, F. E. Spada, F. T. Parker, A. Hutten, G. Thomas, J. Appl. Phys. 73 (1993) 5320.
[11] H. Zaman, A. Yamada, H. Fukuda, J. Ueda, J. Electrochem. Soc. 145 (1998) 565.
[12] S. Kenane, E. Chainet, B. Nguyen, A. Kadri, N. Benbrahim, J. Voiron, Electrochem. Comm. 4 (2002) 167.
[13] S. Kenane, J. Voiron, N. Benbrahim, E. Chainet, F. Robaut, J. Magn. Magn. Mat. 297 (2006) 99.
[14] J. Garcia-Torres, E. Gómez, E. Vallés, Cryst. Growth. Design. 9(4) (2009) 1671.
[15] M. J-Liew, S. Sobri, S. Roy, Electrochim. Acta 51 (2005) 877.
[16] Chemical Equilibrium Diagrams Hydra/Medusa software (http://web.telia.com/~u115651596).
[17] E. Gómez, J. Garcia-Torres, E. Vallés, Anal. Chim. Acta 602 (2007) 187.
[18] E. Gómez, J. Garcia-Torres, E. Vallés, J. Electroanal. Chem. 615 (2008) 213.
[19] N. Sulitanu, Mat. Sci. Eng. B77 (2000) 32.
[20] PDF #05-0727 JCPDS-International Centre for Diffraction Data
[21] E. Gómez, E. Vallés, J. Appl. Electrochem. 32 (2002) 693.
[22] H. Sakuma, H. Tai, K. Ishii, IEEJ Trans. 3 (2008) 375.
[23] E. Gómez, E. Pellicer, E. Vallés, J. Electroanal. Chem. 517 (2001) 109.
[24] E. Gómez, E. Pellicer, X. Alcobé, E. Vallés, J. Solid State Electrochem. 8 (2004) 497.
[25] M. S. Bhuiyan, B. J. Taylor, M. Paranthaman, J. R. Thompson, J. W. Sinclair, J. Mat. Sci. 43 (2008) 1644.
[26] T. Watanabe, Nano-plating: microstructure control theory of plated films and data base of plated film microstructure; Elsevier: Amsterdam, 2004
[27] W. Wang, F. Zhu, W. Lai, J.-q. Wang, G. Yang, J. Zhu, Z. Zhang, J. Phys. D: Appl. Phys. 32 (1999) 1990.

4.5. Improved giant magnetoresistance

Due to the deleterious effect of inclusions in general and sulphur in particular on giant magnetoresistance, a free-sulphur bath was employed to grow the granular films. A chloride-based electrolyte was selected as chloride ions play a double function. On one hand, it is a well-known fact that chloride ions strongly adsorb over the cathode surface [109] which may avoid out of control growth processes. On the other hand, the most important role is that chloride ions act as a complexing agent for silver.

In this sense, the electrolyte employed was 0.002 mol dm^{-3} $AgNO_3$ + x mol dm^{-3} $CoCl_2$ + 3.5 mol dm^{-3} NaCl, with 0.02 mol dm^{-3} ≤ x ≤ 0.4 mol dm^{-3} at a pH of 2.7. A high concentration of NaCl was selected in order to avoid the precipitation of AgCl. However, Ag(I) concentrations higher than 0.002 mol dm^{-3} led to solubility problems.

A first study by cyclic voltammetry was essential to be performed because it provided with basic information about the electrochemical processes. Silver deposition potential was greatly shifted toward negative potentials and no signs of side reactions were observed at the codeposition potentials, hydrogen evolution reaction was only observed at highly negative potentials, potentials out of the range useful to prepare the films. Moreover, this technique allowed discarding Co-Ag solid solution formation as two well-defined peaks were recorded during the anodic scan, being attributed to independent oxidation of cobalt and silver. Chronoamperometry and pulse deposition were the methods selected to prepare the films.

The heterogeneity of the films, although detected by the electrochemical characterization, was corroborated by transmission electron microscopy. A random distribution of nanometric cobalt particles in the silver matrix was observed. From these analyses, important parameters directly affecting the magnetotransport properties i.e. particle size or size distribution, could also be determined and subsequently related with the MR values.

Electrodeposition parameters i.e. applied potential, bath Co(II) concentration or deposition time, were observed to greatly modify the magnetotransport properties of the prepared films. The main explanation was the modification of the cobalt content into the film as well as the particle size. GMR values up to 5.85 % were measured at room temperature in Co-Ag deposits prepared by potentiostatic control. However, GMR values up to 7 % were obtained in deposits grown by pulse deposition. But, Why the electrochemical technique may affect the magnetoresistance? The answer to the question is that the main factors governing the transport properties are modified because of the nucleation and growth processes are dependent on the applied signal either continuous or pulses. The main difference detected by both anodic linear sweep voltammetry (ALSV) and TEM

studies was the particle size distribution and this directly affected the magnetoresistance. It is worthy to mention that the GMR values reported here are larger than those published by others dealing with the electrodeposition of Co-Ag granular films [86-89].

Common characteristics of all the magnetoresistance curves (MR(*H*)) recorded are the non-saturating behaviour detected even at the highest applied magnetic field and the splitting recorded around zero field. Both effects indicate that a size distribution from superparamagnetic to ferromagnetic particles exists, in agreement with previous studies by TEM.

Some models were developed to study the MR dependence on the magnetic field [110-113]. Gittleman observed that MR depended on the square of the magnetization (*M*) when only SPM particles were present [110,113]. Shortly later, Wiser and Hickey [112,113] observed a linear dependence of the MR with *M*, which was attributed to a particle size distribution covering the range from SPM to FM particles. According to them, three possible electron paths "magnetic region 1 → non-magnetic region → magnetic region 2" which contribute in a different manner to the total MR could be described: I) both magnetic regions are SPM, II) both magnetic regions are FM and III) one magnetic region is SPM and the other is FM. Their conclusion was that the spin dependent scattering processes that mainly contribute to the total magnetoresistance effect are those involving ferromagnetic particles. Thus, case II) and case III) are the most contributing to the total magnetoresistance. Later, Bakonyi *et al.* [76] taking profit of Wiser and Hickey findings, elaborated a model to describe the field dependence of the magnetoresistance in magnetic multilayers with both ferromagnetic and superparamagnetic regions. The last model was thus applied to decompose the MR(*H*) curves into the GMR_{FM} (ferromagnetic contribution) and GMR_{SPM} (superparamagnetic contribution) terms, corresponding to case II) and case III), respectively. There was no need to account for a term involving only with superparamagnetic particles (a quadratic dependence of MR on magnetization) as very good fits were observed in all cases. In this regard, the decomposition process allowed obtaining quantitative values about the ferromagnetic and superparamagnetic contributions to the total magnetoresistance.

A clear dominance of the superparamagnetic contribution was detected in all the samples analyzed. However, significant variation was detected depending on the electrodeposition condition i.e. bath Co(II) concentration, applied potential or deposition time, and the electrochemical method employed to grow the material. Clear dependencies of the GMR values and GMR_{FM} and GMR_{SPM} terms on the previous parameters were got from the numerical analysis.

GMR values were also found to dependent on the measurement temperature. A clear increase on its magnitude was observed at temperatures down to 20 K. The highest GMR value achieved was 14%. The comparison of the different MR(*H*) curves revealed that the superparamagnetic contribution was retained even at the lowest temperature. This finding was explained on the basis of the dipolar interaction of the superparamagnetic particles. On the other hand, the thermal treatment was also observed to greatly influence the magnetotransport properties. A sharp decrease in the GMR values was observed at all annealing conditions.

Group of articles included in section 4.5.

Page 161: Relevant GMR in as-deposited Co-Ag electrodeposits. Chronoamperometric preparation

Jose Garcia-Torres, Elisa Vallés and Elvira Gómez, Submitted.

Page 175: Relevant GMR in as-deposited Co-Ag electrodeposits. Pulse plating preparation

Jose Garcia-Torres, Elisa Vallés and Elvira Gómez, Submitted.

Page 187: Temperature dependence of GMR and effect of annealing on electrodeposited Co-Ag granular films

Jose Garcia-Torres, Elisa Vallés and Elvira Gómez, Submitted.

Relevant GMR in as-deposited Co-Ag electrodeposits. Chronoamperometric preparation

Submitted

Relevant GMR in as-deposited Co-Ag electrodeposits. Chronoamperometric preparation

J. García-Torres*, E. Vallés, E. Gómez
Electrodep, Departament de Química Física i Institut de Nanociència i Nanotecnologia (IN^{2}UB), Universitat de Barcelona, c/ Martí i Franquès, 1. 08028 Barcelona (Spain)

Keywords:
Cobalt-silver granular films
Electrodeposition
GMR
FM and SPM contribution

A B S T R A C T

Electrodeposited Co-Ag granular films were prepared by potentiostatic deposition from a chloride-based electrolyte. Different Co(II)/Ag(I) ratios were tested in order to study the influence of the composition bath on the magnetotranport properties. All the as-deposited samples showed GMR effect since both longitudinal and transverse magnetoresistances were negative in the whole field range. GMR values up to 5.85 % were measured at room temperature. Electrochemical and structural techniques (XRD, TEM and electron diffraction) as well as magnetoresistance measurements confirmed the heterogeneity of the deposits with a size distribution from superparamagnetic to ferromagnetic particles. Fcc-Ag and a mixture of hcp-Co and fcc-Co were present in the coatings. An analysis of the magnetotransport properties based on the decomposition of the total magnetoresistance into its ferromagnetic and superparamagnetic contributions revealed a high superparamagnetic contribution in all the samples.

1. Introduction

One of the most fascinating discoveries in the last decades has been the giant magnetoresistance effect and so an important institution as the Nobel Foundation which awards with the Noble Prizes has recognized. The giant magnetoresistance could be defined as the change in the electrical resistance of a material upon the application of an external magnetic field. The discovery was firstly found in layered systems [1,2] but it was not an exclusive property of multilayered structures as it was lately observed in the so called granular films [3,4]. A granular film could be defined as a composite material consisting of nanoscale magnetic granules (Co, Fe,…) embedded in an immiscible metallic matrix (Ag, Cu,...). In such systems, the GMR is due to the spin-dependent scattering of electrons either within or at the interfaces of the ferromagnetic particles dispersed in the non-magnetic matrix. When the particle moments are randomly oriented, the resistivity of the material is higher than when they are aligned by the application of an external magnetic field. The magnitude of the GMR has been found to strongly depend on the size and the concentration of the ferromagnetic particles but also on the fabrication procedure

Several methods have been used to prepare granular materials, among them the physical methods have been extensively used [5-8]. One of the systems with the largest GMR reported is the Co-Ag granular material as some previous studies based on the physical deposition of it have revealed [9-15]. Co-Ag system is a very interesting material due to the total immiscibility of both metals as the phase diagram reveals [16]. Immiscibility favours the formation of granular structures with sharp interfaces which is desired as intermixing at the magnetic/non-magnetic limit is not favourable to GMR. Moreover, the percolation threshold concentration is larger for the Co-Ag system than for others, thus a larger concentration of magnetic scattering centres would contribute to magnetoresistance.

On the other hand, electrodeposition has been revealed as an alternative to the physical deposition to grow high-quality GMR materials. This technique has been mainly employed to obtain Co-Cu (or Co-Cu-X) granular systems [17-21]. However, too much effort has not been dedicated to the electrodeposition of the Co-Ag system [22,23]. The importance of the presence of GMR in the granular electrodeposits also stems from the fact that preparation of such films is rather simple and lesser expensive than by physical deposition methods, and thus they have a higher potential for commercial applications.

In this work we report the presence of important GMR values in electrodeposited Co-Ag granular films obtained by a simple step potential method in a wide range of preparation conditions. A chloride bath without additives was used to

prepare the deposits in order to avoid the possible contamination of the interfaces that might exert a deleterious effect to GMR. The relationship between structure, magnetic and magnetotransport properties is also discussed. In order to gain an insight into the magnetoresistance mechanism, an exhaustive analysis of the field dependence of the magnetoresistance will be presented. The analysis consists on the quantitative decomposition into ferromagnetic (FM) and superparamagnetic (SPM) contribution to the total magnetoresistance in order to gain knowledge about the most likely electron path to contribute to the total magnetoresistance in granular materials.

2. Experimental

Co-Ag thin films were prepared by electrodeposition from solutions containing $AgNO_3$, $CoCl_2$ and NaCl, all reagents being of analytical grade. All the solutions were freshly prepared with water first double-distilled and then treated with a Millipore Milli-Q system. The composition of the solutions was 0.002 M $AgNO_3$ + x M $CoCl_2$ + 3.5 M NaCl with 0.02 M $\leq x \leq$ 0.4 M. The pH was kept around 2.7 and the temperature was maintained at 25 ºC. Solutions were de-aerated by argon bubbling before each experiment and maintained under argon atmosphere during it.

Electrochemical experiments were performed in a conventional three-electrode cell using an Autolab with PGSTAT30 equipment and GPES software. Working electrodes were vitreous carbon (Metrohm) and indium tin oxide (ITO) thin films sputtered on glass plates (thickness of ITO layer=25 nm). The vitreous carbon electrode was polished to a mirror finish using alumina of different grades (3.75 and 1.87 μm) and ultrasonically cleaned for 2 min in water before each experiment. ITO was cleaned with acetone, ethanol and rinsed in water before deposition. The reference electrode was an Ag/AgCl/1 M NaCl electrode and all potentials were referred to it. The counter electrode was a platinum spiral.

Voltammetric experiments were carried out at 50 mV s^{-1}, scanning at first towards negative potentials. Only one cycle was run in each voltammetric experiment. Vitreous carbon was used to perform the electrochemical study. On the other hand, deposits were prepared by chronoamperometry under stirring conditions (ω = 100 rpm) over ITO substrate.

Deposit morphology was observed using Hitachi H-4100 FE field emission scanning electron microscope (FE-SEM). Elemental composition was determined with an X-ray analyser incorporated in Leica Stereoscan S-360 equipment. The samples were dissolved in HNO_3 30% and analyzed by the methods described in reference [24] in order to know the weight of each metal into the samples.

The structure of the deposits was studied with X-ray powder diffraction (XRD) using a conventional Bragg-Brentano diffractometer Siemens D-500. The Cu K_α radiation (λ= 1.5418 Å) was selected using a diffracted beam curved graphite monochromator. The X-ray powder diffraction diagrams were created in the 20-105º 2θ range with a step range of 0.05º and a measuring time of 9 seconds per step. The structure was also studied by using high resolution transmission electron microscopy (HRTEM) combined with selected area electron diffraction (SAED) and fast fourier transformation (FFT) using a JEOL 2100.

Magnetic measurements were taken in a SQUID magnetometer at room temperature in helium atmosphere. The magnetization-magnetic field curves were recorded maintaining the samples parallel to the applied magnetic field. Saturation magnetization values were given in emu g^{-1}, where g is the total weight of the sample.

The magnetoresistance (MR) measurements were performed at room temperature with the four-point-in-line method in magnetic fields between –8 kOe and +8 kOe in the field-in-plane/current-in-plane geometry. Both the longitudinal (LMR) and the transverse magnetoresistance (TMR) (field parallel to current and field perpendicular to current, respectively) components were recorded for each sample. The magnetoresistance was defined as follows:

$$MR(H) = 100*[R(H)-R(0)]/R(0)$$

where R(H) is the resistance in the magnetic field H and R(0) is the resistance when H=0.

3. Results and discussion

3.1.- Electrochemical study

This work was initiated with a voltammetric characterization of the deposition process in order to test if the selected bath allows obtaining heterogeneous films, characteristic required to show the magnetic/non-magnetic films magnetoresistance. Voltammetric experiments were made under quiescent conditions. The scan was initiated at a potential were no current was detected. Figure 1A shows the cyclic voltammetry recorded from the 0.002 M Ag(I) + 0.02 M Co(II) + 3.5 M NaCl solution. A small peak located at -0.4 V (see inset Fig. 1A) corresponding to silver reduction was observed whereas, for sufficient negative potentials a significant negative current increase (mainly attributed to cobalt reduction) was detected. During the positive scan, two well separated oxidations peaks were recorded related to cobalt and silver oxidation. This assignment was confirmed because of the oxidation peak potential of each metal fitted well with those obtained from similar solutions containing only one of the electroactive metals. Upon increasing bath cobalt concentration the potential gap between both oxidation peaks decreased as a consequence

of the shift in the equilibrium potential of the Co/Co^{2+} pair (Fig. 1B). In spite of this approximation it was still possible to clearly observe the independency of the peaks ruling out the Co-Ag alloy formation at any Co(II)/Ag(I) ratio.

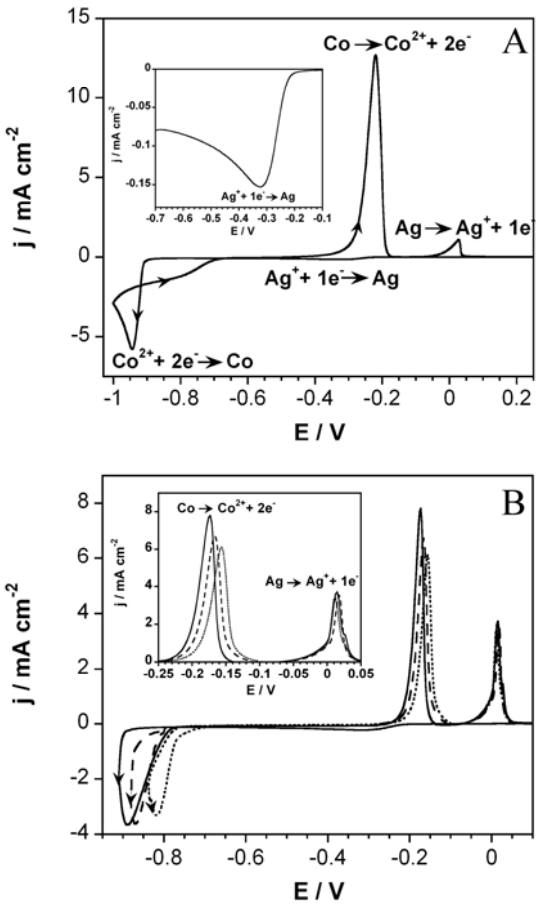

Figure 1. A) Cyclic voltammetry recorded from 0.002 M $AgNO_3$ + 0.02 M $CoCl_2$ + 3.5 M NaCl over vitreous carbon. Inset shows an amplification of the silver reduction peak. B) Cyclic voltammetry recorded from 0.002 M $AgNO_3$ + x M $CoCl_2$ + 3.5 M NaCl, continuous line) x = 0.02, dashed line) x = 0.1 and dotted line) x = 0.4. Inset shows an amplification of the anodic-going scan.

Deposits were prepared potentiostatically over ITO substrate and under stirring conditions in order to keep the contribution of the electroactive species throughout the electrode constant as well as to favour composition constancy along the thickness of the deposit. The applied potentials were more negative than that corresponding to the onset of cobalt deposition in each solution. The current density-time transients showed a monotonic current increase, they being more pronounced as the potential was made more negative (Fig. 2A). A clear film composition-applied potential dependence was observed: cobalt incorporation into the films increased as the applied potential was made more negative. SEM micrographs (Fig. 2B) show compact deposits with nodular morphology in the whole potential range studied. The rounded grains homogeneously cover the entire substrate.

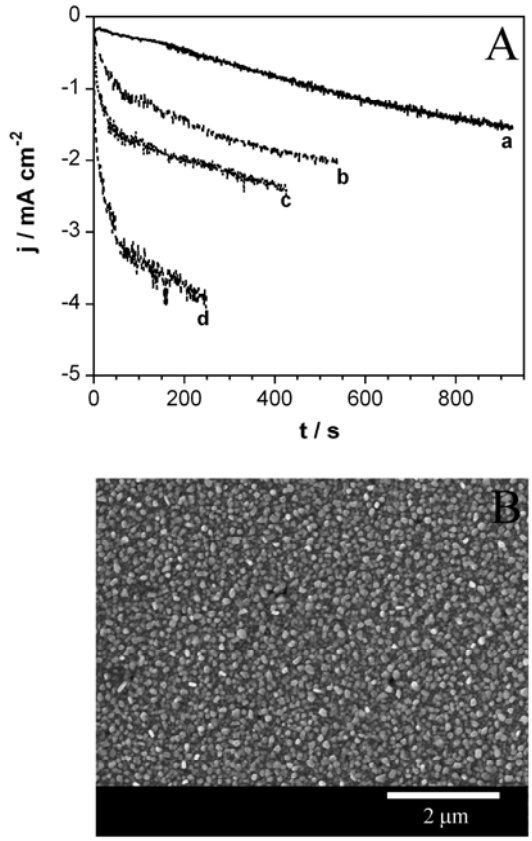

Figure 2. A) Current density-time transients recorded from the solution 0.002 M $AgNO_3$ + 0.02 M $CoCl_2$ + 3.5 M NaCl at different applied potentials. a) -750 mV, b) -800 mV, c) -850 mV and d) -870 mV. B) SEM image of the deposit prepared at -870 mV. Nominal thickness 1050 nm.

3.2.- Structural characterization

The crystalline structure of the deposits was examined by XRD technique (Fig. 3). The peaks in the diffractogram correspond mainly to a polycrystalline fcc-Ag structure with a preferred orientation along the direction (1 1 1). On the other hand, two small peaks located at 41.6 º and 75.9 º could be attributed to the hcp-Co (1 0 0) and hcp-Co (1 1 0) reflections, respectively. It is worthy to mention that no shift in the silver peak positions was detected. Moreover, the calculated silver lattice parameter (0.4085 nm) was in agreement with that tabulated (0.40779 nm). Both findings suggest the no incorporation of Co into the Ag lattice, and hence no Co-Ag alloy formation.

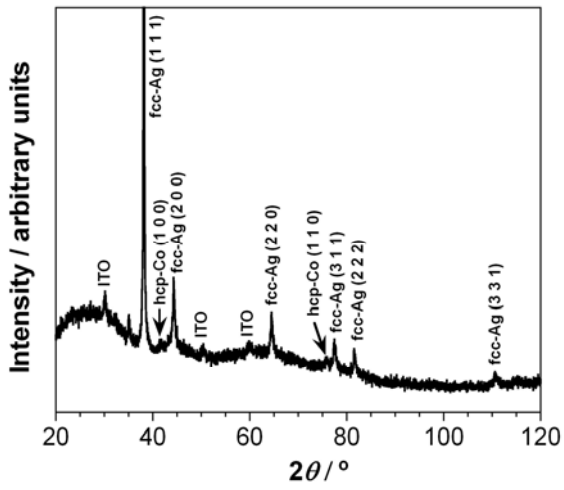

Figure 3. XRD pattern of Co-Ag deposit. 27.5 wt.% Co.

Figure 4A shows a TEM image of as-deposited Co-Ag films prepared from a bath containing 0.4 M in Co(II). A random distribution of nanometric particles (darker areas) in a matrix (lighter background) can be observed with a particle size distribution centred around 2-3 nm. However, particles of a few tens of nanometers are also detected (inset Fig. 4A). Keeping in mind that the maximum size of the cobalt clusters to be superparamagnetic is about 10 nm [25] we can say that a high percentage of the particles (around 70 %) are in the superparamagnetic regime. However, it is noteworthy that although the ferromagnetic particles are smaller in number, their volume fraction is important. When Co(II) bath cobalt concentration decreased, a narrower size distribution was observed.

The SAED pattern of the granular coatings (Fig. 4B) is a complex ring pattern characteristic for polycrystalline materials. The *d* values calculated from the positions of the most intense spots in the electron diffraction pattern agreed well with the *d* values reported for hcp-Co (100) and hcp-Co (101) planes and for the fcc-Ag (111) plane. Moreover, *d* values of 2.050 Å were also detected may corresponding to (0 0 2) hcp-Co, (1 1 1) fcc-Co or (2 0 0) fcc-Ag. The presence of fcc-Co is corroborated as less intense spots showed the characteristic 1.764 Å interplanar spacing for (2 0 0) fcc-Co. Those reflections observed by XRD have been also observed by TEM, both techniques being in agreement to each other.

HRTEM analyses were also performed in order to univocally establish the crystalline structure of films. Fast Fourier Transformation (FFT) analyses were performed on the HRTEM images (Fig. 5). Interplanar spacings typical of hcp-Co ($d_{(1\,0\,1)}$ = 1.992 Å and $d_{(1\,0\,0)}$ = 2.175 Å) were detected in the darker areas (spots 1, 2 and 3, 4, respectively. Upper FFT). Moreover, lattice spacings with *d* = 1.777 Å were found in some regions confirming the presence of fcc-Co. However, it is believed that hcp-Co is the main phase as it was more easily detected not only in all the FFT patterns taken but also in the SAED ones. On the other hand, *d* spacings of 2.344 Å attributed to fcc-Ag (1 1 1) were detected when the FFT analysis was performed in the lighter matrix (spots 5, 6. Lower FFT). Unlike it was expected, darker areas corresponds to cobalt-rich particles and the lighter matrix to silver. These results are in agreement with other related works [24,27].

From TEM analyses one can corroborate once again the heterogeneous nature of the material with a size distribution from superparamagnetic to ferromagnetic particles. Although intermixing between cobalt and silver at the interfaces can not be completely discarded, sharp magnetic/non-magnetic interfaces are expected as cobalt-rich particles surrounded by silver have been observed.

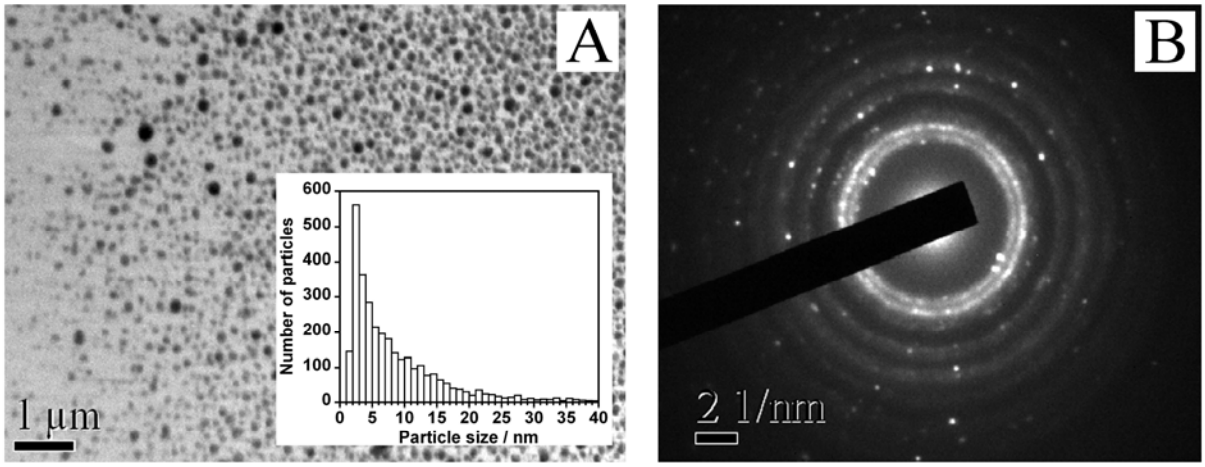

Figure 4. A) TEM micrograph of the as-deposited Co-Ag film with 40 wt.% Co and obtained from the solution 0.002 M $AgNO_3$ + 0.4 M $CoCl_2$ + 3.5 M NaCl. Inset shows the cobalt particles size distribution. B) SAED pattern.

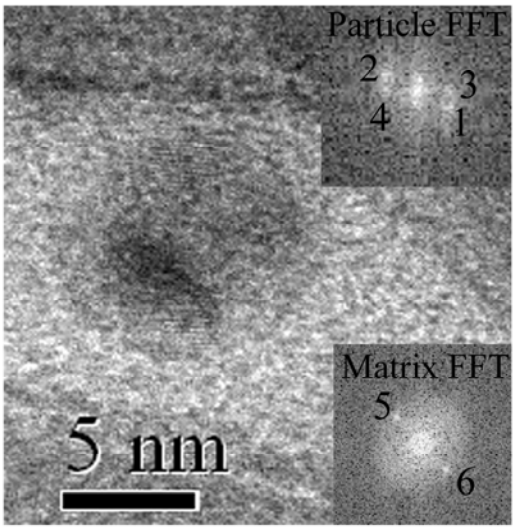

Figure 5. HRTEM micrograph of the as-deposited Co-Ag film with 40 wt.% Co and obtained from the solution 0.002 M $AgNO_3$ + 0.4 M $CoCl_2$ + 3.5 M NaCl. Insets show the FFT patterns taken in both the matrix and the particles.

3.3.- Magnetoresistance

The magnetotransport properties of the Co-Ag samples obtained from the 0.02 M Co(II) solution were firstly studied. All the samples measured showed GMR behaviour, since both LMR and TMR curves are negative in the whole field range. Figure 6 shows a typical room-temperature magnetoresistance curve. All the MR curves measured share some characteristics. On one hand, the saturation of the magnetoresistance can not be achieved even at the + 8 kOe field limit due to the presence of superparamagnetic particles. On the other hand, a clear splitting of the MR curves is observed in all the samples measured. Comparing LMR and TMR curves one could observe that LMR was normally slightly smaller in magnitude. The difference between the LMR and TMR components is defined as the anisotropic magnetoresistance AMR = LMR-TMR and arises from the presence of ferromagnetic particles. The highest magnetoresistance measured in the whole composition range studied was 1.23 %. These results make this electrolyte feasible to be used as electrodeposition bath, however further optimization is required. In this sense, it was decided to increase cobalt concentration in the electrolyte.

3.3.1.- Influence of cobalt concentration in solution

The dependence of both bath cobalt concentration and percentage of cobalt into the Co-Ag films on the GMR values has been studied. In this sense, different series of films were made. The series consisted on the preparation of Co-Ag thin films of various compositions from solutions containing 0.1 M, 0.2 M, 0.3 M and 0.4 M Co(II) concentrations. Again, all the samples measured showed GMR. The magnetoresistance curves presented the same features than those previously described.

A clear film composition dependence of the magnetoresistance has been observed for all the solutions tested (Fig. 7). For a certain Co(II) concentration, the magnetoresistance values increase with the ferromagnetic metal content up to a maximum and then drop off at higher cobalt contents. The maximum GMR values were observed in the range 28-36 wt.% Co, however the wt.% Co corresponding to the magnetoresistance peak value depended on the solution Co(II) concentration. The maximum GMR shifts toward higher wt.% Co and diminishes its value as bath cobalt concentration increases. The maximum magnetoresistance value achieved was 5.75 % obtained from the 0.1 M Co(II) solution.

Giant magnetoresistance mainly arises from the spin-dependent scattering at the interfaces between granules and the matrix, and to a lesser extent from that within the granules. Assuming this mechanism, the grain size, the surface area to volume ratio as well as the density of particles plays an important role on the magnetoresistance.

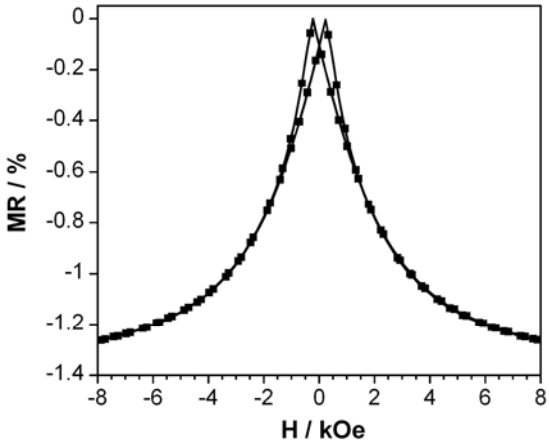

Figure 6. Magnetoresistance curve of the as-deposited Co-Ag film with 25 wt.% Co obtained from the solution 0.002 M $AgNO_3$ + 0.02 M $CoCl_2$ + 3.5 M NaCl at room temperature.

For films with low cobalt content, the low GMR values measured could be explained in view of the large interparticle separation and the small number of particles. Both factors reduce the scattering centres, thus leading to small magnetoresistance values. Moreover, there is less likelihood of coupling between the magnetic regions which could be a contributing factor to the decreased GMR. The later increment in the MR with cobalt content is related to the higher surface area to volume ratio. The higher this ratio is, the higher the scattering centres number is, and hence the higher the GMR is.

Beyond the maximum, the weakening of GMR is related to the clustering of Co granules giving rise to larger particle sizes, conditions where percolation effect sets in. At these conditions, a slight anisotropic contribution was observed in thin films with Co contents higher than around 60 wt.%. These results are in agreement with previous works in which GMR only appears in samples with volume fraction less than 55 %, which is precisely the percolation volume threshold for granular systems [28-30]. At these conditions, large clusters would lead to a decrease in the surface area to volume ratio, which in turn implies a decrease in the scattering centres with a consequent decrease in GMR.. The observed MR decrease with bath Co(II) concentration could also be related with the higher cobalt particle size.

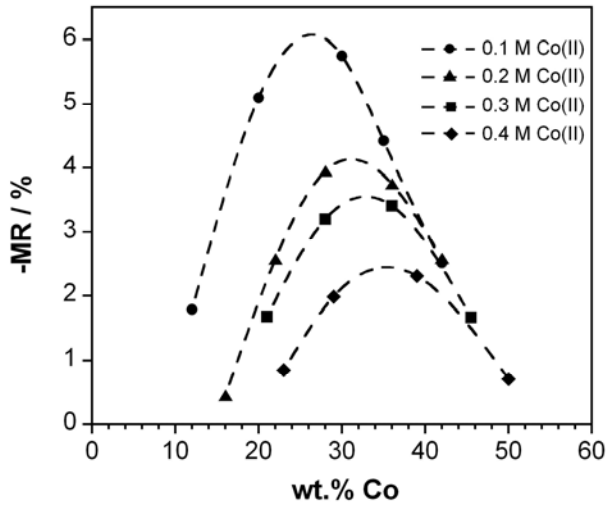

Figure 7. GMR dependence on film's cobalt percentage and bath cobalt content.

The explanation of the observed differences should be made according to the underlying electrochemical processes governing the film's growth. The electrochemical method used for the fabrication of the samples is based on the application of a fixed potential during a given time to make the desired charge flow. The applied potential is modified in order to get a composition range. However, we must keep in mind that the more negative potentials favour nucleation against growth in such a way that the more negative the applied potential, the higher the cobalt particle number and the smaller the particle size. All these factors contribute positively to the GMR leading to an increase in it as the cobalt content increases. However, applying even more negative potentials the nearness between the particles favours coalescence which is detrimental to GMR.

In an opposite way, grain growth is favoured over nucleation as bath cobalt concentration increases leading to bigger cobalt grains. According to it, GMR values are expected to be lower when comparing deposits with the same cobalt percentage but obtained from more cobalt-concentrated solutions, results in agreement with those obtained by TEM. Likewise, the maximum in the MR versus wt.% Co curve is reached at higher Co contents as it is necessary to apply more negative potentials to attain an important cobalt particle number of low size to favour GMR.

Another piece of evidence of the cobalt particle mean size variation is the higher or lesser AMR contribution. In granular systems containing only SPM particles the LMR and TMR components are usually indistinguishable since bulk-like scattering events leading to AMR cannot occur due to the small size of the magnetic (SPM) regions. In this study, the no coincidence between LMR and TMR curves is indicative of the presence of some FM particles. Despite the presence of anisotropic magnetoresistance, very low AMR values were detected making clear that the main contribution to the total magnetoresistance comes from the presence of the superparamagnetic particles. Table 1 shows the AMR values obtained in films with different cobalt percentages. The lowest AMR value is detected in the film with the highest GMR as the smallest particles are present. On the other hand, the effect of the electrolyte composition on the AMR is also shown (Table 2). The observed increase in the particle size as solution cobalt concentration increases leads to an increase in the AMR contribution.

Table 1. Anisotropic magnetoresistance dependence on film's composition obtained from a solution containing 0.1 M Co(II).

wt.% Co	$-LMR_{Experimental}$ / %	$-TMR_{Experimental}$ / %	AMR / %
12.0	1.79	1.91	0.12
20.0	5.10	5.18	0.08
30.0	5.75	5.80	0.05
35.0	4.42	4.59	0.17
42.0	2.51	2.73	0.22

Table 2. Anisotropic magnetoresistance dependence on bath composition.

wt.% Co	[Co(II)] / M	$-LMR_{Experimental}$ / %	$-TMR_{Experimental}$ / %	AMR/%
28.0	0.02	1.23	1.23	0.00
30.0	0.10	5.75	5.80	0.05
28.0	0.20	3.95	4.12	0.17
28.0	0.30	3.20	3.42	0.22
29.0	0.40	1.99	2.26	0.27

3.3.2.- Film thickness dependence

The influence of the nominal film thickness on the GMR values was investigated in films obtained from the 0.1 M Co(II) solution, as the highest GMR values were measured. Films with the same cobalt content but different thicknesses were prepared. The observed tendency for all the film compositions investigated is an increase of the MR values with increasing film thickness up to around 840 nm (Fig. 8). Further increase of the thickness led to a decrease on the magnetoresistance values.

The observed trend may be explained by a slight increase in the particle size as the thickness increases until reaching the optimum value. Further increase leads to a diminution of the surface area to volume ratio and thus a GMR decrease. A maximum GMR of 5.85 % was obtained.

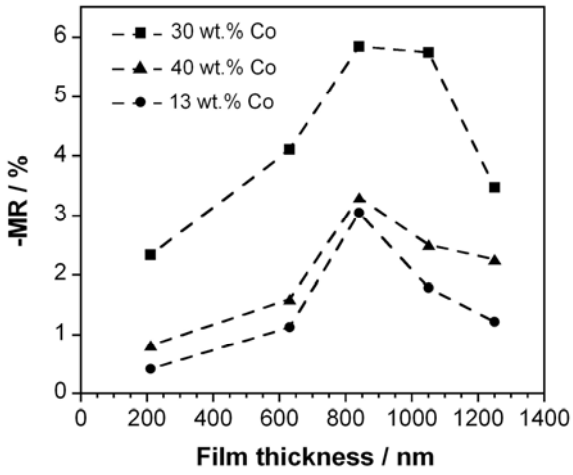

Figure 8. GMR dependence on film's thickness.

3.3.3.- Numerical analysis

Depending on the intrinsic characteristic of the magnetic/non-magnetic metallic nanostructures the field dependence of the giant magnetoresistance can be described by different models. Whereas for granular systems composed exclusively of superparamangetic (SPM) particles the field dependence of the magnetoresistance was found to be proportional to the square of the magnetization (MR(H) α $[L(x)]^2$) [31,32], granular systems with a particle size distribution (from SPM to FM particles) follow a linear dependence (MR(H) α L(x)) (Wiser-Hickey model) [33,34], where L(x) is the Langevin function and $x=\mu H/K_BT$ with μ as the average magnetic moment of the SPM particles (it is usual to write $\mu=N\mu_B$, where μ_B is the Bohr magneton and then N can be used as a parameter characterizing the average macrospin of the particle).

The simultaneous presence of both SPM and FM particles requires distinguishing between three cases when considering the spin-dependent scattering events taking place along the general path "magnetic region 1 → non-magnetic region → magnetic region 2": I) both magnetic particles are SPM, II) both magnetic particles are FM and III) one of the magnetic particles is SPM and the other is FM. Each of these three contributions is different to the field dependence of the magnetoresistance because of the magnetic field needed to align the magnetic moments of either FM or SPM particles is very different. Whereas for FM particles the magnetic field is typically a few kOe, fields above a ten of kOe are required to saturate the SPM granules. Case I) corresponds to that previously described for which MR(H) depends on the square of the magnetization as all the granules are SPM. For case II), small magnetic fields are needed to saturate the magnetic moments of the FM particles, and hence no further effect of the magnetic field on the resistance is observed. Therefore, case II) makes no contribution at all to MR(H) at large fields. However, when considering case III) at high magnetic fields where the magnetic moments of the FM particles are completely aligned, the correlation of the magnetic moments involved in the scattering process depends on the time average of the spatial orientation of one SPM particle moment following the MR(H) α L(x) relation. Accordingly, the spin-dependent scatterings that mainly contribute to the GMR effect are those involving FM particles (case II) and case III)). These contributions will be denoted as GMR_{FM} (FM contribution) and GMR_{SPM} (SPM contribution), respectively.

Keeping in mind the HRTEM and magnetotransport measurements presented above, the electrodeposited Co-Ag thin films analyzed in this work show a particle size distribution. For this reason, the procedure suggested in ref. [35] was applied to decompose the magnetoresistance into its FM and SPM contributions. Assuming that for magnetic fields $H > H_S$, the MR(H) data can be well described as

$$MR(H) = MR_{FM} + GMR_{SPM}\, L(x) \qquad (1)$$

whereby $MR_{FM} = AMR + GMR_{FM}$ is a constant term and H_s is the saturation field of the FM region.

The measured MR(H) data are fitted with the Langevin function for magnetic fields beyond the FM saturation ($H_s \approx$ 1.7 kOe) for both the LMR and TMR components and this provides the $GMR_{SPM}(H)$ contribution. When subtracting this contribution from the experimental data, we are left with the $MR_{FM}(H)$ contribution. As it can be observed in Figure 9, the MR(H) data above H_s was reasonably well fitted with the MR(H) α L(x) relation. Moreover, the analysis is able to reflect the different SPM and FM contribution of the magnetoresistance curves. Table 3 shows the measured GMR values as well as the results obtained from the numerical

analysis as the GMR once all the magnetic moments would be aligned with the applied magnetic field ($GMR_{Saturation}$), the GMR_{SPM} and the MR_{FM} terms and the relative weight of each contribution (%SPM, %FM) for the different electrodeposition baths. A common characteristic of all the samples measured is the clear dominance of the GMR_{SPM} term whatever the longitudinal or transverse magnetoresistance is measured. Similar general trends have been observed for all the baths analyzed: the relative weight of the SPM contribution (% SPM) initially increases up to a maximum and then drops off as the wt.% Co increases into the film. It is important to highlight that the highest superparamagnetic contributions were observed in the deposits obtained from the 0.1 M $CoCl_2$ solution, deposits which also showed the highest GMR values. Moreover, for a given bath composition the highest GMR is observed when the SPM contribution is also the highest. These data are in agreement with the electrochemical interpretation of the process: as the applied potential is made more negative cobalt granules are smaller in size, thus SPM contribution increases. Beyond the maximum, the coalescence of the particles gives rise to a SPM contribution diminution. On the other hand, the higher the bath Co(II) concentration, the higher the FM contribution as higher particle sizes were probably obtained.

The decomposition procedure was also applied to the MR curves of the films with different thicknesses. Films with the same cobalt content but different thicknesses were compared (Table 4). For a given film composition, the thicker the film is the lower the SPM contribution is. The same trend has been observed in the whole composition range studied. Similar results were obtained when TMR curves were analyzed.

The above discussion and the experimental data support the statement that in granular systems containing a particle size distribution (from SPM to FM particles) and whatever the applied magnetic field the main electron path leading to spin-dependent scattering events is "FM particle → non-magnetic region → SPM particle (or the inverse path). The reason for such scattering to take place along the whole magnetic field range is the random distribution of the SPM magnetic moments even at the highest applied field. Electrons polarized in a FM(SPM) particle will reach within the mean free path length another SPM(FM) particle with a high probability of a different local magnetization orientation and hence it will undergo a spin-dependent scattering. On the other hand, the electron path "FM particle 1→ non-magnetic region → FM particle 2 also contributes to the GMR at low applied magnetic fields. As it has been previously shown, the MR_{FM} term is the sum of two contributions: AMR + GMR_{FM}. Although up to now there is no way to quantitatively know each contribution separately, it can be said that GMR_{FM} term is dominant in these granular films as the AMR values found are very small.

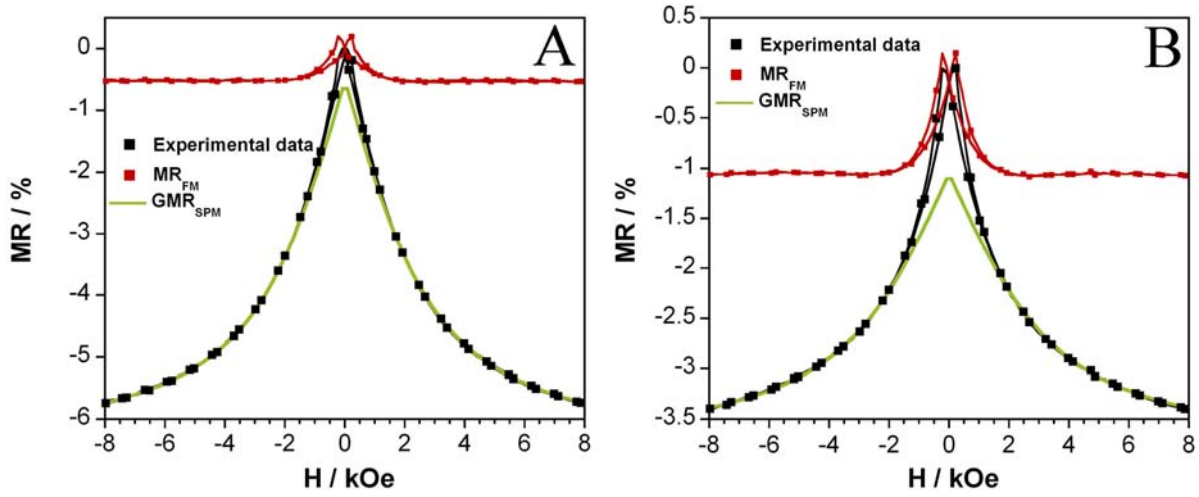

Figure 9. Decomposed longitudinal magnetoresistance data for Co-Ag coatings with different SPM and FM contributions. Co-Ag coatings obtained from the solutions A) 0.002 M $AgNO_3$ + 0.1 M $CoCl_2$ + 3.5 M NaCl and 30 wt.% Co and B) 0.002 M $AgNO_3$ + 0.3 M $CoCl_2$ + 3.5 M NaCl and 40 wt.% Co.

Table 3. Magnetoresistance dependence on film's composition. Decomposition of the total magnetoresistance into its superparamagnetic (GMR_{SPM}) and ferromagnetic (GMR_{FM}) contributions. The relative weight of the SPM (%SPM) and FM (%FM) contributions are also shown.

[Co(II)] = 0.1 M						
wt.% Co	$-GMR_{Experimental}$ / %	$-GMR_{Saturation}$ / %	$-GMR_{SPM}$ / %	$-MR_{FM}$ / %	% SPM	% FM
12.0	1.79	1.86	1.63	0.23	87.63	12.37
20.0	5.10	5.95	5.38	0.57	90.42	9.58
30.0	5.75	6.69	6.15	0.54	91.93	8.07
35.0	4.42	5.65	4.96	0.69	87.79	12.21
42.0	2.51	2.93	2.51	0.42	85.67	14.33
[Co(II)] = 0.2 M						
wt.% Co	$-GMR_{Experimental}$ / %	$-GMR_{Saturation}$ / %	$-GMR_{SPM}$ / %	$-MR_{FM}$ / %	% SPM	% FM
16.0	0.45	0.54	0.43	0.11	79.63	20.37
22.0	2.57	3.22	2.6	0.62	80.75	19.25
28.0	3.95	4.49	3.71	0.78	82.63	17.37
35.0	3.41	3.98	3.22	0.76	80.90	19.10
42.0	2.58	2.98	2.31	0.67	77.52	22.48
[Co(II)] = 0.3 M						
wt.% Co	$-GMR_{Experimental}$ / %	$-GMR_{Saturation}$ / %	$-GMR_{SPM}$ / %	$-MR_{FM}$ / %	% SPM	% FM
21.0	1.68	2.01	1.52	0.49	75.62	24.38
28.0	3.20	3.70	2.87	0.83	77.57	22.43
36.0	3.41	3.90	3.05	0.85	78.21	21.79
45.5	1.67	2.01	1.51	0.50	75.12	24.88
[Co(II)] = 0.4 M						
wt.% Co	$-GMR_{Experimental}$ / %	$-GMR_{Saturation}$ / %	$-GMR_{SPM}$ / %	$-MR_{FM}$ / %	% SPM	% FM
23.0	0.85	0.97	0.65	0.32	67.01	32.99
29.0	1.99	2.23	1.51	0.72	67.71	32.29
39.0	2.31	2.62	1.81	0.81	69.08	30.92
50.0	0.71	0.93	0.62	0.31	66.67	33.33

Table 4. Magnetoresistance dependence on film's thickness. Decomposition of the total magnetoresistance into its superparamagnetic (GMR_{SPM}) and ferromagnetic (MR_{FM}) contributions. The relative weight of the SPM (%SPM) and FM (%FM) contributions are also shown.

Thickness / nm	wt.% Co	$-GMR_{Experimental}$ / %	$-GMR_{Saturation}$ / %	$-GMR_{SPM}$ / %	$-MR_{FM}$ / %	% SPM	% FM
210	12.0	0.42	0.49	0.45	0.04	91.84	8.16
630	12.0	1.13	1.22	1.11	0.11	90.98	9.02
840	12.0	3.05	3.63	3.27	0.36	90.08	9.92
1050	12.0	1.79	1.86	1.63	0.23	87.63	12.37
1250	12.0	1.22	1.39	1.16	0.23	83.45	16.55
210	30.0	2.34	2.60	2.45	0.15	94.23	5.77
630	30.0	4.11	4.77	4.42	0.35	92.66	7.34
840	30.0	5.85	7.33	6.76	0.57	92.22	7.78
1050	30.0	5.75	6.69	6.15	0.54	91.93	8.07
1250	30.0	3.48	4.10	3.64	0.46	88.78	11.22
210	42.0	0.82	0.91	0.85	0.06	93.41	6.59
630	42.0	1.60	1.90	1.72	0.18	90.53	9.47
840	42.0	3.31	3.94	3.54	0.40	89.85	10.15
1050	42.0	2.51	2.93	2.51	0.42	85.67	14.33
1250	42.0	2.26	2.69	2.25	0.44	83.64	16.36

3.4.- Magnetic properties

The magnetic properties of Co-Ag films were analyzed by recording hysteresis loops. Figure 10A shows two representative magnetization-magnetic field dependences. A clear ferromagnetic behaviour is observed whatever the film cobalt content is. No important changes in the coercive field were obtained. On the other hand, saturation magnetization (M_s) is reached at relatively small magnetic fields, the saturation field being smaller for a film with 20 wt.% Co than for a 30 wt.% Co film. This result is in agreement with the MR(*H*) decomposition procedure in which a higher ferromagnetic contribution was observed for the film with 20 wt.% Co. The saturation value of the magnetization (which has been calculated dividing by the total weight of the sample) is around 30 emu/g for 20 wt.%Co and 80 emu/g for 30 wt.% Co. If the weight of the ferromagnetic metal is only taken into account, the magnetization of saturation is fairly close to that of pure cobalt metal. This fact suggests that the phase separation between Co and Ag is nearly complete.

Figure 10B displays the MR(*H*) dependencies for the same samples than in figure 10A. Apparent disagreement between both measurements seems to be observed: *M*(*H*) curves saturate at relatively low magnetic fields, whereas MR(*H*) show no sign of saturation even in the maximum field available. Such difference is attributed to the fact that magnetization is determined by the volume fraction of the two components only; whereas magnetoresistance strongly depends on the mutual spatial arrangement of the two kinds of regions. Keeping in mind the TEM results, the volume fraction of the ferromagnetic particles is important if comparing with that of the superparamagnetic particles, being the FM particles the responsible for the magnetic behaviour. On the other hand, the non-saturating behaviour of the MR(*H*) curves is due to the high number of superparamagnetic particles.

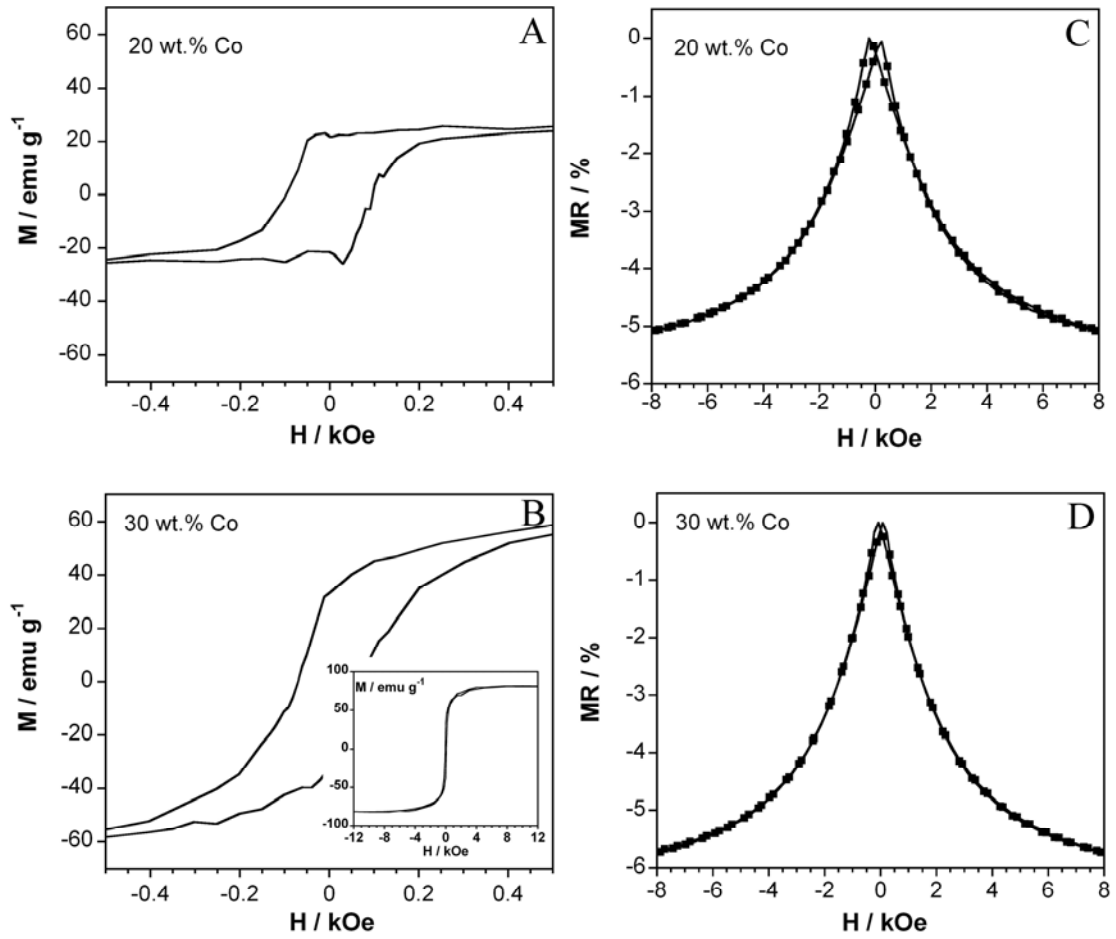

Figure 10. A, B) *M-H* loops of Co-Ag coatings obtained from the solution 0.002 M $AgNO_3$ + 0.1 M $CoCl_2$ + 3.5 M NaCl and different cobalt percentages and C, D) MR(*H*) curves.

4. Conclusions

We have investigated the structural, magnetic and magnetotransport properties of Co-Ag heterogeneous films prepared by electrodeposition. A simple method as chronoamperometry technique was employed to grow the magnetoresistive material. The deposition conditions (i.e. Co(II) concentration in the electrolyte, applied potential) and the film thickness were modified in order to gain knowledge on the influence of those parameters on the magnetoresistance effect.

The electrochemical and structural techniques revealed the GMR-required film heterogeneous nature as Co-rich particles (with a mixture of hcp and fcc structures) dispersed into the fcc-silver matrix were detected. Clear film composition-magnetoresitance dependence was observed for all the baths studied: as the film Co content increases, the number of scattering centres and then magnetoresistance increases up to a maximum. The connection between particles plays the main role in the decrease of MR for higher Co contents. GMR values up to 5.85 % were measured at room temperature in the as-deposited samples.

The understanding of the electrochemistry of the process has been helpful in understanding the GMR variation in electrodeposited films. The electrodeposition conditions clearly influenced the deposit's microstructure (different superparamagnetic particle/ferromagnetic particle ratios) which in turn affected the magnetotransport properties.

It is also worthy to mention that the GMR values reported here are higher than those published in previous works dealing with electrodeposited Co-Ag granular films [22,23]. Moreover, these values are even higher than those published in recent studies in which physical methods as RF sputtering were employed [36] but lower than other physical methods [37].

Acknowledgments

This paper was supported by contract MAT-2006-12913-C02-01 from the Comisión Interministerial de Ciencia y Tecnología (CICYT). J. García-Torres would also like to thank the Departament d'Innovació, Universitats i Empresa of the Generalitat de Catalunya and Fons Social Europeu for their financial support.

References

[1] M. N. Baibich, J. M. Broto, A. Fert, F. Nguyen Van Dau, F. Petroff, P. Etienne, G. Creuzet, A. Friederich and J. Chazelas, *Phys. Rev. Lett.*, 1988, **61**, 2472.

[2] G. Binasch, P. Grünberg, F. Saurenbach and W. Zinn, *Phys. Rev.* B, 1989**,** **39**, 4828.

[3] A. E. Berkowitz M. J. Carey, J. R. Michell, A. P. Young, S. Zhang, F. E. Spada, F. T. Parker, A. Hutten and G. Thomas**,** *Phys. Rev. Lett*., 1992**,** **68**, 3745.

[4] J. Q. Xiao, J. S. Jiang and C. L. Chien, *Phys. Rev. Lett*., 1992**,** **68**, 3749.

[5] A. Tiwari, S. Rout, P. B. Patil and M. S. Kumar, J. *Nanoscience and Nanotechnology*, 2007, **7(6)**, 2076.

[6] C. Wang, X. Xiao, H. Hu, Y. Rong and T. Y. Hsu, *Physica B: Condensed Matter,* 2007, **392 (1-2)**, 72.

[7] B. Larde, J. M. Le Breton, F. Richonme, A. Maignan and J. Teillet, *J. Magn. Magn. Mat.*, 2004, **272-276**, 1714.

[8] G. Xiao, J. Q. Wang and P. Xiong, *Appl. Phys. Lett.*, 1993, **62**, 420.

[9] J. A. Barnard, S. Hossain, M. R. Parker, A. Waknis and M. L. Watson, *J. Appl. Phys.*, 1993, **73**, 6372.

[10] S. Rubin, M. Holdenried and H. Micklitz, *J. Magn. Magn. Mat.*, 1999, **203**, 97.

[11] T. Sugiyama and O. Nittono, *Thin Solid Films*, 1998, **334(1-2)**, 206.

[12] S. Honda, H. Yamane, M. Nishino and M. Nawate, *J. Magn. Magn. Mat.*, 1998, **193(1-3)**, 492.

[13] K. Tonooka and O. Nishinura, *Appl. Surf. Science*, 2001, **169-170**, 500.

[14] J. Q. Wang and G. Xiao, *Phys. Rev. B,* 1994, **49**, 3982.

[15] S. S. P. Parkin, R. F. C. Farrow, T. A. Rabedeau, R. F. Marks, G. R. Harp, Q. H. Lam, M. Toney, R. Savoy and R. Geiss, *Euro. Phys. Lett.*, 1993, **22**, 455.

[16] Alloy phase diagram in: Hugh Barker (Eds), ASM Handbook, vol 3. ASM International. Ohio 1992.

[17] T. Cohen-Hyams, W. D. Kaplan, D. Aurbach, Y. S. Cohen and J. Yahalom, *J. Electrochem. Soc.*, 2003, **150(1)**, C28.

[18] G. R. Pattanaik, D. K. Pandya and S. C. Kashyap, *J. Alloys and Compounds*, 2001, **326(1-2)**, 260.

[19] S. Ge, H. Li, C. Li, L. Xi, W. Li and J. Chi, *J. Phys. Condens. Matter*, 2000, **12(27)**, 5905.

[20] V. M. Fedosyuk, D. Ravinder and J. Blythe, *J. Magn. Magn. Mat.*, 1996, **156(1-3)**, 77.

[21] S. Pané, E. Gómez and E. Vallés E., *J. Electroanal. Chem.*, 2006, **596(2)**, 87.

[22] S. Kenane, J. Voiron, N. Benbrahim, E. Chainet and F. Robant, *J. Magn. Magn. Mat.*, 2006, **297(2)**, 99.

[23] H. Zaman, A. Yamada, H. Fakuda and Y. Hueda, *J. Elechem. Soc.*, 1998, **145(29)**, 565.

[24] E. Gómez, J. Garcia-Torres and E. Vallés, *Anal. Chim. Acta,* 2007, **602**, 187.

[25] V. F. Puentes and K. M. Krishnan, *IEEE transactions on magnetics*, 2001, **37(4)**, 2210.

[26] W. Wang, F. Zhu, W. Lai, J-Q Wang, g. Yang, J. Zhu and Z. Zhang, *J. Phys. D: Appl. Phys*, 1999, **32**, 1990.

[27] H. Sang, N. Xu, J.H. Du, G. Ni, S. Y. Zhang and Y. W. Du, *Phys. Rev. B*, 1996, **53**, 15023.

[28] C. L. Chien, Q. Xiao and J. Jiang, *J. Appl Phys.*, 1993, **73(10)**, 5309.
[29] P. L. Li and B. E. Paton, *Phys. Lett.*, 1976, **56A**, 225.
[30] A. K. Nigam and A. K. Majumdar, *Phys. Rev. B*, 1983, **27**, 495.
[31] J. L. Gittleman, Y. Goldstein and S. Bozowski, *Phys. Rev. B*, 1972, **5**, 3609.
[32] S. Zhang, *Appl. Phys. Lett.*, 1992, **61**, 1855.
[33] N. Wiser, *J. Magn. Magn. Mater.*, 1996, **159**, 119.
[34] B. J. Hickey, M. A. Howson, S.O. Musa and N. Wiser, *Phys. Rev. B*, 1995, **51**, 667.
[35] I. Bakonyi, L. Péter, Z. Rolik, K. Kiss-Szabó, Z. Kupay, J. Tóth, L. F. Kiss and J. Pádár, *Physical Review B*, 2004, **70**, 054427.
[36] V.V. Hiep, N. Chau, D.M. Hong and N.H. Luong, *J. Magn. Magn. Mat.*, 2007, **310**, 2524.
[37] A. E. Berkowitz, J. R. Michell, M. J. Carey, A. P. Young, D. Rao, A. Starr, S. Zhang, F. E. Spada, F. T. Parker, A. Hutten and G. Thomas, *J. Appl. Phys.*, 1993**, 73(10)**, 5320.

Relevant GMR in as-deposited Co-Ag electrodeposits. Pulse plating preparation

Submitted

Relevant GMR in as-deposited Co-Ag electrodeposits: Pulse plating deposition

J. García-Torres*, E. Vallés, E. Gómez
Electrodep, Departament de Química Física i Institut de Nanociència i Nanotecnologia (IN²UB), Universitat de Barcelona, c/ Martí i Franquès, 1. 08028 Barcelona (Spain)

Keywords:
Co-Ag granular films
Heterogeneous films
Pulse plating
Giant magnetoresistance

A B S T R A C T

Electrodeposited cobalt-silver heterogeneous films with giant magnetoresistance prepared by means of pulse technique have been investigated. The size distribution indicates that films are composed of superparamagnetic particles, however ferromagnetic cobalt granules are also present. Magnetic and magnetotransport measurements support the presence of both kinds of particles. Structural analysis of the Co-Ag granular films revealed the presence of fcc-Ag and a mixture of hcp-Co and fcc-Co. No signs of solid solution were detected. GMR values up to 7% were measured at room temperature for the as-deposited films. High superparamagnetic contribution was observed in all conditions analyzed after the decomposition of the total magnetoresistance into its superparamagnetic and ferromagnetic contribution.

1. Introduction

The electrodeposition and the magnetotransport properties of electrodeposited Co-Ag granular films have been a very little-studied issue [1-3]. In such heterogeneous systems, GMR effect is mainly governed by the spin-dependent scattering of conduction electrons in the magnetic/non-magnetic interfaces. Thus, the magnitude of the GMR strongly depends on the size and the concentration of the ferromagnetic particles and therefore on the preparation method [4,5].

In a previous work of ours, we reported on the preparation of Co-Ag electrodeposits with GMR by chronoamperometry [6]. The selected electrolyte to perform the electrodeposition was 0.002 M $AgNO_3$ + x M $CoCl_2$ + 3.5 M NaCl, where $0.02 < x < 0.4$. In the electrodeposition bath the chloride ions act as complexing agent for silver. The highest solubility allowed for Ag(I) was 0.002 M. The influence of applied potential and hence film's composition, electrolyte Co(II)/Ag(I) ratio and film's thickness on the properties of Co-Ag films was analyzed. In all conditions tested, heterogeneous Co-Ag deposits with no signs of solid solution formation were detected. TEM analyses revealed that the deposits consisted of a random distribution of cobalt particles immersed in a silver matrix with a particle size distribution centred around 2-3 nm. Particles of a few tens of nanometers (up to 40 nm) were also detected.

A clear splitting around zero field and a non-saturating behaviour of the MR(*H*) curves measured at room temperatures were recorded being attributed to the presence of particles with ferromagnetic and superparamagnetic behaviour, respectively. A clear film composition dependence of the magnetoresistance was observed for all the solutions tested. The maximum GMR value measured was 5.85 % for a film with 30 wt.% Co and obtained from the solution containing 0.1 M Co(II). Out of this maximum, lower GMR values were measured attributed to either the low cobalt percentage or the coalescence of cobalt granules giving rise to larger particle sizes.

A quantitative analysis based on the decomposition of the MR(*H*) curves into its superparamagnetic (SPM) and ferromagnetic (FM) contributions allowed to discriminate the main electron path responsible of the GMR in these samples. The analysis revealed that the superparamagnetic contribution amounted up to around 90 % to the total magnetoresistance.

Keeping in mind the effect that the granule size exerts on the GMR and the possibility to modify it by the applied electrochemical signal i.e. shape and kind of the applied signal, in this work we report on the fabrication of Co-Ag granular films by pulse deposition. Different pulse sequences will be studied in order to try to improve the magnetotransport properties. An exhaustive analysis of the field dependence of the magnetoresistance will be presented. A comparison between the results obtained from both techniques is also considered.

2. Experimental

Co-Ag granular films were prepared from solutions containing $AgNO_3$, $CoCl_2$ and NaCl, all reagents being of analytical grade. All the solutions were freshly prepared with water first

double-distilled and then treated with a Millipore Milli-Q system. The composition of the solutions was 0.002 M $AgNO_3$ + x M $CoCl_2$ + 3.5 M NaCl with 0.1 M ≤ x ≤ 0.3 M. The pH was kept around 2.7 and the temperature was maintained at 25 ºC. Solutions were de-aerated by argon bubbling before each experiment and maintained under argon atmosphere during it.

Electrochemical experiments were performed in a conventional three-electrode cell using an Autolab with PGSTAT30 equipment and GPES software. Working electrodes were vitreous carbon (Metrohm) used for the basic electrochemical study and indium tin oxide (ITO) thin films sputtered on glass plates (thickness of ITO layer=25 nm) employed to grow the films. The vitreous carbon electrode was polished to a mirror finish using alumina of different grades (3.75 and 1.87 μm) and ultrasonically cleaned for 2 min in water before each experiment. ITO was cleaned with acetone, ethanol and rinsed in water before deposition. The reference electrode was an Ag/AgCl/1 M NaCl electrode. All potentials were referred to this electrode. The counter electrode was a platinum spiral.

In-situ electrochemical characterization was performed on low-charge deposits by anodic linear sweep voltammetry (ALSV). Voltammetric *stripping*s were always run in a blank solution (3.5 M NaCl) immediately after deposition and at a scan rate of 10 mV s^{-1}.

Deposit morphology was observed using Hitachi H-4100 FE field emission scanning electron microscope (FE-SEM). Elemental composition was determined with an X-ray analyser incorporated in Leica Stereoscan S-360 equipment. The samples were dissolved in HNO_3 3 % and analyzed by the electroanalytical methods previously developed [7] when it was necessary to determine the weight of the samples.

The structure of the deposits was studied with X-ray powder diffraction (XRD) using a conventional Bragg-Brentano diffractometer Siemens D-500. The Cu Kα radiation (λ= 1.5418 Å) was selected using a diffracted beam curved graphite monochromator. The X-ray powder diffraction diagrams were created in the 20-105º 2θ range with a step range of 0.05º and a measuring time of 9 seconds per step. The structure was also studied by using high resolution transmission electron microscopy (HRTEM) combined with selected area electron diffraction (SAED) using a JEOL 2100.

Magnetic measurements were taken in a SQUID magnetometer at room temperature in helium atmosphere. The magnetization-magnetic field curves were recorded maintaining the samples parallel to the applied magnetic field. Saturation magnetization values were given in emu g^{-1}, where g is the total weight of the sample.

The magnetoresistance (MR) measurements were performed at room temperature with the four-point-in-line method in magnetic fields between –8 kOe and +8 kOe in the field-in-plane/current-in-plane geometry. Both the longitudinal (LMR) and the transverse magnetoresistance (TMR) (field parallel to current and field perpendicular to current, respectively) components were recorded for each sample. The magnetoresistance was defined as follows:

$$MR(H) = 100*[R(H)-R(0)]/R(0)$$

where R(*H*) is the resistance in the magnetic field *H* and R(0) is the resistance when *H*=0.

3. Results and discussion

3.1.- Electrochemical study

Cyclic voltammograms performed on the studied solutions indicated two reduction peaks attributed to the deposition of both metals separately. Moreover, two oxidations peaks were recorded during the anodic-going scan related to the independent oxidation of the previously deposited elements. From these experiments, the potential window at which each process took place has been determined owing to establish potential ranges for film's electrodeposition.

Co-Ag films were grown by pulse deposition over ITO substrate. This electrochemical method is based on the application of alternating potentials for silver and cobalt deposition during short times. The electrodeposition parameters were carefully selected after an optimization process in which composition, and morphology were the parameters controlled. Silver deposition potential was selected sufficiently negative so that cobalt oxidation did not take place. In all the solutions studied, silver electrodeposition parameters were set at: E_{Ag} = -700 mV, t_{Ag} = 0.3 s; and the pulse length for cobalt deposition (t_{Co}) was 0.35 s. Cobalt applied potential (E_{Co}) was varied in order to modulate film's composition. Moreover, a third step was included at a potential where cobalt oxidation took place in a controlled manner in order to avoid the overgrowth of cobalt particles (E_{Ox} = -500 mV and t_{Ox} = 0.035 s). The applied signal to grow the films is shown in Figure 1A. Figure 1B shows the current profile recorded during one cycle of the deposition process. Due to the different concentration of both metals, cobalt-related current is much higher than that related to silver deposition. On the other hand, no significant increase on the reduction current density was observed during successive cycles probably associated to a no important increase on the surface roughness. Figure 1C shows a SEM image of a Co-Ag film obtained by pulse deposition. Independently of the pulse sequence applied all the films showed granular morphology. Moreover, compact and continuous deposits with no cavities were obtained in all the conditions tested and from the very beginning of the electrodeposition.

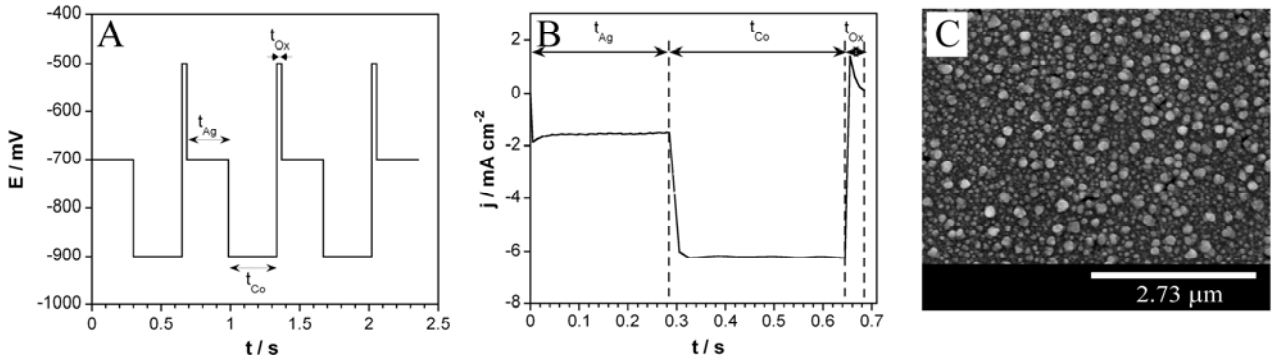

Figure 1. A) Applied signal to grow the Co-Ag films. B) Real signal recorded during the deposition process from the solution 0.002 M $AgNO_3$ + 0.2 M $CoCl_2$ + 3.5 M NaCl applying the signal of Fig. 1A. C) SEM image of the deposit prepared under the signal of Fig. 1B.

As the applied electrochemical signal may exert some changes in the microstructure of the deposits, i.e. variation of the grain size, *in-situ* electrochemical characterization was initially performed in order to compare the oxidation responses of low charge deposits (a few nanometers thick) obtained by the two different applied signals (either single step or pulse). Figure 2 shows the voltammetric *stripping* corresponding to potentiostatic and pulse deposited films with similar charge. Independently of the electrodeposition technique two clear oxidation peaks, attributed to cobalt and silver oxidation, were recorded and in agreement with the results found by cyclic voltammetry. Although both voltammetric *strippings* are qualitatively similar, an important difference can be observed: the width of the cobalt oxidation peak is greater in the potentiostatic deposits (Figure 2A, dashed line) than in the pulse deposited films (Figure 2A, continuous line). The difference could be attributed to the different cobalt particle size distribution obtained by means of both techniques. While a narrower size distribution is expected to be obtained by pulse deposition in accordance with the non-continuous nature of the applied signal; a broader size distribution is expected with potentiostatic method. The no observance of a sharp oxidation peak in the voltammetric *stripping* for the potentitiostatic deposits could be due to the fact that bigger particles are more difficult to be oxidized.

In order to confirm this hypothesis, the influence of the deposition potential and film's charge over the shape of the voltammetric curve for both kinds of deposits is examined. When comparing potentiostatic deposits of the same charge but prepared at different potentials one can observe that the more negative the applied potential the narrower the cobalt oxidation peak width (Figure 2B). This is due to the fact that nucleation is favoured over grain growth as the applied potential is made more negative, so grains with more similar and smaller size will be obtained at those potentials, in other words, the size distribution will be narrower and shifted toward smaller sizes. On the other hand, deposition charge clearly influences the shape of the cobalt oxidation peak depending on the applied signal (Figure 2C, 2D). Meanwhile a sharp decay of the current to zero is observed independently of the charge for the pulse deposited films, a continuous current decrease is observed in cobalt oxidation for the potentiostatic deposits, the zero current being not reached for higher charges (Figure 2D, dashed and dotted line). All the above exposed make think that pulse plating technique allows obtaining films with a narrower size distribution. Due to the observed differences between both techniques, it was decided to investigate the properties of Co-Ag films prepared by pulse deposition.

3.2.- Structural characterization

The XRD pattern of an as-deposited Co-Ag granular film is shown in Figure 3. Although the dominant peaks are due to the substrate because of the low thickness of the films, peaks attributed to the fcc structure of the silver matrix can be detected. As reported previously, it appears extremely difficult to detect cobalt in thin films by XRD [8], just two small peaks place at $2\theta = 47.1º$ and 56.7º could be attributed to hcp-Co (1 0 1) and fcc-Co (2 0 0), respectively. On the other hand, the no shift in the silver peaks and the observed agreement between the calculated silver lattice parameter (0.4083 nm) and that tabulated (0.4078 nm) suggested that Co-Ag solid solution formation did not take place.

TEM analyses demonstrate the heterogeneity of the Co-Ag films prepared. TEM image in Figure 4A shows quasi-spherical cobalt particles randomly dispersed in the silver matrix confirming the granular structure. Although the particle size distribution is centred around 1-2 nm, some particles up to around 20 nm could be detected. This size distribution is narrower than that observed in potentiostatic films by TEM, these results being also in agreement with

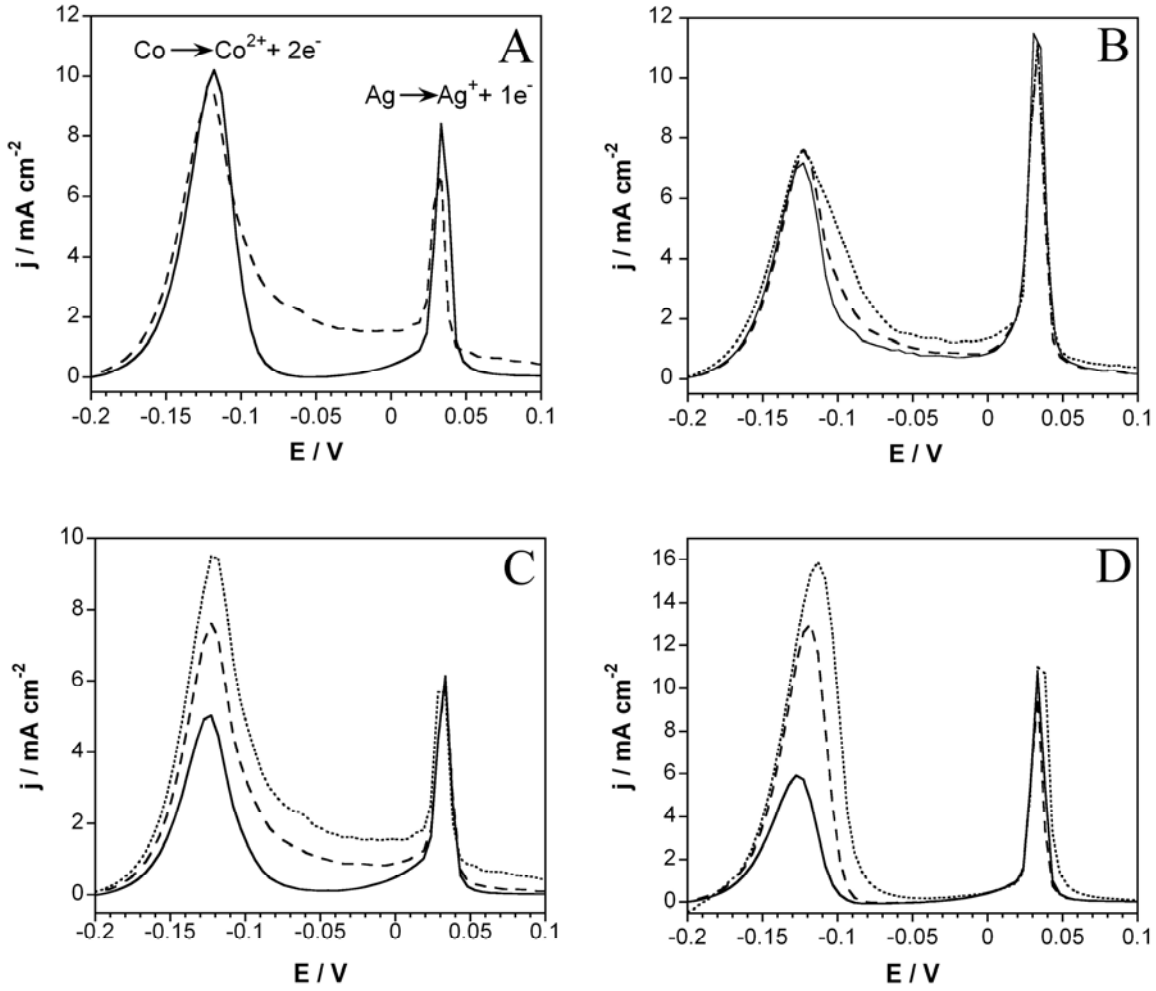

Figure 2. Voltammetric *strippings* of low-charge Co-Ag deposits prepared from the solution 0.002 M $AgNO_3$ + 0.2 M $CoCl_2$ + 3.5 M NaCl. A) Comparison of deposits prepared by means of different techniques: dashed line) potentitostatic film, Q = -110 mC cm^{-2} and continuous line) pulse deposited film, Q = -120 mC cm^{-2}. B) Comparison of the applied potential on potentiostatic films: continuous line) -850 mV, dashed line) -830 mV and dotted line) -800 mV. C) Comparison of the deposition charge on potentiostatic films: continuous line) -35 mC cm^{-2}, dashed line) -64 mC cm^{-2} and dotted line) – 110 mC cm^{-2}. D) Comparison of the deposition charge on pulse deposited films: continuous line) -45 mC cm^{-2}, dashed line) -60 mC cm^{-2} and dotted line) – 75 mC cm^{-2}.

those previously raised by ALSV electrochemical technique. On the other hand, electron diffraction was employed in order to clearly distinguish the crystalline structure of both metals. The SAED pattern (Figure 4B) not only confirms the presence of fcc-Ag but also indicates the presence of hcp-Co and fcc-Co. The *d* values calculated from the electron diffraction pattern agreed well with the values reported for the fcc-Ag (1 1 1) plane, hcp-Co (1 0 0) and hcp-Co (1 0 1) planes and for the fcc-Co (2 0 0) plane, results in agreement with those obtained by XRD.

3.3.- Magnetoresistance and magnetic properties

Figure 5 shows some longitudinal magnetoresistance (LMR) curves recorded from Co-Ag films obtained from the 0.2 M Co(II) solution with different composition. All the MR curves are characterized by a splitting around 0 kOe

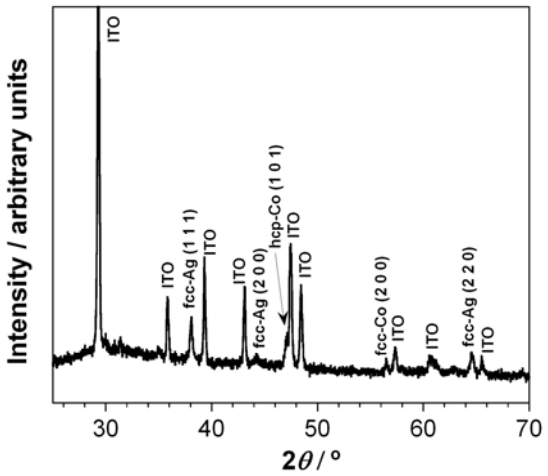

Figure 3. XRD pattern of an as-deposited Co-Ag film (28 wt.% Co) obtained from the solution 0.002 M $AgNO_3$ + 0.2 M $CoCl_2$ + 3.5 M NaCl. Nominal thickness 450 nm.

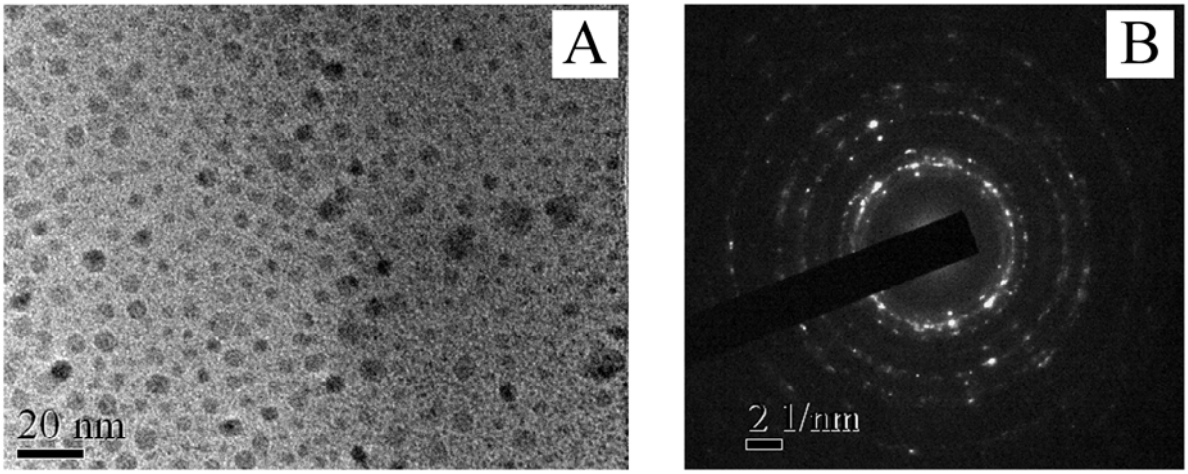

Figure 4. TEM micrograph of an as-deposited Co-Ag film (30 wt.% Co) obtained from the solution 0.002 M $AgNO_3$ + 0.2 M $CoCl_2$ + 3.5 M NaCl. B) SAED pattern.

related to the presence of ferromagnetic particles. No saturation of the MR field dependence was recorded even for the highest applied magnetic fields (+ 8 kOe) indicative of the superparamagnetic (SPM) character of some of the cobalt granules. The same behaviour was detected in the transverse magnetoresistance (TMR) curves. A clear film composition dependence of the magnetoresistance is observed (Figure 5). GMR initially increases with cobalt content up to a maximum and then it decreases as cobalt percentage increases. At low cobalt percentages, the low GMR is due to the small number of cobalt particles contributing to the magnetoresistance effect. On the other hand, at high cobalt contents the clustering of cobalt granules leads to a decrease in the surface-area to volume ratio with a consequent decrease in GMR. The same behaviour was observed in all the solutions tested (Table 1). Table 1 shows both the GMR experimental values measured at + 8 kOe ($GMR_{Experimental}$) and the calculated ones after complete alignment of the cobalt granules along the magnetic field direction, that is the GMR achieved at saturation ($GMR_{Saturation}$). The maximum experimental magnetoresistance value achieved was 7 % in a film with 25 wt.% Co obtained from the 0.2 M Co(II) solution.

Due to the alternation on the deposition potentials of both metals, the nucleation of one metal over the other is more favoured than grain growth. Moreover, nucleation is also favoured as the applied potential is made more negative. Keeping it in mind, the first observed increase in the magnetoresistance with the increase in cobalt content (increase associated with the more negative potential values) is related to the increase in the surface area to volume ratio due to the higher number of magnetic particles with a smaller size. Beyond the maximum, the nearness of the particles favours coalescence which is detrimental to GMR. The same behaviour has been observed for all the solutions tested. Too high bath cobalt concentrations could lead to the formation of extended ferromagnetic regions instead of small particles with a negative consequence on the magnetoresistance. The two opposite effects (the pulse signal favours nucleation but high Co(II) concentrations could give rise to the formation of extended magnetic regions) led obtaining the highest GMR value at an intermediate concentration (0.2 M Co(II)) as the most appropriate values for grain size, surface area to volume ratio and density of particles must be obtained, factors that play an important role in the magnetoresistance.

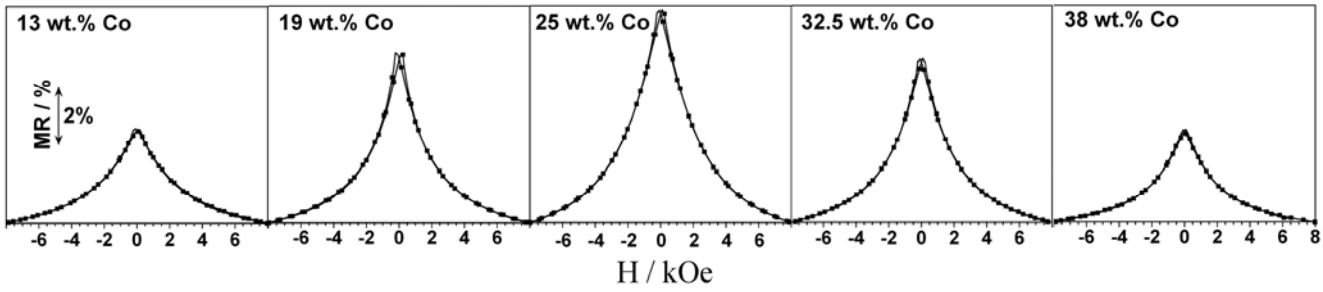

Figure 5. Longitudinal magnetoresistance curves measured at room temperature of as-deposited Co-Ag films with different compositions obtained from the solution 0.002 M $AgNO_3$ + 0.2 M $CoCl_2$ + 3.5 M NaCl.

Table 1. Magnetoresistance dependence on film's composition. Decomposition of the total magnetoresistance into its superparamagnetic (GMR_{SPM}) and ferromagnetic (GMR_{FM}) contributions. The relative weight of the SPM (%SPM) and FM (%FM) contributions are also shown. The magnetoresistance value once the magnetic moments are all aligned (GMRSaturation) is also obtained from the numerical analysis.

[Co(II)] = 0.1 M						
wt.% Co	$-GMR_{Experimental}$ / %	$-GMR_{Saturation}$ / %	$-GMR_{SPM}$ / %	$-GMR_{FM}$ / %	% SPM	% FM
13.00	2.48	2.98	2.73	0.25	91.61	8.39
23.00	5.39	6.23	5.78	0.45	92.74	7.26
27.00	2.89	3.21	2.94	0.27	91.59	8.41
32.00	2.30	2.64	2.47	0.17	93.56	6.44
45.00	1.24	1.39	1.21	0.18	87.13	12.87
[Co(II)] = 0.2 M						
wt.% Co	$-GMR_{Experimental}$ / %	$-GMR_{Saturation}$ / %	$-GMR_{SPM}$ / %	$-GMR_{FM}$ / %	% SPM	% FM
13.00	3.14	3.86	3.42	0.44	88.60	11.40
19.00	5.56	6.41	5.83	0.58	91.01	8.99
25.00	7.00	7.79	7.22	0.57	92.68	7.32
28.00	5.92	6.91	6.35	0.56	91.90	8.10
32.50	5.37	6.15	5.48	0.67	89.11	10.89
38.00	2.90	3.26	2.81	0.45	86.20	13.80
[Co(II)] = 0.3 M						
wt.% Co	$-GMR_{Experimental}$ / %	$-GMR_{Saturation}$ / %	$-GMR_{SPM}$ / %	$-GMR_{FM}$ / %	% SPM	% FM
14.00	2.38	2.72	2.23	0.49	81.99	18.01
17.00	3.00	3.34	2.77	0.57	82.93	17.07
20.00	3.56	4.28	3.59	0.69	83.88	16.12
24.50	5.27	6.21	5.32	0.89	85.67	14.33
31.00	5.38	6.29	5.58	0.71	88.71	11.29
35.00	3.84	4.40	3.72	0.68	84.46	15.54
43.00	1.80	2.12	1.75	0.37	82.57	17.43

The influence of the film's thickness was investigated in deposits obtained from the solution containing 0.2 M Co(II), after verifying that composition was nearly constant throughout the thickness. Figure 6 shows the magnetoresistance dependence on the nominal film's thickness for deposits with the same cobalt content. As it can be observed GMR initially increases with thickness up to around 450 nm and then it drops off at higher thicknesses. The observed increase in the GMR with the thickness could be related with the increase in the number of scattering centres. Further increase on the thickness could give rise to a more disordered distribution of both metals, leading to a GMR decrease.

A slight difference was recorded between LMR and TMR curves being attributed to bulk-like scattering events in the ferromagnetic particles, thus leading to the anisotropic magnetoresistance (AMR) term (AMR = LMR-TMR). The low values for the AMR term agree well with the quasi-spherical shape of the particles observed by TEM. Despite these low values, some tendencies could be observed depending on the film composition and bath

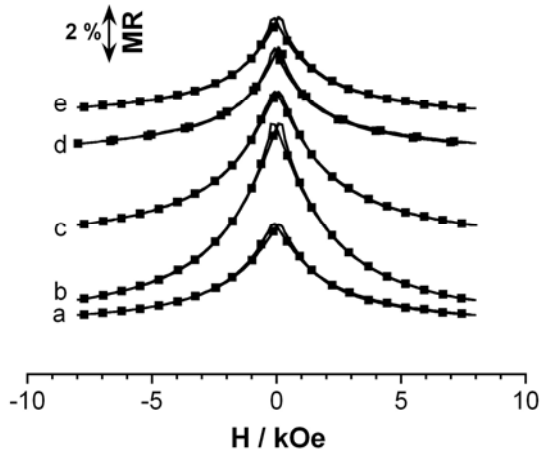

Figure 6. GMR dependence on film's thickness for an as-deposited Co-Ag film (28 wt.% Co). a) 225 nm, b) 450 nm, c) 900 nm, e) 1300 nm and f) 1800 nm.

Co(II) concentration (Table 2). From all the solutions AMR initially decreases with cobalt content which is in agreement with the presence of smaller particles obtained at higher potentials. However, further increase on the cobalt percentage leads to an increase in the AMR term as corresponds to the coalescence of the cobalt granules and the lost of spherical symmetry. However, slightly higher AMR values were obtained when bath cobalt concentration increased up to 0.3 M as corresponds to higher particle sizes.

Table 2. Anisotropic magnetoresistance dependence on film's composition for deposits obtained from the solution containing 0.2 M Co(II). Nominal thickness 450 nm.

wt.% Co	$-LMR_{Experimental}$ / %	$-TMR_{Experimental}$ / %	AMR / %
13.00	3.14	3.22	0.08
19.00	5.56	5.62	0.06
25.00	7.00	7.03	0.03
28.00	5.92	6.00	0.08
32.50	5.37	5.51	0.14
38.00	2.90	3.08	0.18

The field dependence of the magnetoresistance in granular systems can be described by different models depending on the size distribution. Whereas this dependence was found to be proportional to the square of the magnetization ($MR(H) \alpha [L(x)]^2$) in systems composed exclusively of SPM particles [9,10], granular systems with a particle size distribution (from SPM to FM particles) follow a linear dependence ($MR(H) \alpha L(x)$) [11,12], where $L(x)$ is the Langevin function. Keeping in mind TEM analyses and magnetotransport measurements presented above, the electrodeposited Co-Ag thin films analyzed in this work show a particle size distribution. For this reason, the numerical analysis suggested by Bakonyi *et al.* [13] and based on the Wiser-Hickey model was applied in order to decompose the total magnetoresistance into its FM and SPM contributions. According to [13], the MR(H) data for magnetic fields $H > H_s$ is properly fitted with the following equation

$$MR(H) = MR_{FM} + GMR_{SPM}\, L(x) \qquad (1)$$

whereby $MR_{FM} = AMR + GMR_{FM}$ is a constant term and H_S is the saturation field of the FM region

The measured MR(H) data are fitted with Eq. (1) for magnetic fields beyond the FM saturation ($H_S \approx 1.7$ kOe) for both the LMR and TMR components and this provides the $GMR_{SPM}(H)$ contribution as well as the GMR values once the magnetization of the magnetic particles are completely aligned ($GMR_{Saturation}$). When subtracting this contribution from the experimental data, we are left with the $MR_{FM}(H)$ contribution.

The MR fit results indicates that the main contribution to the total magnetoresistance is attributed to the GMR_{SPM} term whatever is the electrolyte composition (Table 1). The relative weight of the SPM contribution (% SPM) initially increases up to a maximum and then drops off as the wt.% Co increases into the film, so the lowest SPM contributions are observed at the ends of the curve. The maximum in the SPM contribution always corresponds with the highest GMR value measured for each solution. On the other hand, bath Co(II) concentration seems to exert some influence on the SPM contribution. While the superparamagnetic contribution is similar for 0.1 M and 0.2 M electrolyte cobalt concentrations; it significantly decreases for higher concentrations (0.3 M).

The decomposition procedure was also applied to the MR curves of the films with different thicknesses. Figure 7A shows the evolution of the $GMR_{Saturation}$, GMR_{SPM} and GMR_{FM} terms with film thickness for films with 28 wt.% Co. The GMR_{SPM} term is dominant in the whole thickness range studied. On the other hand, Figure 7B shows the evolution of the relative weight of both the SPM and the FM

contributions to the total MR. A slight decrease in the SPM contribution with film thickness is observed. The no significant variation is probably attributed to the pulse nature of the applied signal which assures nearly grain size constancy along thickness. The same trend has been observed in the whole composition range studied. Similar results were obtained when TMR curves were analyzed.

The hysteresis loops of the Co-Ag samples (Figure 8) confirm the ferromagnetic behaviour of all the films analyzed. Saturation magnetization (M_s) increased as cobalt content into the films increased, the M_s values being typical of that of bulk cobalt (around 160 emu g^{-1}) [14] when only the weight of the ferromagnetic metal was taken into account to calculate M_s. This fact corroborates that the phase separation between Co and Ag is complete.

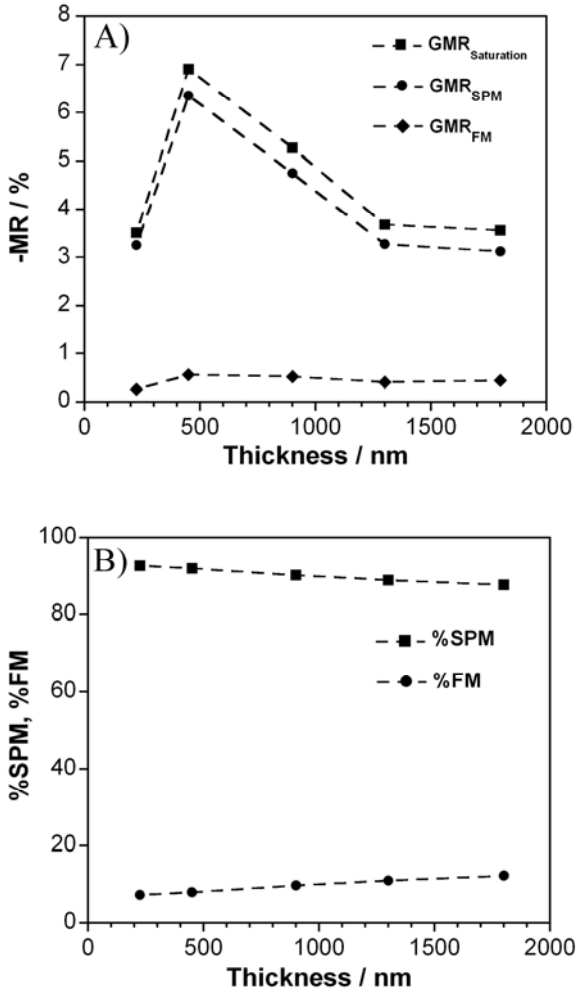

Figure 7. Results of the decomposition of the MR(H) curves into SPM and FM contributions as a function of the film thickness. A) $GMR_{Satutration}$, GMR_{SPM} and GMR_{FM} terms and B) relative weight of the SPM and FM contributions.

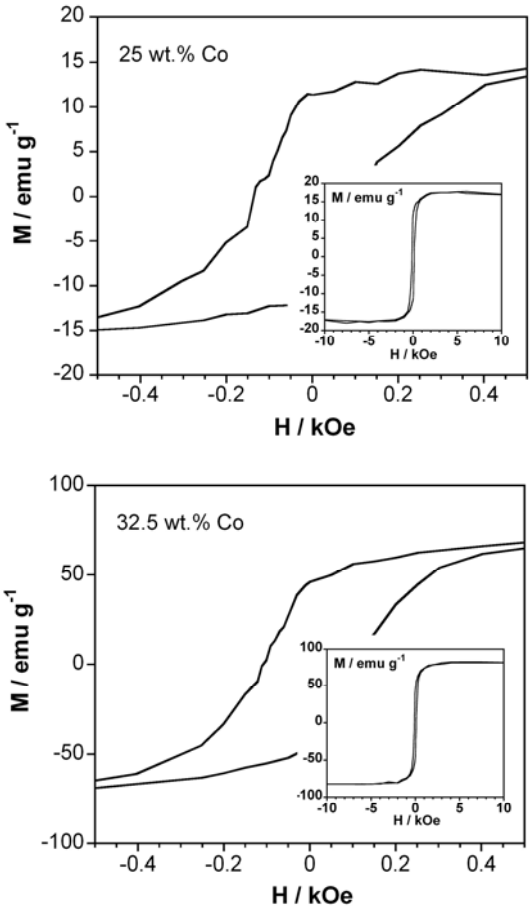

Figure 8. M-H loops of Co-Ag coatings obtained from the solution 0.002 M AgNO3 + 0.2 M CoCl2 + 3.5 M NaCl and different cobalt percentages. Insets try to show the magnetization saturation value.

The comparison between MR(H) curves and *M-H* loops of the same sample (Figure 9) show agreement between them since similar H_c and H_p (peak value in the MR(H) curve) values are recorded. However, unlike the shape of MR(H) curves the *M-H* loops show no signs of superparamagnetic behaviour as small magnetic fields are required to saturate the films. The difference lies on the fact that magnetization is determined by the volume fraction of the superparamagnetic and ferromagnetic particles only, whereas magnetoresistance also depends strongly on the mutual spatial arrangement of the two kinds of regions [15]. According to TEM analyses, although the particle's number of higher size is small, their volume fraction into the sample is important (V α r^3, and $V_{FM} = V_{SPM}(r_{FM}^3 / r_{SPM}^3)$ they being responsible for the observed behaviour in the *M-H* loops. On the other hand, SPM particles are the responsible of the non-saturating behaviour observed in the MR(H) curves.

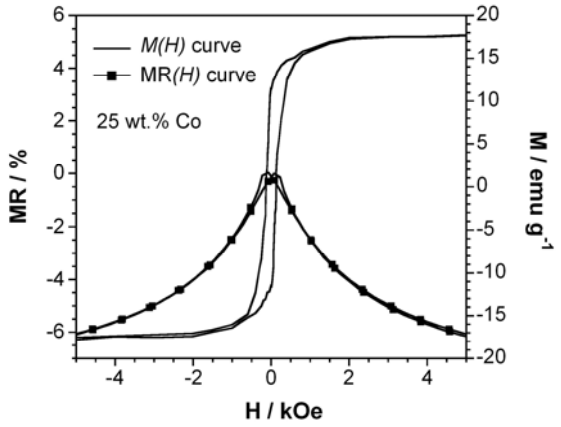

Figure 9. Comparison of MR(*H*) curves and *M-H* loops of the samples containing 25 wt.% Co.

4. Conclusions

The electrodeposition bath employed allowed obtaining films with different giant magnetoresistance values. These values were dependent on bath Co(II) concentration, film's composition and film's thickness and electrochemical technique.

The structural characterization revealed the presence of fcc-Ag and a mixture of hcp-Co and fcc-Co. The TEM analysis indicated that for a fixed solution, cobalt particle size distribution was narrower in pulse deposited films than in potentiostatic films with similar cobalt percentage. At these conditions the GMR values were greater for the deposits obtained by pulse plating, where GMR values as high as 7% on the as-deposited films were measured at room temperature.

Anodic linear sweep voltammetry (ALSV), a simple electrochemical technique, was demonstrated useful to roughly evaluate changes between the sizes distributions of the deposits obtained by means of both electrodeposition techniques employed.

In all conditions, the quantitative analysis of the magnetoresistance curves indicated that the main electron path responsible of the magnetoresistance effect was that involving ferromagnetic and superparamagnetic particles (the GMR_{SPM} term), which was clearly higher than the ferromagnetic contribution. It was also observed that higher SPM contributions were obtained for the pulse deposited films, where the higher GMR values were also measured.

Acknowledgments

This paper was supported by contract MAT-2006-12913-C02-01 from the Comisión Interministerial de Ciencia y Tecnología (CICYT). J. García-Torres would also like to thank the Departament d'Innovació, Universitats i Empresa of the Generalitat de Catalunya and Fons Social Europeu for their financial support.

References

[1] Zaman, H.; Yamada, A.; Fukuda, H.; Hueda, Y. *J. Electrochem. Soc.*, **1998**, *145(2)*, 565.

[2] Kenane, S.; Chainet, E.; Nguyen, B.; Kadri, A.; Benbrahim, N.; Voiron, *J. Electrochem. Comm.*, **2002**, *4*, 167.

[3] Kenane, S.; Voiron, J.; Benbrahim, N.; Chainet, E.; Robant, F. *J. Magn. Magn. Mat.*, **2006**, *297(2)*, 99.

[4] Xiao, J.Q.; Jiang, J.S.; Chien, C.L. *Phys. Rev. B*, **1992**, *46(14)*, 9266.

[5] Honda, S.; Nawate, M.; Tanaka, M.; Okada, T. *J. Appl. Phys.*, **1997**, **82(2)**, 764.

[6] Garcia-Torres, J.; Valles, E.;Gomez, E. Submitted.

[7] Gomez, E.; García-Torres, J.; Valles, E. *Anal. Chim. Acta,* **2007**, *602*, 187.

[8] Ohashi, K.; Ito, M.; Watanabe, M. Electrochemical technology in Electronics. The electrochemical Society Proceedings Series: Pennington (NJ), 1988.

[[9] Gittleman, J.L.; Goldstein, Y.; Bozowski, S. *Phys. Rev. B*, **1972**, *5*, 3609.

[10] Zhang, S. Appl. *Phys. Lett.*, **1992**, *61*, 1855.

[11] Wiser, N. *J. Magn. Magn. Mater.*, **1996**, *159*, 119.

[12] Hickey, B.J.; Howson, M.A.; Musa, S.O.; Wiser, N. *Phys. Rev. B*, **1995**, *51*, 667.

[13] Bakonyi, I.; Péter, L.; Rolik, Z.; Kiss-Szabó, K.; Kupay, Z.; Tóth, J.; Kiss, L. F.; Pádár, *J. Physical Review B*, **2004**, *70*, 054427.

[14] Nishikawa, M.; Kita, E.;Erats, T.; Tasaki, A. *J. Magn. Magn. Mater.*, **1993**, *126*, 303.

[15] Bakonyi, I.; Péter, L.; Weihnacht, V.; Tóth, J.; Kiss, L.F.; Schneider, C.M. *J. Optoelectron. Adv. Mater.*, **2005**, *7(2)*, 589.

Temperature dependence of GMR and effect of annealing on electrodeposited Co-Ag granular films

Submitted

Temperature dependence of GMR and effect of annealing on electrodeposited Co-Ag granular films

J. García-Torres*, E. Vallés, E. Gómez
Electrodep, Departament de Química Física i Institut de Nanociència i Nanotecnologia (IN^{2}UB), Universitat de Barcelona, c/ Martí i Franquès, 1. 08028 Barcelona (Spain)

Keywords:
Co-Ag
Granular films
GMR
Temperature dependence
Annealing

A B S T R A C T

The magnetoresistance of Co-Ag granular films composed of superparamagnetic and ferromagnetic particles was studied at different temperatures. The increase in the GMR values while decreasing temperature down to 20 K was quantified. The non-saturating behaviour of the MR(*H*) curves was retained even at the lowest measurement temperature, which was mainly attributed to the dipolar interaction among the superparamagnetic particles. The influence of the annealing conditions on the magnetoresistance was also studied. In all conditions, a decrease in the GMR values was measured being attributed to an increase in the particle size.

1. Introduction

Giant magnetoresistance in granular magnetic materials arises from the spin-dependent scattering of conduction electrons in the magnetic regions. The resistance at zero magnetic field, where the magnetic moments are randomly oriented, is higher than when they are aligned by the application of a magnetic field [1,2]. In this sense, GMR effect has been found to depend on a great number of parameters i.e. granule size, surface-area to volume ratio or density of particles, among others [3,4].

Moreover, a temperature dependence of the GMR phenomenon has also been found [5,6]. A careful study of the temperature dependence of GMR is not only important in understanding its physical origin, but also beneficial to its practical applications. On the other hand, the annealing treatment also affects the magnetotransport properties. Whereas in some conditions the thermal treatment allows improving the GMR in granular films [7], in others it is detrimental for the magnetoresistance [8], the reason being the change in those parameters in which magnetoresistance depends.

The electrodeposition of Co-Ag granular films from a chloride-based electrolyte has been recently studied in our research group [9,10]. Cobalt-silver heterogeneous films with GMR were prepared by two different electrochemical techniques, chronoamperometry and pulse deposition, and from electrolytes containing different Co(II) concentrations. Although cobalt particle size distributions were always centred at sizes smaller than 4 nm, the distributions were narrower in films prepared from low Co(II) bath concentrations and/or pulse technique. GMR effect was found to depend on film's cobalt content, bath Co(II) concentration, film thickness and electrochemical technique. The GMR values obtained from our experimental conditions were practically double than those reported for electrodeposited Co-Ag granular films [11,12]. Moreover, these GMR values were even higher than those reported by some authors on the physical deposition of the system [13,14].

In this sense, the objective of the present work is to study the temperature dependence and the effect of the annealing treatment on the GMR of Co-Ag granular films obtained by continuous and pulse techniques.

2. Experimental

The samples were prepared by chronoamperometry and pulse deposition. An aqueous electrolyte containing $AgNO_3$, $CoCl_2$ and NaCl, all reagents of analytical grade, was used to prepare the Co-Ag thin films. The composition of the solutions was 0.002 M $AgNO_3$ + x M $CoCl_2$ + 3.5 M NaCl, with 0.1 M ≤ x ≤ 0.3 M. The pH was kept around 2.7 and the temperature was maintained at 25 ºC. Electrodeposition was performed over indium tin oxide (ITO) thin films sputtered on glass plates (thickness of ITO layer=25 nm).

The magnetoresistance (MR) measurements were performed at different temperatures from room temperature down to 20 K with the four-point-in-line method in magnetic fields between –8 kOe and +8 kOe in the field-in-

plane/current-in-plane geometry. Both, the longitudinal (LMR) and the transverse magnetoresistance (TMR) (field parallel to current and field perpendicular to current, respectively) components were recorded for each sample. The magnetoresistance was defined as MR(H)=100*[R(*H*)-R(0)]/R(0), where R(*H*) is the resistance in the magnetic field H and R(0) is the resistance when *H*=0.

Samples were annealed under vacuum conditions at different conditions of temperature and time: 1) 300 ºC during 1h and 2) 150 ºC during 30 minutes. Deposit's morphology, before and after annealing, was observed using Hitachi H-4100 FE field emission scanning electron microscope (FE-SEM).

3. Results and discussion

3.1.- Temperature dependence of giant mangetoresistance

Firstly, the temperature dependence of giant magnetoresistance was studied for the chronoamperometric and pulse deposited films showing the highest GMR values at room temperature, 5.85 % (sample A, obtained from the solution with x = 0.1 M and with 30 wt.% Co) and 7 % (sample B, obtained from the solution with x = 0.2 M and with 25 wt.% Co), respectively. A clear increase in the GMR value was observed as temperature decreased (Fig. 1). GMR values as high as 12 % and 14 % were measured at 20 K for samples A and B, respectively.

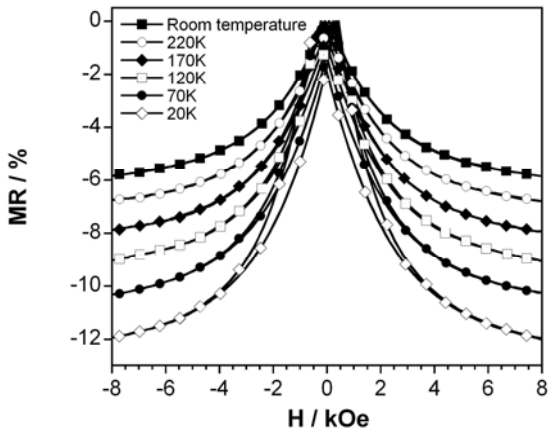

Figure 1. Temperature dependence of the longitudinal magnetoresistance for sample A.

These results are in accordance with the well-known expression of the resistivity of a granular material exhibiting GMR [15]:

$$\rho(H,T) = \rho_0 + \rho_{phonon}(T) + \rho_m(T)\left(1 - F(M/M_s)^2\right) \quad (1)$$

where ρ_0 is the temperature-independent contribution from crystal defects, $\rho_{phonon}(T)$ is the temperature-dependent phonon contribution related to the dispersion of the conduction electrons by the lattice phonons and $\rho_m(T)$ is the contribution due to the scattering of the conduction electrons at the magnetic/non-magnetic interfaces. The temperature dependence of the resistivity is mainly carried by the $\rho_{phonon}(T)$ term as the $\rho_m(T)$ term is weakly dependent on temperature [15]. In this sense, the lower the temperature the lower the electron-phonon interaction because of the number of phonons decreases with temperature and hence the higher the magnetoresistance.

A common characteristic of all the MR(*H*) curves recorded is the non-saturating behaviour indicating an important contribution of the superparamagnetic particles to the total magnetoresistance at all the temperatures measured. The numerical analysis of the magnetoresistance field dependence curves suggested by Bakonyi *et al.* [16] was applied to quantitatively decompose the total GMR into its superparamagnetic (GMR_{SPM}) and ferromagnetic (GMR_{FM}) contribution in which the magnetoresistance can be expressed as [16]:

$$MR(H) = MR_{FM} + GMR_{SPM}\, L(x), \quad (2)$$

for magnetic fields $H > H_s$. Whereby $MR_{FM} = AMR + GMR_{FM}$ is a constant term, H_s is the saturation field of the FM region and $L(x)$ is the Langevin function where $x=\mu H/kT$ with μ constituting the average magnetic moment of the SPM particles.

The numerical analysis consists on fitting the MR(*H*) curves with Eq. (2) for magnetic fields beyond $H_s \approx 1.7$ kOe which provides with the $GMR_{SPM}(H)$ contribution. The $MR_{FM}(H)$ contribution is obtained when subtracting the $GMR_{SPM}(H)$ from the experimental data. The results from the numerical analysis of the MR(*H*) curves measured at the different temperatures are shown in Fig. 2A for sample A. For all temperatures a clear dominance of the GMR_{SPM} term is observed, the relative weight of the SPM contribution (%SPM) being as high as 90 %. Moreover, both GMR_{SPM} and MR_{FM} terms increase with decreasing temperature maintaining the same proportion, which suggests that the percentage of superparamagnetic contribution to the total magnetoresistance scarcely changes with temperature. Similar tendency was observed for sample B.

On the other hand, the observed decrease with temperature of the average magnetic moment μ of the SPM regions (Fig. 2B), also extracted from the magnetoresistance curve fitting analysis, could be interpreted on the basis of the blocking of smaller and smaller clusters with decreasing temperature. However, this is in opposition to the observation that the SPM

character is retained at low temperatures which suggests the idea that not all SPM regions can be blocked even at the lowest temperature applied.

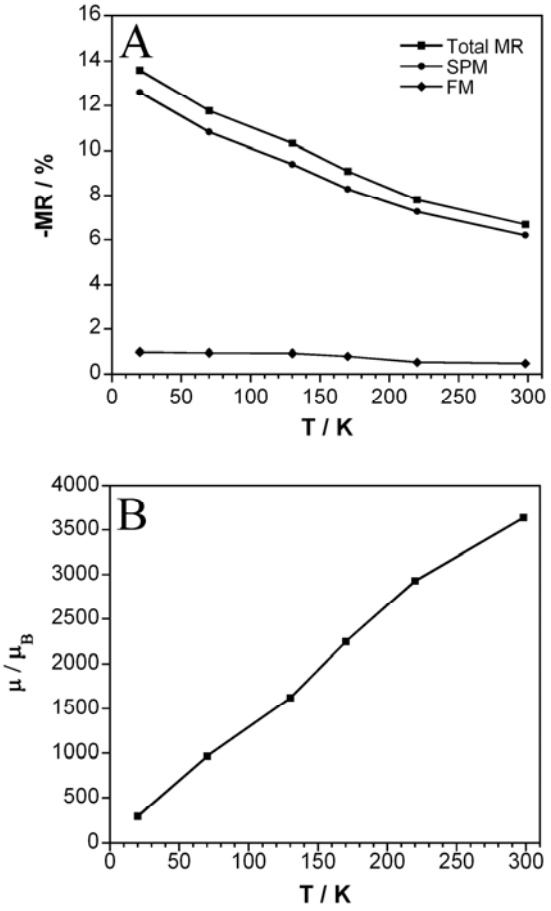

Figure 2. A) Evolution of various magnetoresistance parameters with temperature: longitudinal magnetoresistance at saturation ($GMR_{Saturation}$) and its SPM and FM contributions (GMR_{SPM} and MR_{FM}, respectively). B) Dependence of the average magnetic moment (μ) of the SPM regions on the temperature.

An effective dipolar interaction between the magnetic regions (mainly between the superparamagentic particles) could reasonably explain not only why the MR(*H*) curves retain the Langevin-like character at low temperatures but also the decrease in the apparent SPM particle size with temperature. In order to take into account the interacting behavior of the SPM particles, the modification of the argument of the Langevin function was required and hence the reformulation of the magnetoresistance expression [17,18]:

$$MR(H) = MR_{FM} + GMR_{SPM} L\left(\frac{\mu' H}{k(T+T^*)}\right) = MR_{FM} + GMR_{SPM} L\left(\frac{H}{k\lambda}\right) \quad (3)$$

where the GMR_{SPM} and MR_{FM} terms have the same meaning than in Eq. (2), μ' is the actual SPM magnetic moment and T* is the term that accounts for the dipolar interaction. The parameter $\lambda = T^*/\mu' + T/\mu'$ is defined to simplify the fitting procedure.

The representation of $\lambda\mu_B$ versus temperature shows a linear dependence in the whole temperature range (Fig. 3). From the linear fit, μ' and T* parameters have been obtained from the slope ($1/\mu'$) and the ordinate at the origin (T^*/μ'), respectively (Fig. 3). The obtained μ' value (22570 μ_B) is higher than that obtained from the conventional Langevin fit to the room temperature data (around 3600 μ_B) which indicates that the interacting SPM particles behave as bigger ones. On the other hand, the fact that the T* value (1648 K) is high enough if compare with the measurement temperature justifies the non-saturating behavior of the MR(*H*) curves observed in all the temperature range studied.

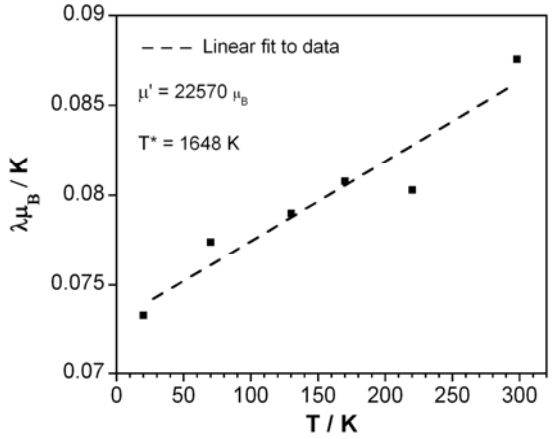

Figure 3. Evolution of parameter $\lambda\mu_B$ as a function of temperature as obtained from the longitudinal magnetoresistance data. μ'and T* parameters are also indicated.

3.2.- Influence of annealing

Annealing treatments at different temperatures and times were performed on different series of Co-Ag granular films obtained both potentiostatic and pulse deposition from the selected solutions. Fig. 4A shows the evolution of GMR with film's cobalt content for potentiostatic films before and after the annealing at 300 ºC during 1h. Independently of the thermal treatment, magnetoresistance initially increases with the ferromagnetic metal content up to a maximum and then drop off for higher cobalt contents. However, it is important to highlight here the sharp decay in the magnetoresistance values after the annealing. The maximum GMR value achieved in potentiostatic films decreased almost twenty times after the annealing. Bath cobalt concentration also exerted influence on

the GMR of the annealed films (Fig. 4B): the higher the Co(II) concentration the lower the GMR. It is also important to remark that GMR practically vanished for the films obtained from the most concentrated electrolyte in Co(II) (0.3M). On the other hand, the GMR decrease was lower for the pulse deposited films in which the maximum GMR decreased around ten times after the annealing (Fig. 4C). The difference would be related to the smaller grain size detected in the as-deposited state of pulse deposited films if compare with potentiostatic films [10]. Independently of the electrochemical technique, the reason for such sudden decrease could be attributed to a notable increase in the cobalt granule size after the thermal treatment as complete phase separation between cobalt and silver exists in the as-deposited state. This is in contrast to other electrodeposited systems in which a solid solution in the as-deposited state is obtained [7] and the subsequent annealing favours cobalt segregation leading to an increase in the GMR.

In all the samples measured, the comparison of the shape of the MR curves before and after the annealing allows observing that magnetoresistance curves (both LRM and TMR) recorded before the annealing (Fig. 5A) display a more non-saturating behaviour than those measured after the thermal treatment (Fig. 5B) in which a more sudden drop of the resistance at low magnetic fields was observed. These results are in agreement with the increase on the cobalt particle size after annealing treatment.

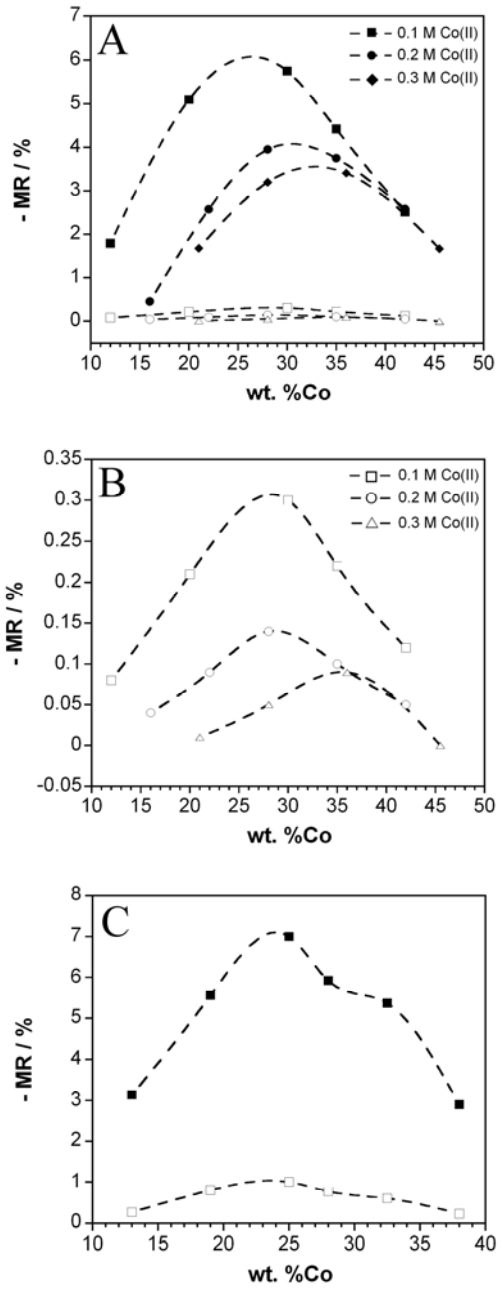

Figure 4. A) Influence of annealing on the GMR of Co-Ag granular films obtained by chronoamperometry and from different bath Co(II) concentrations. Full symbols are the GMR values in the as-deposited state, whereas empty symbols are the GMR after annealing. B) Magnification of the GMR values after annealing for the different bath Co(II) contents. C) Influence of the annealing on the GMR of Co-Ag granular films obtained by pulse deposition. Bath Co(II) content 0.2 M. Full symbols are the GMR values in the as-deposited state, whereas empty symbols are the GMR after annealing.

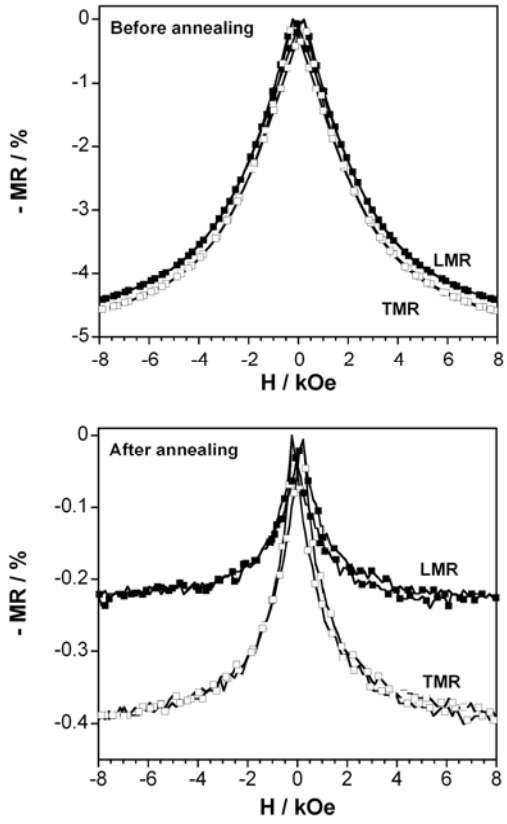

Figure 5. Shape of the MR(H) curves both longitudinal (LMR) and transverse (TMR) A) before and B) after the annealing.

Table 1. Influence of the annealing on the GMR values and ferromagnetic contribution for different bath cobalt concentrations and different techniques.

Method	Co(II) / M	wt.% Co	as-deposited		annealed (300ºC,1h)		annealed (150ºC,30min)	
			GMR	% FM	GMR	% FM	GMR	% FM
Potentiostatic	0.1	12.0	1.79	12.37	0.08	44.44	0.20	32.38
		30.0	5.75	8.07	0.30	30.30	1.04	22.73
		42.0	2.51	14.33	0.12	53.85	0.31	37.50
Potentiostatic	0.2	16.0	0.45	20.37	0.04	52.00		
		28.0	3.95	17.37	0.14	37.50		
		42.0	2.58	22.48	0.05	61.82		
Pulse plating	0.2	13.0	3.14	11.40	0.27	37.93		
		25.0	7.00	7.32	1.00	24.30		
		38.0	2.90	13.80	0.28	45.83		

Another piece of evidence was supplied by the difference between the longitudinal (LMR) and transverse (TMR) magnetoresistance curves, which is defined as anisotropic magnetoresistance term (AMR = LMR-TMR). Although the AMR value was almost the same before and after the annealing (Fig. 5), its percentage contribution to the total magnetoresistance is much higher after the annealing due to the significant smaller GMR values measured. This result is indicative of the bigger size of the cobalt granules.

The FM and SPM ratio is clearly affected by the annealing temperature (Fig. 6). While the SPM contribution is the dominant term before the annealing (Fig. 6A), a higher FM contribution is observed after the thermal treatment in all cases (Fig. 6B), the FM contribution being even higher than SPM contribution in some occasions. The higher FM contribution explains the observed sharp decrease in the GMR after the annealing because of the coalescence of the cobalt granules during the thermal treatment. Table 1 summarizes some of the results obtained from the numerical analysis of the MR(H) curves before and after the annealing in which the ferromagnetic contribution is given.

Despite the small GMR values measured for the annealed samples, some general trends have been observed in all the baths analyzed (Table 1): the relative weight of the FM contribution (% FM) initially decreases down to a minimum and then increases as film wt.% Co increases. It is important to remark that even after annealing the deposits showing the highest GMR values always presented the smallest FM contribution. These results are in agreement with those found in the as-deposited state.

In view of the last results, some of the Co-Ag films were annealed under milder conditions (150 ºC during 30 minutes). Although a decay of the MR was again observed, it was not as sharp as in the former annealing, the maximum GMR value decreasing from 5.75 % to 1.04 % after the annealing. The numerical analysis also indicated a lesser FM contribution when deposits were annealed at lower temperatures (Table 1).

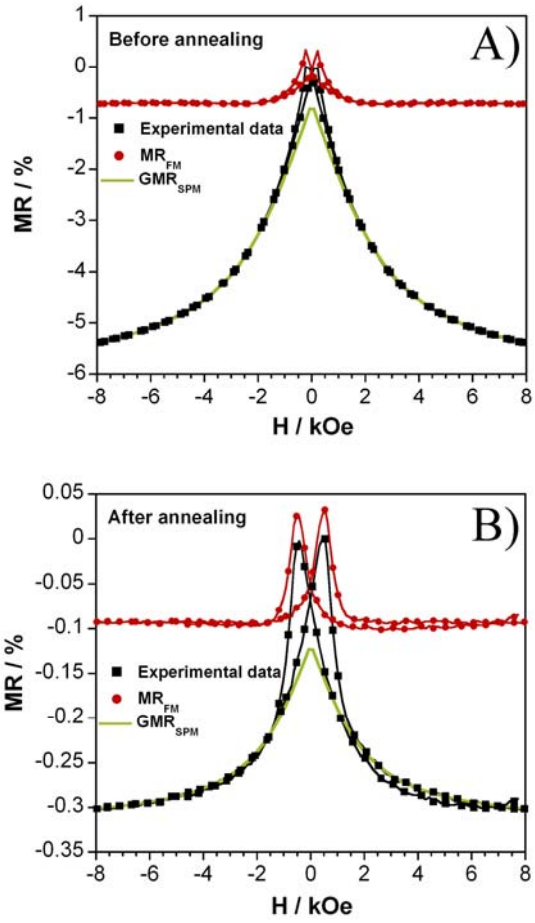

Figure 6. . Influence of the annealing treatment on the SPM and FM contribution. A) before and B) after the annealing.

The annealing effect was also observed on the morphology. Independently of the thermal treatment conditions, granular morphology was observed (Fig. 7). However, coarser grains were detected after the annealing (Fig. 7B). This SEM image also shows the way in which the grains coalesce. The increase in the atomic diffusion by the increase in temperature gives rise to the increment in the contact area between the particles and subsequent formation of the neck between them (see arrows and inset in Fig. 7B). Finally, the coalescence between the particles takes place leading to the formation of bigger particles. Although cobalt and silver grains can not be independently observed by SEM, it is expected that silver and cobalt grains growth also takes place in the manner schematized in Fig. 7C.

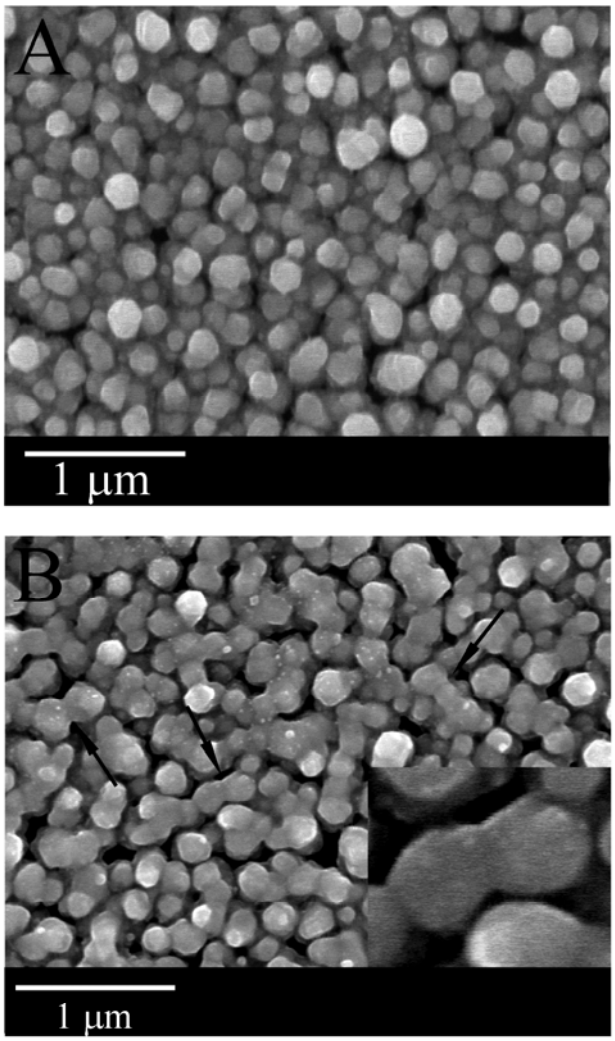

Figure 7. SEM micrographs of Co-Ag granular films A) before and B) after the annealing. C) Scheme of the coalescence and growth of the grains with thermal treatment.

4. Conclusions

The temperature dependence of the magnetoresistance of Co-Ag granular films prepared by different electrochemical techniques has been studied. A continuous increase in the magnetoresistance was observed while temperature was decreased down to 20 K, so that GMR values are double at low temperature. The MR(*H*) curves measured at the different temperatures were characterized by a non-saturating behaviour. The decomposition of such curves into its superparamangetic and ferromagnetic contributions revealed that the SPM contribution was retained even at cryogenic temperatures. This fact was explained by the dipolar interaction among the SPM particles.

Thermal treatment was also found to influence the magnetotransport properties. For the films prepared, even a moderate thermal treatment is detrimental to magnetotransport properties. A sharp decrease in the GMR values was observed at all the annealing conditions tested which was attributed to a pronounced increase on the size of the cobalt granules. Such increment led to observe a more saturating behaviour on the MR(*H*). On the other hand, the FM contribution increased from less than 10 % up to around 50 % after the annealing. Finally, SEM images revealed that the growth of bigger particles at the expense of smaller ones took place.

Acknowledgments

This paper was supported by contract MAT-2006-12913-C02-01 from the Comisión Interministerial de Ciencia y Tecnología (CICYT). J. García-Torres would also like to thank the Departament d'Innovació, Universitats i Empresa of the Generalitat de Catalunya and Fons Social Europeu for their financial support.

References

[1] A.E. Berkowitz, M.J. Carey, J. R. Michell, A.P. Young, S. Zhang, F.E. Spada, F.T. Parker, A. Hutten, G. Thomas, Phys. Rev. Lett. 68, 1992**,** 3745.

[2] I. Bakonyi, L. Peter, Prog. Mater. Sci. 55(3), 2010, 107.

[3] A. Tsoukatos, H. Wan, G.C. Hadjipanayis, Appl. Phys. Lett. 61(25), 1992, 3059.

[4] W-J. Song, R. Yang, Physica B: Condensed Matter 279(1-3), 2000, 181.

[5] Y. Ju, C. Xu, Z-Y. Li, J. Magn. Magn. Mat. 223, 2001, 267.

[6] F. Spizzo, E. Angeli, D. Bisero, F. Ronconi, P. Vavassori, P. Allia, V. Selvaggini, M. Coisson, P. Tiberto, F. Vinai, J. Magn. Magn. Mat. 262(1), 2003, 88.

[7] E. Gómez, A. Labarta, A. Llorente, E. Vallés, J. Electrochem. Soc. 151, 2004, C731.

[8] Z. Li, Z. Zhang, H. Zhao, B. Ma, Q.Y. Jin, J. Appl. Phys., 106(1), 2009, 013907/1.

[9] J. Garcia-Torres, E. Valles, E. Gomez. Submitted

[10] J. Garcia-Torres, E. Valles, E. Gomez. Submitted.

[11] S. Kenane, J. Voiron, N. Benbrahim, E. Chainet, F. Robant, J. Magn. Magn. Mat. 297(2), 2006, 99.

[12] H. Zaman, A. Yamada, H. Fakuda, Y. Hueda, J. Elechem. Soc. 145(29), 1998, 565.

[13] V.V. Hiep, N. Chau, D.M. Hongk, N.H. Luong, J. Magn. Magn. Mat. 310, 2007, 2524.

[14] F. Parent, J. Tuaillon, L.B. Stern, V. Dupuis, B. Prevel, A. Perez, P. Melinon, G. Guiraud, R. Morel, A. Barthelemy, A. Fert, Phys. Rev. B, 55 (1997) 123.

[15] J.Q. Xiao, J. Samuel, C.L. Chien, Phys. Rev. B 46, 1992, 9266.

[16] I. Bakonyi, L. Péter, Z. Rolik, K. Kiss-Szabó, Z. Kupay, J. Tóth, L. F. Kiss, J. Pádár, Phys. Rev. B 70, 2004, 054427.

[17] P. Allia, M. Coisson, P. Tiberto, F. Vinai, M. Knobel, M.A. Navak and W.C. Nunes, Phys. Rev. B 64, 2001, 144420.

[18] L. Péter, Z. Rolik, L.F. Kiss, J. Tóth, V. Weihnacht, C.M. Schneider, I. Bakonyi, Phys. Rev. B, 73, 2006, 174401.

4.6. Summary and outlook

The preparation of cobalt-silver films was demonstrated to be feasible from the different electrolytic baths tested. Co-Ag films with modulated composition were obtained in all cases. However, third species (sulphur) were incorporated into the deposits coming from sulphur-containing substances present in the bath. The electrolyte composition clearly influenced the microstructure/nanostructure of the films prepared, the crystalline structure being the most affected parameter. A weaker ferromagnetic behaviour was observed in Co-Ag films prepared from electrolytes based on sulphur-containing species as low M_s values were measured. On the other hand, magnetoresistance was only measured at cryogenic temperatures in Co-Ag deposits containing sulphur. The most plausible explanation was that sulphur placed at the magnetic/non-magnetic interfaces exerts a deleterious effect on the magnetoresistance, confirming that the magnetic/non-magnetic interface plays a main role in the MR of granular films. This result was corroborated when sulphur-free films were prepared from a chloride-based electrolyte. GMR values were measured at room temperature indicating that the unblocked interface allows the magnetoresistance effect taking place.

GMR phenomenon was found to depend on the electrodeposition conditions such as applied potential or deposition time, as these parameters directly influenced the microstructure/nanostructure of the deposits: grain size and size distribution, their volume fraction or the surface area to volume ratio. The electrochemical technique also exerted some influence on the magnetoresistance. The GMR values achieved in this work (up to 7%) practically double those found by other researchers dealing with the electrodeposition of Co-Ag granular films. Moreover, these values are even higher than those measured by some authors preparing them by physical methods [114,115].

As a conclusion we could say that electrodeposition has been revealed as an alternative technique to prepare Co-Ag granular films with giant magnetoresistance. However, much more progress could be made in the Co-Ag electrodeposition field. A series of parameters could be modified in order to study their influence on the magnetoresistance. The shape of the pulse signal applied, the working temperature or the pH could be some of the parameters to investigate.